CRACK HEALING AS A FUNCTION OF pOH^- AND FRACTURE MORPHOLOGY

A Thesis

by

JESSICA ANNE FALLON

Submitted to the Office of Graduate Studies of
Texas A&M University
in partial fulfillment of the requirements for the degree of

MASTER OF SCIENCE

December 2004

Major Subject: Geology

CRACK HEALING AS A FUNCTION OF pOH^- AND FRACTURE MORPHOLOGY

A Thesis

by

JESSICA ANNE FALLON

Submitted to Texas A&M University
in partial fulfillment of the requirements
for the degree of

MASTER OF SCIENCE

Approved as to style and content by:

Andreas K. Kronenberg (Co-Chair of Committee)	James E. Russell (Member)
William M. Lamb (Co-Chair of Committee)	Richard L. Carlson (Head of Department)
Robert K. Popp (Member)	

December 2004

Major Subject: Geology

ABSTRACT

Crack Healing as a Function of pOH^- and

Fracture Morphology. (December 2004)

Jessica Anne Fallon, B.S., The University of Oklahoma

Co-Chairs of Advisory Committee: Dr. Andreas K. Kronenberg
Dr. William M. Lamb

Crack healing in quartz has been investigated by optical microscopy and interferometry of rhombohedral $(10\bar{1}1)$ cracks in polished Brazilian quartz prisms that were annealed hydrothermally at temperatures of 250°C and 400°C for 2.4 to 240 hours, fluid pressure $P_f = P_c = 41$ MPa, and varying pOH^- (from 5.4 to 1.2 at 250°C for fluids consisting of distilled water and NaOH solutions with molalities up to 1). Crack morphologies before and after annealing were recorded for each sample in plane light digital images. Crack apertures were determined from interference fringes recorded using transmitted monochromatic light ($\lambda = 598$ nm). As documented in previous studies, crack healing is driven by reductions in surface energy and healing rates are governed by diffusional transport; sharply defined crack tips become blunted and split into fluid-filled tubes and inclusions. A rich variety of fluid inclusion geometries are also observed with non-equilibrium shapes that depend on initial surface roughness.

Crack healing is significant at T=400°C. Crack healing is also observed at T=250°C for smooth cracks with apertures <0.6 mm or cracks subject to low pOH^-. The extent of crack healing is sensitive to crack aperture and to hackles formed by fine-scale crack branching during earlier crack growth. Crack apertures appear to be controlled by hackles and debris, which prop the crack surfaces open. Upon annealing, crack apertures are reduced, and these reduced crack apertures govern the kinetics of diffusional crack healing that follows. Hackles are sites of either enhanced or reduced

loss of fluid-solid interface, depending on slight mismatches and sense of twist on opposing crack surfaces. Hackles are replaced either by healed curvilinear quartz bridges and river patterns surrounded by open fluid-filled crack, or by fluid-filled tubes surrounded by regions of healed quartz. For a given temperature, aperture and anneal time, crack healing is enhanced at low pOH^- (≤ 1.2) either because of changes in the hydroxylated quartz-fluid interface that enhance reaction rates or because of increased rates of diffusional net transport of silica at high silica concentrations.

DEDICATION

This thesis is dedicated to everyone who believed in me, who listened to me, and who kept me from quitting. I love all of y'all.

ACKNOWLEDGEMENTS

I would like to thank my advisor and my committee for invaluable suggestions and advice. I would also like to particularly thank Dr. Popp for supplying the experimental materials and apparatus. Without his gold and bombs, this project would not have been possible.

TABLE OF CONTENTS

Page

LIST OF FIGURES

FIGURE Page

FIGURE Page

LIST OF TABLES

1. INTRODUCTION

Mechanical and transport properties of rocks and fault zones of the Earth's upper crust depend on the presence of cracks. Effective elastic properties of rocks are largely governed by the populations of pores and cracks (Wyllie et al., 1956; Domenico, 1977; Gregory, 1977; Bourbie and Zinszner, 1985; Winkler and Murphy, 1995). Brittle failure and fault development depend on local stress concentrations at microcracks where critical conditions for crack extension are met (Griffith, 1921; Brace et al., 1966; Segall and Pollard, 1981; Wong 1982). Transport and storage of fluids in sedimentary rocks and fault zones depend on interconnected porosity consisting of pores, microcracks and fracture networks (Brown and Scholz, 1985; Brown, 1987; Wong et al., 1989; Brown and Bruhn, 1998; Brown et al., 1998).

Populations of cracks in rocks depend in turn on the presence of fluids and chemical rock-fluid interactions that accelerate rates of crack growth and crack healing. Crack growth is known to be accelerated by aqueous fluids through hydrolysis reactions at crack tips that weaken bonds and allow crack growth under low, sub-critical stresses (e.g., Atkinson, 1979; Atkinson and Meredith, 1981; Michalske and Freiman, 1982; Dove, 1995). Studies of crack healing and sealing have shown that silica precipitation, local dissolution and diffusional transport are involved (Smith and Evans, 1984; Hickman and Evans, 1987; Brantley et al., 1990; Brantley, 1992; Fischer and Brantley, 1992; Beeler and Hickman, 1996; Laubach et al., 2004), and all of these depend on the presence and character of fluids that fill cracks.

Evidence for crack healing and crack sealing is abundant in rocks subjected to subsurface fluids. Healed cracks are commonly decorated by fluid inclusions, which are found in curvi-planar arrays (Sprunt and Nur, 1979; Shelton and Orville, 1980; Roedder,

---

This thesis follows the style of *Journal of Geophysical Research.*

1984; Boullier, 1999; Lespinasse, 1999). Crack sealing has been documented in many deformed rocks, marked by vein fillings (Fischer and Brantley, 1992; Tenthorey et al., 1998; Lee and Morse, 1999; Renard et al., 2000; Means and Li, 2001; Wiltschko and Morse, 2001; Hilgers et al., 2004; Laubach et al., 2004) that reduce porosity and permeability through precipitation, with either local or distant sources providing the solute.

Crack growth in aqueous environments has been studied extensively, both for silicate glass and crystalline geologic materials under varying mechanical loads and thermodynamic conditions (Wiederhorn, 1967, 1969; Wiederhorn and Bolz, 1970; Ritter and LaPorte, 1975; Atkinson, 1979; Atkinson and Meredith, 1981; Dunning et al., 1984; Freiman, 1984; Dove, 1995). By comparison, relatively little work has addressed crack healing in silicate minerals. Yet, crack healing is likely important to the mechanical and transport properties of rocks in a number of geologic settings. Mechanical compaction of reservoir sands involves grain crushing (Zhang et al., 1990; Zhu et al., 1997; Karner et al., 2003) and crack healing may restrengthen, and reduce fracture porosity of these sedimentary lithologies (Dewers and Ortoleva, 1994; Zhang et al., 2001). Crack healing may contribute to re-strengthening of faults and damaged host rocks surrounding faults during inter-seismic periods (Chester, 1995; Hickman et al., 1995; Karner, et al., 1997; Cowie, 1998; Kanagawa, 2000; Tenthorey et al., 2003). Thus, stresses required to reactivate a fault will depend on the extent of crack healing. Crack healing is expected to govern the evolution of transport properties of groundwater aquifers and hydrocarbon reservoirs and it may alter fluid flow patterns through fracture networks (Brown and Scholz, 1985; Brown, 1987; Wong et al., 1989; Brantley et al., 1990; Brown and Bruhn, 1998; Brown et al., 1998)

Crack healing has been investigated for aluminum oxide and calcite at high temperatures that promote surface diffusion (Evans and Charles, 1977; Hickman and Evans, 1987), and for quartz subjected to hydrothermal conditions that promote diffusive transport of

solute through the fluid (Smith and Evans, 1984; Brantley et al., 1990; Brantley, 1992; Beeler and Hickman, 1996). In their study of crack healing in alumina, Evans and Charles (1977) observed that healing follows a diffusion rate-limited model of surface area reduction described by Nichols and Mullins (1965). They also measured increases in strength of aluminum oxide associated with the extent of crack healing. Similar processes of diffusive transport and surface area reduction have been documented for calcite at high temperatures and for quartz in the presence of aqueous fluids. Sharply defined crack tips are replaced by blunt crack terminations of increased aperture, and crack terminations recede as local dissolution (or ablation), diffusive transport of solid components and precipitation lead to the formation of tubes and then near-spherical, fluid-filled inclusions or voids (Shelton and Orville, 1980; Roedder, 1984; Sterner and Bodnar, 1984; Smith and Evans, 1984; Bodnar and Sterner, 1985; Brantley et al., 1990).

The growth of cracks in quartz is known to depend on pH and there are a number of reasons to suspect that crack healing depends on polar molecules near mineral-fluid interfaces. When OH- molecules react with high-energy, unsatisfied Si and O bonds at a crack surface, they produce lower energy Si-OH complexes (Parks, 1990; Kronenberg 1994). High OH- activity increases the solubility of silica in solution and allows more of the OH- molecules to bond to the fracture surface, leading to reduced surface energy and enhanced dissolution rates.

Crack healing is known to depend on crack aperture, time, temperature, and pore fluid chemistry. Smith and Evans (1984) documented the morphological changes in cracks within hydrothermally annealed quartz. They concluded that healing rates of thermally-induced cracks are limited by diffusion rates, and showed that the extent of healing depends on time, temperature, and silica concentration in the fluid. However, they also noted that some cracks healed while others didn't, with variations depending solely on crack aperture. Brantley (1990) investigated crack healing in quartz and found that healing was thermally activated, but rates were also found to vary with crack aperture

and geometry. Hickman and Evans (1987) investigated healing in calcite, and observed that hackles had some morphological control on healing. In all of these studies, crack healing was shown to be driven by surface energetics and the kinetics of healing were compared with a relationship of the form:

$$\left|L - L_0\right| = \Lambda\left[\frac{t\ \exp(-Q/RT)}{T}\right]^n \qquad (1)$$

where $L\text{-}L_0$ is the change in crack length during annealing, Λ is a constant that includes a diffusion coefficient and geometrical terms that describe crack aperture, t is time, Q is an activation energy, R is the gas constant, T is temperature, and n is a parameter related to crack geometry and load distribution (Hickman and Evans, 1987). Assuming that diffusive mass transport is the rate-limiting process during crack healing, the activation energy Q is expected to be given by the energy barrier for diffusion of solute in the fluid. Crack healing in quartz has been shown to depend on fluid chemistry; variations in healing in brines of differing ionic strength have been interpreted to result from a SiO_2 solubility effect on diffusive net transport (Brantley, 1992).

Crack aperture depends on debris generated during crack propagation and elastic crack closure as debris is dissolved (Beeler and Hickman, 2004). In their study of crack closure in quartz, Beeler and Hickman (2004) investigated crack closure in quartz prior to diffusional crack healing, and found that apertures decrease almost instantaneously as temperature is increased. They fit profiles of crack half-aperture (w) with distance from the crack tip by using a hyperbolic function:

$$\frac{w}{w_b} = \frac{b}{a}\sqrt{(x+a)^2 - a^2} \qquad (2)$$

where w_b is the widest half-aperture, x is the distance from the tip, normalized by the tip to initiation point length, and a and b are constants. From in-situ interferometry of rhombohedral cracks in quartz subjected to elevated temperatures and silica-saturated fluid, Beeler and Hickman (2004) found that crack apertures decreased by as much as 80% at T = 400°C to 530°C.

Despite the experimental care exercised in previous studies of crack healing, scatter in healing rate data is significant. This may be due to uncertainties in crack aperture and variations in crack morphology that influence healing.

This research investigates how fracture geometry and the OH^- activity of pore fluids affect the extent and rates of crack healing in quartz by way of controlled hydrothermal annealing experiments performed on pre-cracked quartz single crystals. Microcracks formed sub-parallel to the rhombohedral r face of quartz were imaged before and after hydrothermal annealing experiments in plane light and crack apertures were determined by interferometry using monochromatic light. Crack closure and healing are characterized at $P_c = P_f = 41$ MPa, T = 250°C or 400°C and $pOH^- = 5.94$ (H_2O at 400°C) to 1.18 (1 molal NaOH at 250°C). This study demonstrates a strong relationship between fracture morphology and healing, and a strong relationship between pOH^- and crack healing. While first order dependencies of crack healing on time and temperature are predicted by the diffusional healing model, these relationships are not as strong as the geometric and pOH^- sensitivities.

2. EXPERIMENTAL DETAILS

2.1 Preparation of Pre-cracked Specimens and Fluids

Oriented quartz samples used for this study were prepared from a single inclusion-free crystal of Brazilian quartz with well formed prismatic and rhombohedral faces (FIGURE 1). Quartz plates were cut parallel to the rhombohedral r-plane $(10\bar{1}1)$ and the r-surfaces were ground and wet-polished to 2 mm thickness using glass plates and alumina powders with sequentially finer sizes, starting with 400 grit and finishing with a 0.3 μm slurry. Using a thin kerf (0.33 mm) diamond wafer saw, the polished quartz plates were cut into prisms with dimensions of 10 mm by 3 mm measured in the r-plane. A notch was cut along the length of each prism and at two corners (FIGURE 2) to guide crack growth along the r-plane and provide for a decreasing crack extension force as the propagating crack tip moves away from the notched end of the prism. Quartz spacers were cut into similar sized prisms from the same crystal and were left with rough surfaces to be used as a source of SiO_2 during the experiment.

Nearly planar $(10\bar{1}1)$ cracks were introduced by loading each polished and notched quartz prism along its long dimension (F_1) using a precision machinist's vise (FIGURE 3). Extension of the crack across the entire prism was prevented by applying a load (F_2) normal to $(10\bar{1}1)$ by way of a small secondary clamp and two shims made of lead. In most cases, this method resulted in the formation of a crack, extending out through a triangular region with its crack tip mid-way across the prism. However, in some samples, r-cleavage cracks also formed at the opposite prism end and some cracks deflected out of the r-plane.

Fluids prepared for the hydrothermal annealing experiments consisted of doubly distilled water and NaOH solutions with concentrations of 0.01, 0.1, 0.5, and 1.0 molality. Activity coefficients for OH- in these fluids were calculated using data from Simonson

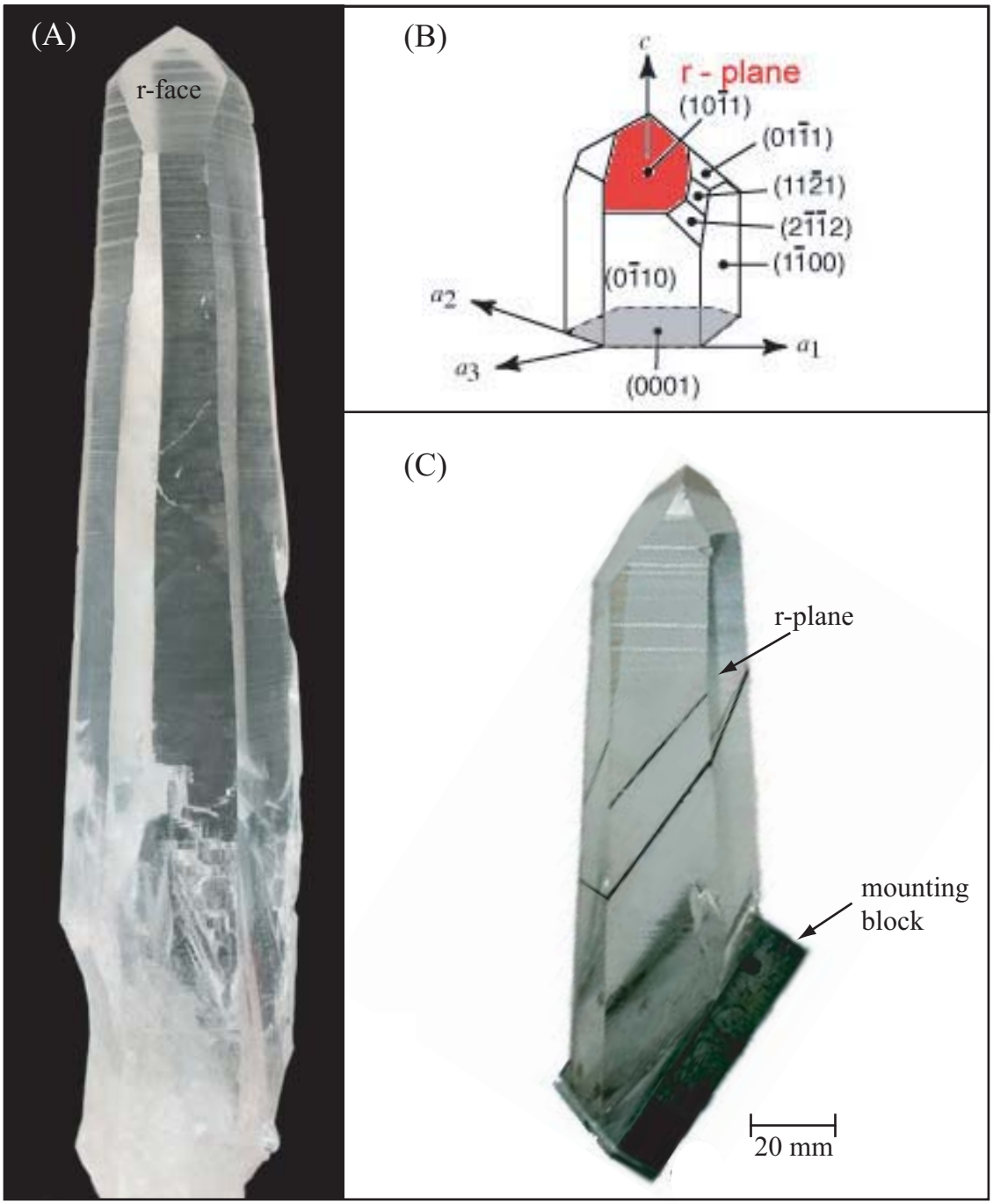

FIGURE 1. Brazilian quartz crystal used to prepare crystallographically oriented quartz samples. (A) The uncut quartz crystal, oriented to show a number of prism faces and the rhombohedral r-face (10$\bar{1}$1). (B) Crystallographic diagram of a quartz prism showing the r-plane. (C) Quartz crystal mounted for cutting plates parallel to the r-plane.

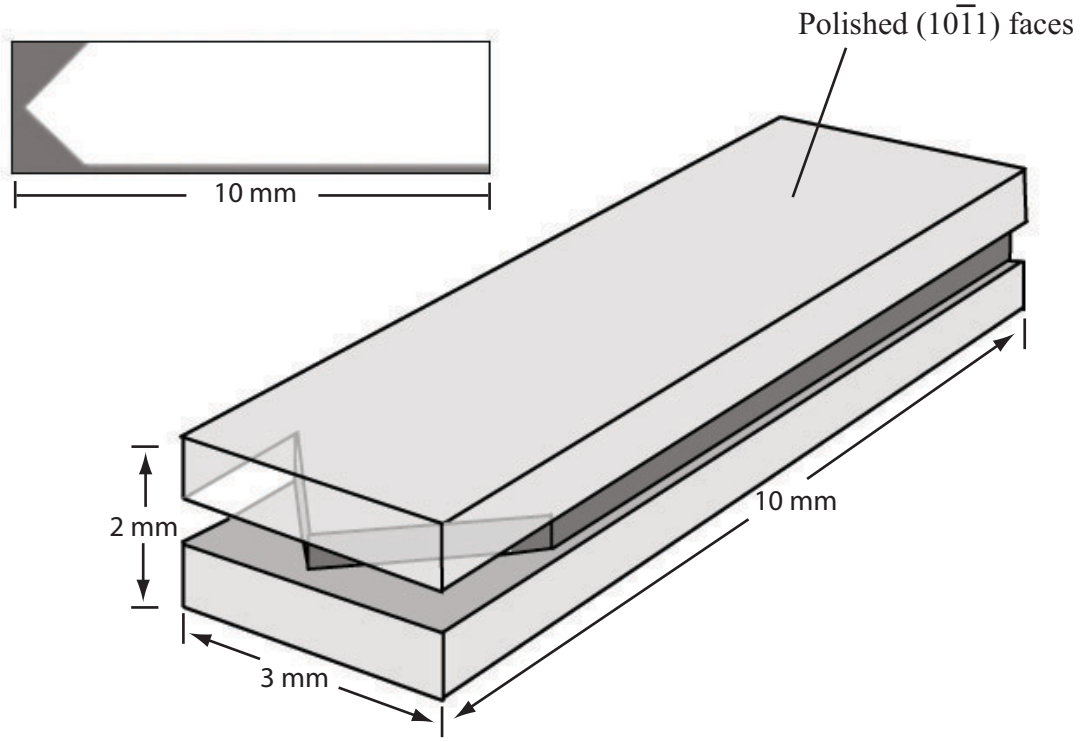

FIGURE 2. Quartz prism prepared for crack growth, with polished (10$\bar{1}$1) faces and notches cut along the prism's length and at two corners to control crack extension.

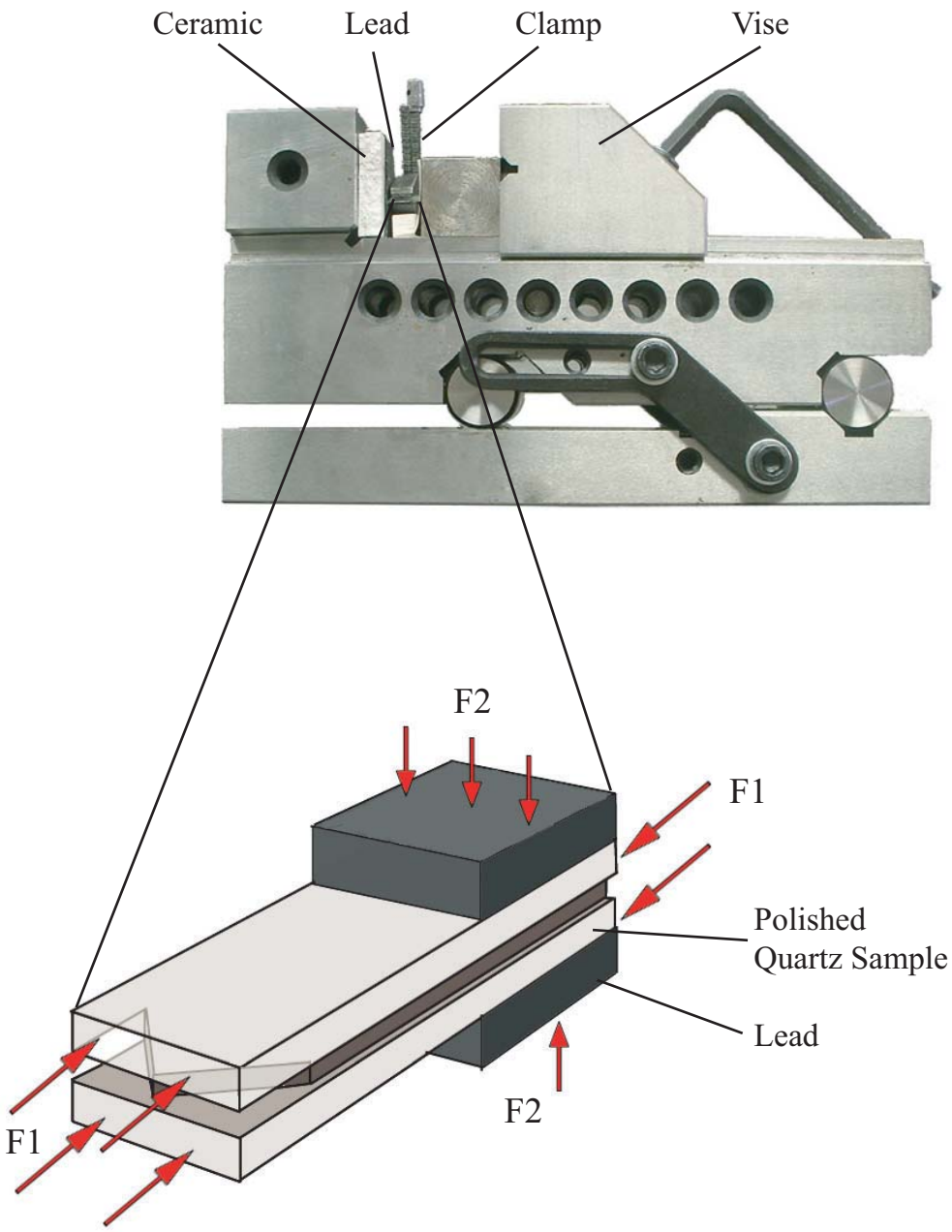

FIGURE 3. Quartz crack generation. Nearly planar $(10\bar{1})$ cracks were generated by loading each quartz prism along the long dimension (load F1) using a precision machinists vise. A small clamp was used to apply a force (F2) normal to the extending crack, thereby preventing extension across the entire sample length. Lead shims ensured an even distribution of the normal load F2.

et al. (1989) and Marshall and Franck (1981), for the chosen experimental conditions. Quartz solubilities for the fluids at experimental conditions were taken from results reported by Walther and Helgeson (1977) and Rumyantsev (1993, 1995). For conditions at which solubility was not measured directly, the equilibrium solubility is estimated by interpolation of experimental results (TABLE 1). The rough non-r surfaces of each quartz prism and the quartz spacers are expected to serve as an effective source of SiO_2 and equilibrium SiO_2 concentrations are assumed to be achieved early in each experiment.

TABLE 1. pOH^- and quartz solubility for pore fluids used in experiments.

NaOH molality at 25°C	mean NaOH activity coefficient at 250°C	OH activity coefficient	OH activity	pOH^-	Quartz Solubility (molality SiO_2)
0.01 m	0.825	0.340	0.0034	2.47	~ 0.005
0.1 m	0.606	0.184	0.0184	1.74	0.071
0.5 m	0.430	0.0925	0.0462	1.34	0.408
1.0 m	0.363	0.0658	0.0658	1.18	~ 1
			Distilled water at 250 °C	5.43	0.009
			Distilled water at 400 °C	5.94	0.016

(Simonson et al., 1989; Marshall and Franck, 1981; Rumyantsev, 1993, 1995; Walther and Helgeson, 1977)

For each experiment, a pre-cracked quartz prism, two quartz spacers, and ~ 0.1 ml fluid were sealed in a gold capsule (4.5 mm inner diameter tube with a wall thickness of ~ 0.12 mm). One end of each gold capsule was arc-welded into a triple-junction (FIGURE 4). The weight of the empty gold capsule was recorded. Weights were sequentially recorded after adding the first quartz spacer, the fluid, the quartz prism, and the second quartz spacer. After loading, the capsule was placed in an ice-water bath, and the open end of each capsule was sealed by arc-welding another triple-junction. The weight of the welded capsule was recorded before experimentation.

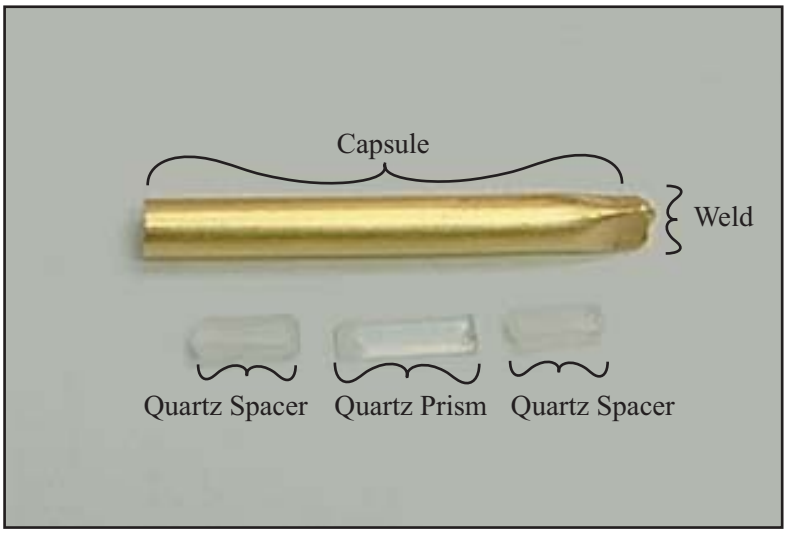

FIGURE 4. Hydrothermal annealing experiment conducted on pre-cracked quartz prism and fluid within gold capsule (first triple-junction weld shown) with quartz spacers on both sides of the quartz prism).

2.2 Experiments

Once sealed, the sample capsules were placed into externally heated cold seal pressure vessels (FIGURE 5). The vessels were sealed, and pressure applied by way of an argon pressure system (FIGURE 6). At a P_c of ~ 50 MPa, the vessel was isolated to check for leaks. After 20 minutes P_c was decreased to the experimental target value of 41 MPa. Given the quantity of fluid (~ 0.1 mL) typically sealed in each gold capsule and the small crack volumes of the quartz samples (~ 2 x 10^{-5} mL), the internal fluid pressure P_f is taken to be equal to the confining pressure P_c applied by argon on the outer surfaces of the gold capsule. Thus $P_f = P_c = 41$ MPa, and the effective pressure $P_e = (P_c - P_f) = 0$. Once the pressure vessel was tested for leaks, the vessel was placed in a furnace and temperature raised, monitoring temperature by way of a K-type Chromel-Alumel thermocouple. The vessel typically required 45 minutes to reach the experimental temperature. At the end of each experiment, the pressure vessel was removed from the furnace and cooled with compressed air to 90°C (over 10-15 minutes). At 90°C, the pressure was released, in order to expand the gold capsule and allow retrieval of the quartz prism from the capsule without damaging or altering the healed crack. Capsules were weighed to test for any leaks and opened to extract the quartz sample. Weight measurements for well-sealed capsules before and after an experiment were the same within +/- 0.001 g. However, a significant number of capsules burst upon expansion at the end of the experiment. For these capsules, water contents of 0.005 to 0.050 g remained, and water was observed inside the capsule. Results reported in this study are restricted to those samples for which capsule weights were unchanged, as well as those capsules in which water was confirmed by observation. Out of 42 experiments run, 21 quartz prisms were successfully retrieved, and 4 of the prisms retrieved had measurable cracks on both sides, resulting in 25 cracks total.

These hydrothermal annealing experiments were performed on samples with r-cleavage cracks of varying aperture and crack morphology at T = 250°C and 400°C (+/- 1°C), Pc

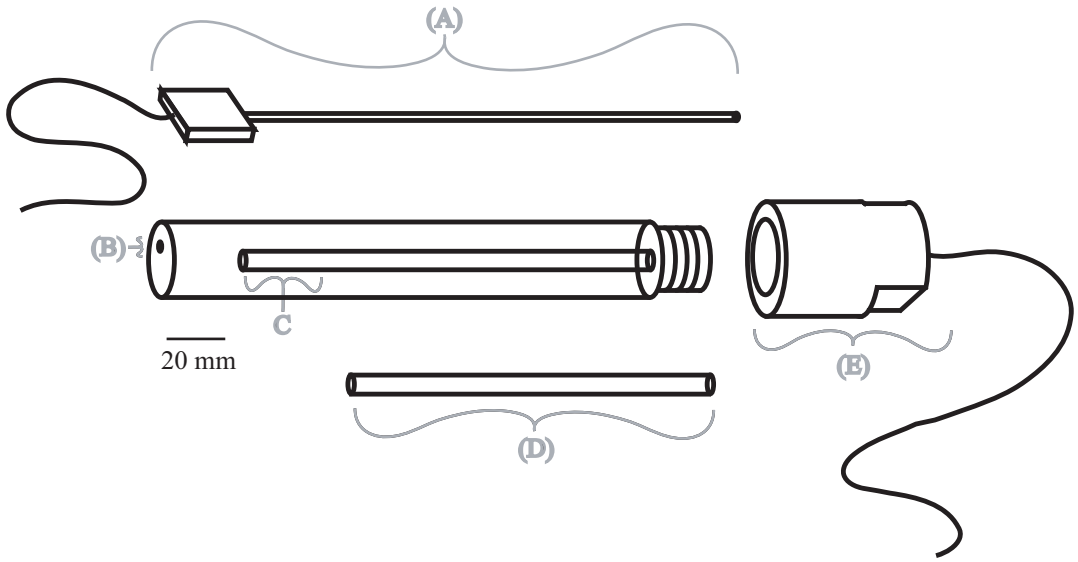

FIGURE 5. Cold seal hydrothermal pressure vessel, shown with end cap, filler rod and thermocouple. (A) K-type thermocouple. (B) Thermocouple well. (C) Capsule location. (D) Filler rod. (E) Pressure vessel end cap and connection to pressure system.

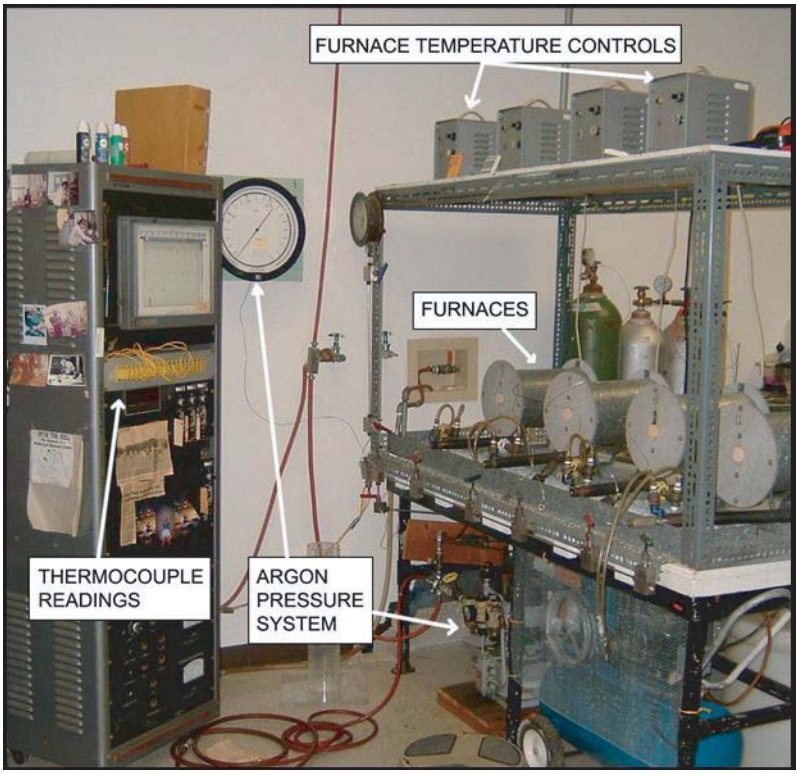

FIGURE 6. Cold seal pressure system, used for the hydrothermal annealing experiments.

= Pf = 41 MPa (+/- 1 MPa), annealing times of 2.4, 12, 24, 96, and 240 hours, and pore fluids with NaOH concentrations of 0 to 1.0 molality (corresponding to a pOH^- of 5.94 to 1.18, respectively). Beginning and ending times of anneals were recorded within one minute, but uncertainty in effective annealing time may be as large as ~ 10 minutes due to the time required to raise the temperature at the beginning of each experiment. The number of successful experiments performed for each set of conditions is given in TABLE 2.

TABLE 2. Numbers of successful hydrothermal annealing experiments on pre-cracked quartz prisms for various conditions and annealing times.

	2.4 hours	12 hours	24 hours	96 hours	240 hours
250°C, Distilled H_2O	1	1	2	1	0
250°C, 0.01 molal NaOH	0	0	1	0	0
250°C, 0.1 molal NaOH	1	0	2	0	1
250°C, 0.5 molal NaOH	0	0	1	0	0
250°C, 1.0 molal NaOH	0	0	1	0	0
400°C, Distilled H_2O	1	0	7	0	1

2.3 Imaging Methods and Interferometry

Cracks in each quartz sample (FIGURE 7) were photographed digitally (using a Zeiss Axioplan 2 microscope, with an Axiocam HRc camera, and Axiovision 3.0 software) before and after the hydrothermal experiments at four magnifications (25X, 100X, 200X and 320X) using plane polarized light, and monochromatic light. Monochromatic light with a wavelength of 589 nm +/- 5 nm was obtained by placing an interference filter in the condensing optics between the light source and sample.

Digital photomontages were compiled from the 25X and 100X images while the 200X and 320X images were used to record fine details in crack morphology. Changes in crack morphology and crack tip location are readily detected by comparing images before and after annealing, at low magnification (FIGURE 7) and at high magnification (FIGURE 8).

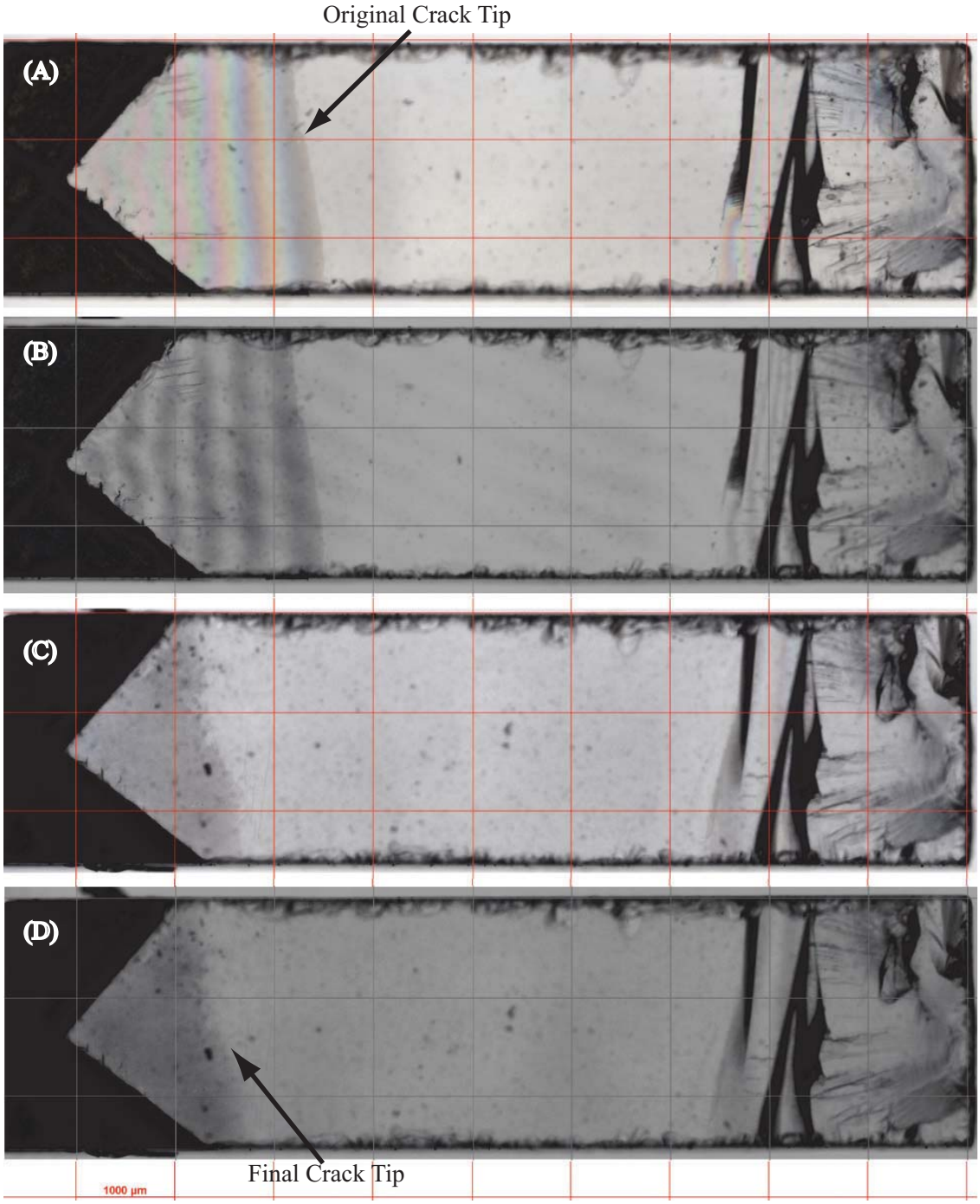

FIGURE 7. Imaging cracked quartz prisms. The rhombohedral r-crack is parallel to the plane of each photomicrograph. (A) Quartz prism 2D#1 with rhombohedral r-crack, photographed before hydrothermal annealing in plane polarized polychromatic light from a 100 W halogen light source. (B) Quartz prism 2D#1 photographed before annealing using monochromatic light with a wavelength of 589 nm +/- 5 nm. (C) Quartz prism 2D#1 photographed after hydrothermal annealing in plane polarized polychromatic light. (D) Quartz prism 2D#1 photographed afterhydrothermal annealing using monochromatic light (λ = 589nm).

(A)

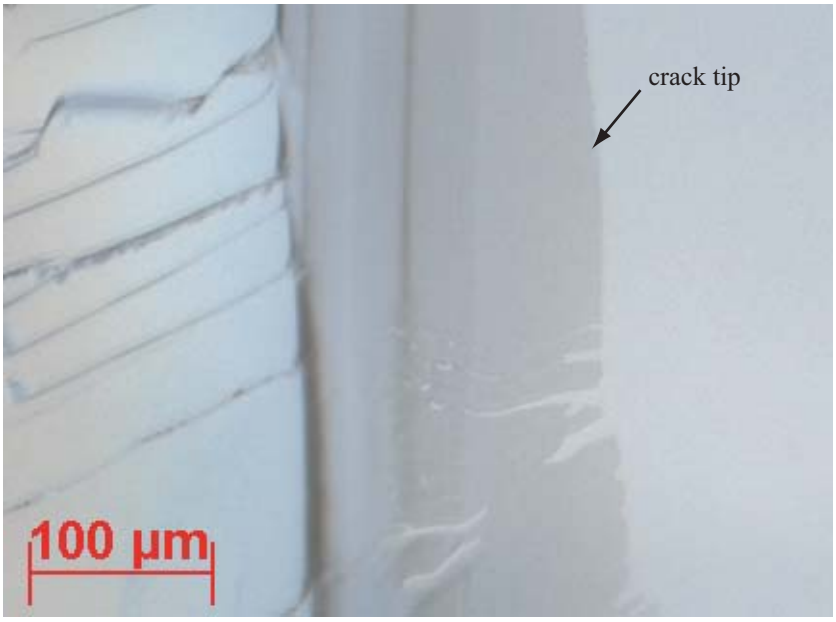

(B)

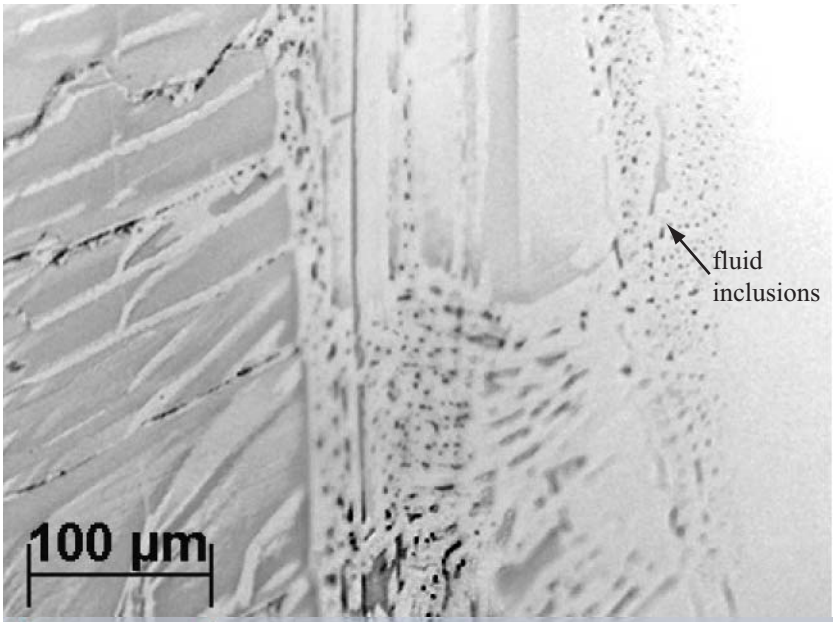

FIGURE 8. Detail of healing at the crack tip. (A) before and (B) after annealing in distilled water at T = 400°C, t = 24 hrs (quartz prism 3F#3).

Crack apertures, changes in crack aperture, and changes in crack morphology were determined from interference fringes detected in transmission, enhancing contrast of the digitally stored images when needed to reveal interference phenomena. Rhombohedral r-cracks $(10\bar{1}1)$ in the oriented quartz prisms represent wedge shaped gaps in the optical path, with reflections at surfaces giving rise to interference (FIGURE 9). The portion of the light traveling through the quartz crystal that is reflected at crack surfaces (both at the top and bottom of the crack) interferes with the transmitted light that has not been reflected, giving rise to constructive and destructive interferences that depend on wavelength λ. Given that the opening angle of a given crack is small, interference fringes appear diffuse and their spacing is broad. Nevertheless, crack apertures can be determined accurately by counting fringes along a transect away from the crack tip, each fringe representing an increase in aperture of ~ 0.3 μm or a 0.15 μm increase in half aperture w of the crack;

$$w = \frac{m\lambda}{4} \tag{3}$$

where m is the fringe number, and λ is the wavelength (Valasek, 1949; Moller 1988; Beeler and Hickman, 2004).

Fringes obtained with monochromatic light (λ = 589) are simple to analyze, yet interference phenomena are also observed for polychromatic light that contain aperture information at larger and smaller wavelengths than λ = 589 nm. Color fringes observed for polychromatic light can be calibrated against fringes of monochromatic light (FIGURE 10) and provide information on the dimensions of cracks when apertures are extremely fine. The apertures of cracks that display only the first destructive fringe or less in monochromatic light have been estimated semi-quantitatively using color fringes from polychromatic light with a resolution given by the smallest visible wavelength of light (λ = 380 nm).

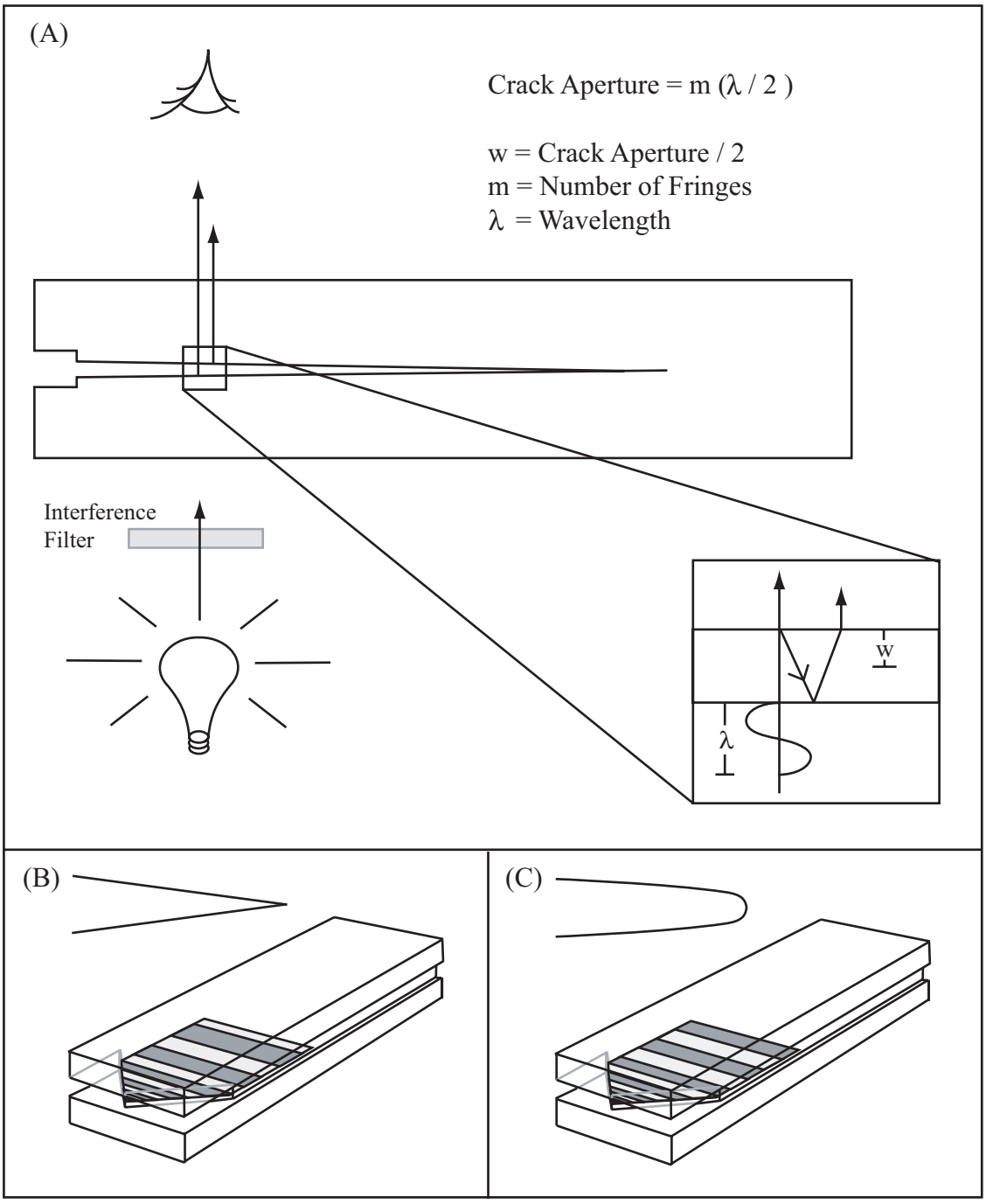

FIGURE 9. Interference fringes from nearly planar rhombohedral crack. (A) Schematic diagram showing how interference fringes are generated from a wedge-shaped crack. (B) Interference fringes expected for a simple wedge-shaped crack with planar walls and sharp crack tip. In transmitted light, transmitted and doubly reflected light combine constructively at the thin crack near its tip, and fringes out from the tip serve as contours of constant crack aperture. (C) Most cracks imaged exhibit destructive interference at the crack tip, associated with a blunt crack tip and non-linear crack walls.

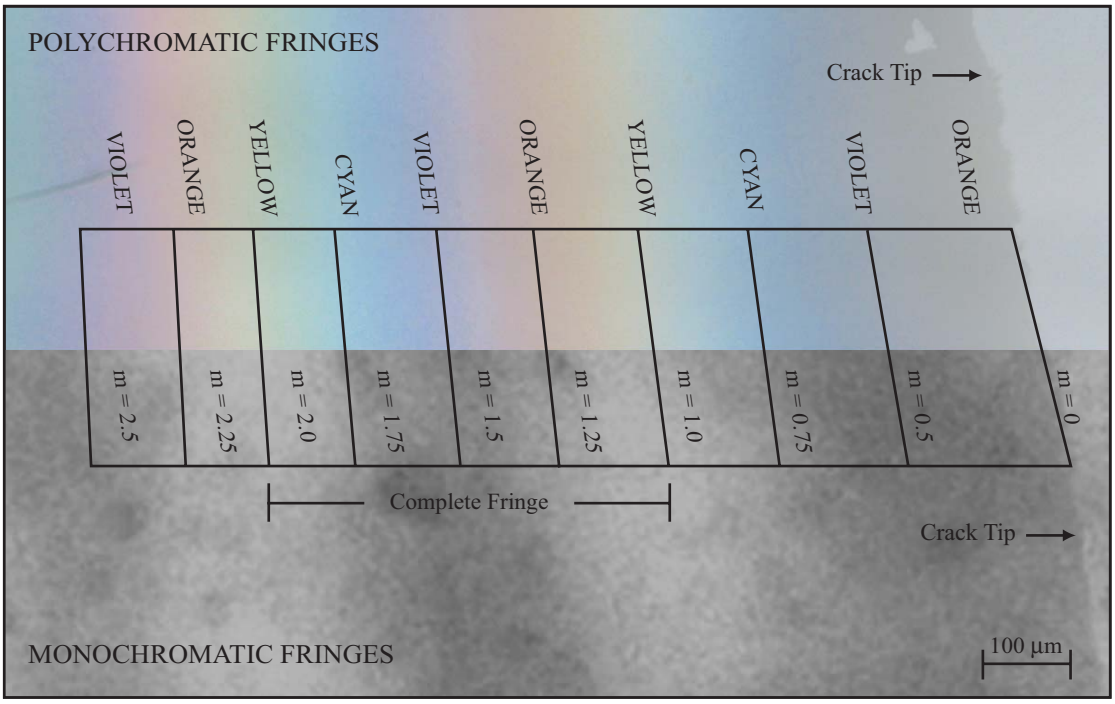

FIGURE 10. Interference fringes for the same rhombohedral crack for monochrommatic (λ = 589 nm) and polychromatic light (100W bulb).

2.4 Crack Mapping and Healing Measurement

Digital photomontages of cracks imaged before and after annealing at 100X magnification were matched by way of a grid that allows accurate point-to-point location. Fracture maps were generated from these photomontages, identifying crack tips before and after the experiments. Crack lengths and areas were determined from these maps using NIH ImageJ.

Crack length is measured along a traverse perpendicular to the aperture fringes for each crack. However, since the cracks are not rectangular in map view, and since healing proceeds irregularly and occasionally occurs in isolated patches far from the crack tip, measures of original length and healed crack length are difficult to evaluate for a number of cracks. While length healed and area healed are proportional for most cracks, healed length and area do not scale well for cracks that healed irregularly. In these cases, healed area is a better representation of total crack healing than any particular healed crack length. Measurements of length are used to evaluate crack aperture profiles and closure, but the measurements of crack area before and after hydrothermal annealing are used to quantify crack healing. Healed crack areas are measured by superimposing crack maps for the same crack before and after annealing and determining the difference in connected crack areas in mm^2. Healed crack areas are taken to be positive. For a few samples, crack areas after annealing were greater than measured before annealing. Changes in crack area determined for these samples are negative, representing further crack extension during the experiment with little or no crack healing. For other samples, fluid inclusions were found extending further into the quartz prism than the original crack tip imaged prior to annealing. For these samples, it is assumed that crack extension proceeded after imaging and before crack healing. In these cases, the original crack area is re-determined, based on the furthest extent of fluid inclusions in the prism and healed crack areas are evaluated from this starting area.

For each rhombohedral r-crack, the crack half-aperture (w) and length to the crack tip were measured along a traverse from the crack tip to the sample edge, based on observed interference fringes and EQUATION 3 (Valasek, 1949; Moller 1988; Beeler and Hickman, 2004). Apertures following annealing experiments were not measured for cracks that healed completely, or that healed irregularly in isolated patches. In addition, some cracks had such small apertures that fringes did not provide quantitative information. In other cases, crack apertures were so large and irregular that fringes could not be accurately identified and counted. With the exception of these instances, crack opening was evaluated by plotting crack half-aperture as a function of distance measured along the crack's length, producing a crack profile. To compare crack profiles for cracks of different lengths, the profiles were normalized following the procedure described by Beeler and Hickman, (2004). For profiles before and after annealing, crack aperture is normalized with respect to the maximum aperture before annealing. For profiles before annealing, distance along the crack length is normalized with respect to the crack length measured prior to annealing. For profiles after annealing, distance along the crack is normalized with respect to the maximum crack length measured before healing (or the maximum crack length as measured from the furthest extent of fluid inclusions to the crack initiation point in the instances where crack length increased after the initial imaging). Observed profiles were compared with crack aperture profiles determined by Beeler and Hickman (2004) from in-situ interference measurements during crack closure experiments. Crack aperture profiles were likewise compared before and after our hydrothermal annealing experiments.

Measures of surface roughness and quantification of the extent that r-surfaces show hackle marks and crack branching are difficult inherently difficult to quantify. In order to characterize crack roughness, cracks are qualitatively evaluated and placed into one of three categories designated as hackle magnitude 1, 2, and 3. Cracks that appear optically smooth or have hackles with widths (as measured in the r-plane) of <=10 μm are classified as "smooth" and designated a hackle magnitude of 1. Cracks that have hackles

with widths greater than 10 μm but less than 50 μm are classified as having a hackle magnitude of 2. Cracks with hackles 50 μm or wider are classified as “rough”, and assigned a hackle magnitude of 3.

3. RESULTS

Crack areas before experimentation range from 0.51 mm^2 to 9.36 mm^2 and maximum crack half-apertures range from 0.074 μm to 2.36 μm. Crack areas are reduced in many of the hydrothermally annealed quartz prisms, with healed areas ranging from 0 to 5.27 mm^2. In a few experiments, crack area increased by as much as 1.66 mm^2. Half-apertures after annealing are reduced, ranging from 0 to 1.62 μm. The results of hydrothermal annealing experiments performed on pre-cracked quartz prisms are listed in TABLE 3, organized by the experimental conditions imposed, and the surface roughness of the initial cracks. Samples are numbered according to the r-plate taken from the parent quartz crystal, and prism cut from the plate (e.g. sample 2C#3 left comes from r-plate 2 with the prism C#3 cut from this plate). For those prisms in which two r-cracks were formed, cracks are identified as left (forming at the end with notches cut at corners) or right (forming at the opposite prism end) and healing data are provided for both. Healed areas are provided in mm^2 where positive values indicate healing and negative values indicate further crack extension. Half-apertures based on interferometry are given in μm for the maximum aperture (at the point of crack initiation).

3.1 Crack Morphology Prior to Hydrothermal Experiments

Cracks formed in the quartz prisms fall into four morphological categories based on their macroscopic geometry: planar, lobate, curved-tip and planar branched (FIGURE 11). Examination of these cracks by optical microscopy reveals fracture morphologies common to fracture surfaces in other crystalline materials as illustrated schematically in FIGURE 12 (after Bahat, 1991). Fractures in crystalline solids typically initiate at a surface flaw and follow a crystallographic plane of low relative surface energy. As the crack propagates, it forms a smooth region surrounding the initiation point, referred to as the mirror (after its smooth reflective surface). The mirror grades into a less smooth region identified as the mist, and the mist grades into the rough, stepped hackled region

TABLE 3. Healed area and half-aperture data.

Sample #	Temp (°C)	Time (hrs)	Pore Fluid	Hackle Magnitude	Crack area before Experimentation (mm^2)	Half-Aperture Before Experimentation (μm)	Healed Area (mm^2)	Half-Aperture After Experimentation (μm)	Apparent Healing Rate (mm^2/s)
2C#3 left	250	2.4	H_2O	1	0.509869	0.220875	0.437	0.000	5.06E-05
2C#3 right	250	2.4	H_2O	3	1.974756	0.2945	0.195	0.295	2.25E-05
2B#3	250	2.4	0.1m NaOH	1	1.715895	0.073625	1.653	0.000	0.000191
2E#4	250	12	H_2O	3	0.764382	1.178	-0.753	0.000	-1.7E-05
2B#1	250	24	H_2O	1	3.807329	0.2945	2.365	0.147	2.74E-05
1A#2	250	24	H_2O	3	9.363347	2.0615	-1.656	2.945	-1.9E-05
1B#5	250	24	0.01m NaOH	3	4.577151	0.515375	0.000	0.884	0
2D#3 left	250	24	0.1m NaOH	1	1.934892	0.589	1.329	0.147	1.54E-05
2E#5	250	24	0.1m NaOH	1	1.866941	0.73625	1.793	0.000	2.08E-05
2D#3 right	250	24	0.1m NaOH	3	7.027884	0.73625	0.000	0.884	0
2F#3	250	24	0.5m NaOH	2	7.826218	2.20875	3.195	0.295	3.7E-05
2A#6 left	250	24	1.0m NaOH	3	1.926225	0.073625	1.791	0.000	2.07E-05
2A#6 right	250	24	1.0m NaOH	2	9.240167	2.0615	3.876	0.000	4.49E-05
2C#5	250	96	H_2O	2	1.003257	0.073625	0.976	0.000	2.82E-06
3C#3	250	240	0.1m NaOH	1	5.737001	1.178	5.272	0.000	6.1E-06
2D#1 left	400	24	H_2O	1	5.035353	0.8835	2.367	0.147	2.74E-05
3E#2	400	2.4	H_2O	2	3.670928	0.662625	0.476	0.442	5.51E-05
3C#2	400	24	H_2O	1	1.532031	0.220875	1.457	0.000	1.69E-05
3C#4	400	24	H_2O	1	1.899939	0.73625	1.366	0.442	1.58E-05
2F#2	400	24	H_2O	2	3.415685	0.44175	0.561	0.147	6.49E-06
3D#2	400	24	H_2O	2	4.004219	0.73625	0.488	0.295	5.65E-06
3E#3	400	24	H_2O	3	5.267596	0.2945	0.651	0.221	7.53E-06
3F#1	400	24	H_2O	3	4.645325	2.356	0.209	3.240	2.42E-06
2D#1 right	400	24	H_2O	3	3.335805	0.73625	0.321	0.589	3.72E-06
2A#2	400	240	H_2O	1	2.741741	0.257688	2.742	0.000	3.17E-06

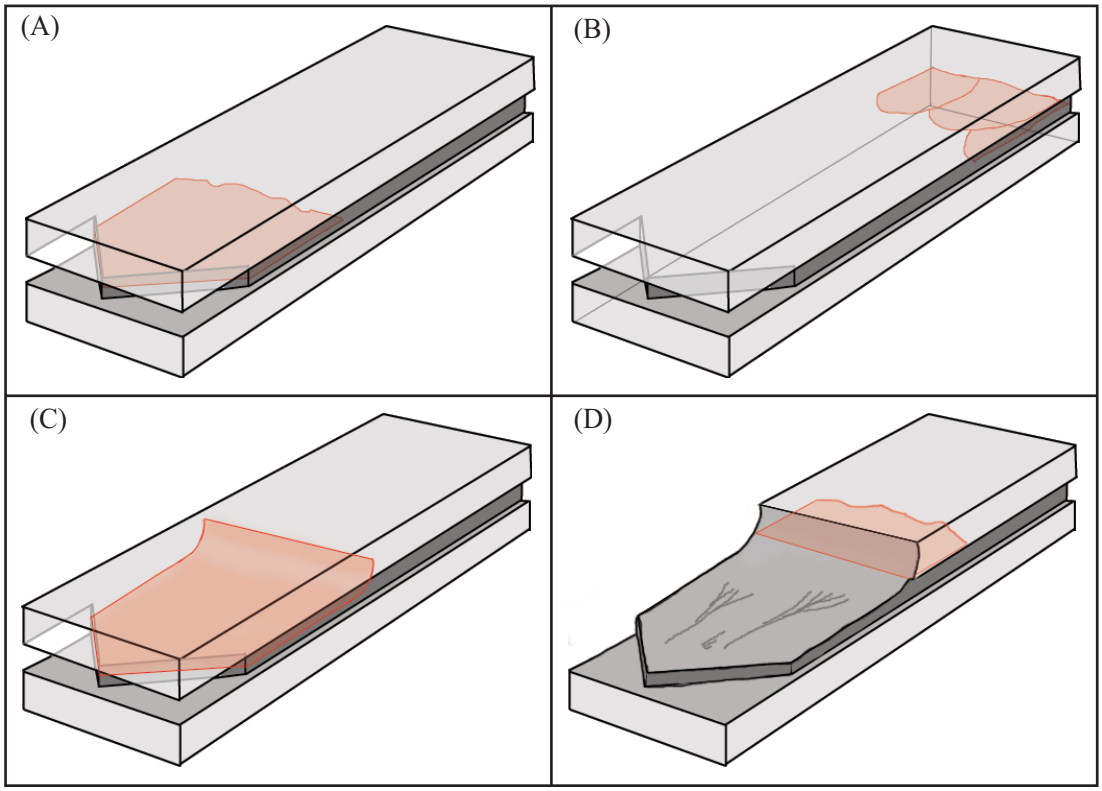

FIGURE 11. Fractures generated in quartz prisms of varying form. (A) Planar cracks originate from the triangular notched end, and propagate into the prism, maintaining a planar form. (B) Lobate cracks initiate on the opposite square end of the prism and propagate inward as fan-shaped lobes. (C) Curved-tip cracks are initiated as planar cracks that curve sharply out of plane at the tip. (D) Branched cracks initiate from the triangular notched end as a single planar r-crack which splits into two propagating cracks, one continuing in the r-plane, and the other curving out of plane.

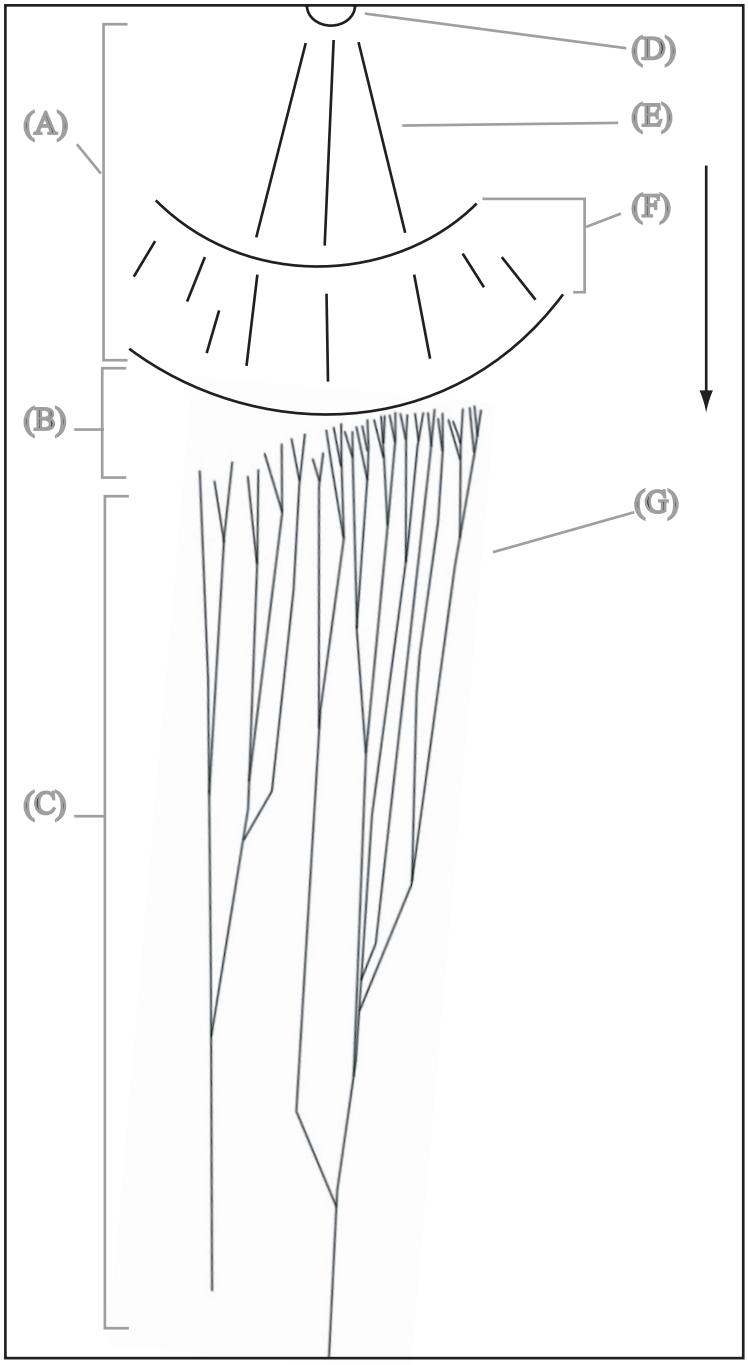

FIGURE 12. Fracture surface features identified in crystalline materials. The crack propagation direction is shown with the black arrow. (A) The relatively smooth fracture mirror. (B) The fracture mist, which is a transition zone between the smooth mirror, and the hackled region of the crack. (C) The hackled region, characterized by high relief hackle markings and steps in the crack (traced from crack micrograph, sample 1A#2). (D) The crack initiation point. (E) Radial striae, which are fine lineations on the surface of the mirror parallel to the crack propagation direction. (F) Rib markings, which are low relief undulations on the fracture surface perpendicular to the crack propagation dirction. (G) Hackles forming a river pattern, parallel to the crack propagation direction.

(Bahat, 1991). Rhombohedral r cracks formed in quartz exhibit smooth areas in some regions, and hackle marks in other regions, with hackles of varying step height and step angle with respect to the r-plane. In many cases, hackle marks are observed to merge to form larger hackles with larger step heights, forming well developed river patterns. Hackles and river patterns develop between pairs of cleavage planes when the non-coplanar cracks are bridged by shear cracks or secondary cleavages as a result of combined tension and shear stresses (Bahat, 1991). Rhombohedral r cracks in the pre-cracked quartz prism also show linear surface features perpendicular to the direction of crack propagation, referred to as rib markings. These features develop due to stress fields that progressively bend the crack front away from the original direction of propagation (Bahat, 1991). Small subsidiary microcracks are also seen associated with crack branching at large magnitude hackles (FIGURE 13). Despite the complexities associated with hackle formation and crack branching, the apertures of cracks formed in these quartz prisms vary systematically from the crack tip to the prism end where the crack initiated. Aperture profiles (FIGURE 14) determined by interferometry for many of the cracks generated in quartz prisms are consistent with the hyperbolic function (EQUATION 3) used to fit r-cracks in quartz by Beeler and Hickman (2004), although some cracks show varying curvature from crack tip to prism end and complex profiles that are associated with roughness of the crack surface.

3.2 General Description of Crack Healing

Healing of cracks due to hydrothermal annealing is most apparent near the original crack tip where apertures are smallest, though in some circumstances healing initiates from features in the interior of the crack. The process of crack tip recession may leave behind fluid-filled tubes and fluid inclusions (FIGURE 15) much as documented by Smith and Evans (1984), as well as large regions of optically continuous quartz without resolvable fluid inclusions (FIGURE 15). Fluid inclusions and healed crack morphologies appear to be affected by the occurrence of hackle marks (FIGURE 16, 17). At the same time

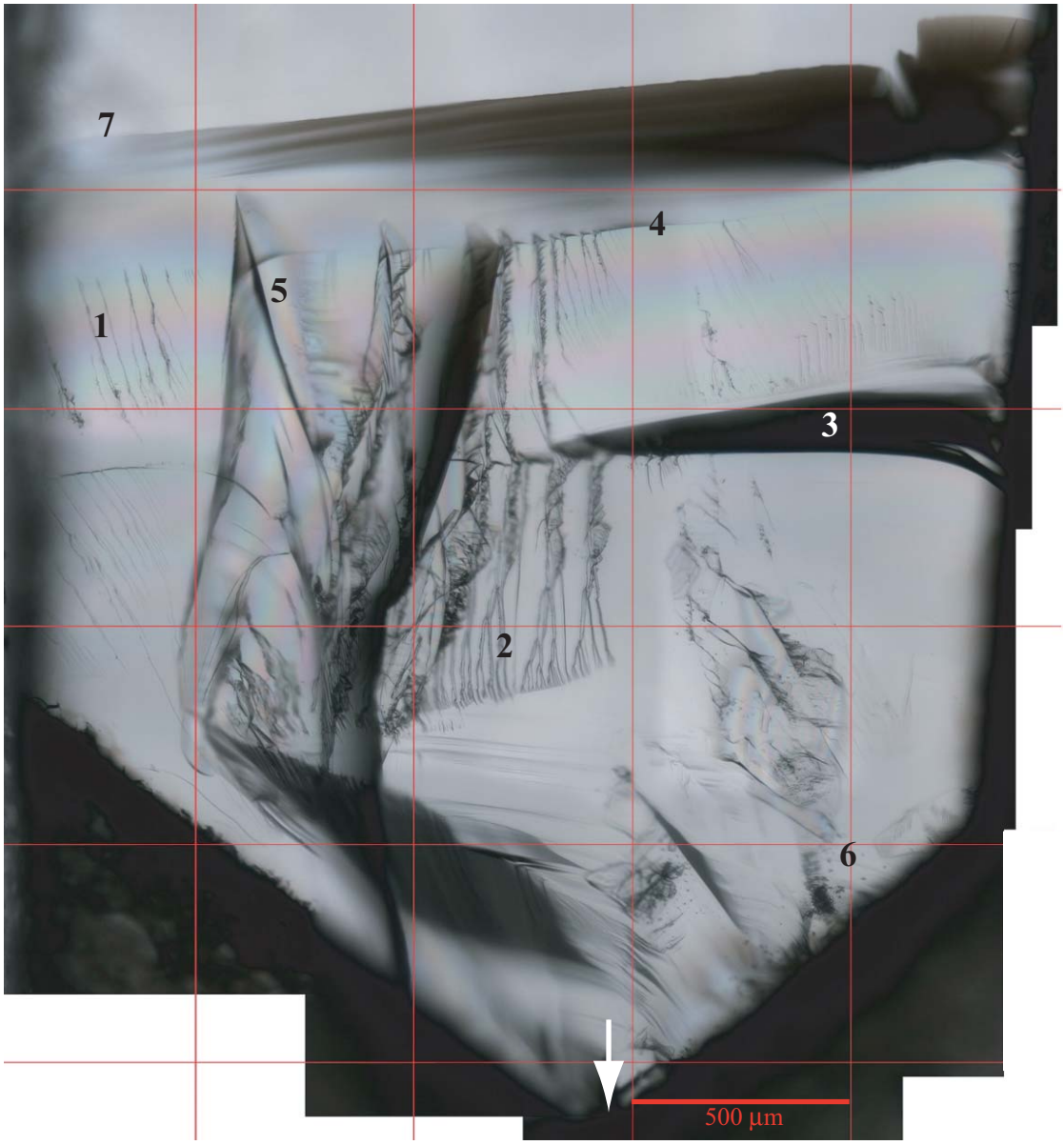

FIGURE 13. Quartz crack 3F#1 before hydrothermal annealing, showing typical fracture features. The white arrow indicates the direction from the crack tip to the crack initiation point. (1) Hackles consisting of fine steps in the crack surface due to fine-scale crack branching during crack propagation. (2) Hackles that merge during propagation into river patterns. (3) Larger fracture step. (4) Rib marking. (5) Subsidiary microcracks that form as sub-parallel branches from the main r-plane crack. (6) Debris within the crack formed during crack propagation. (7) Crack tip.

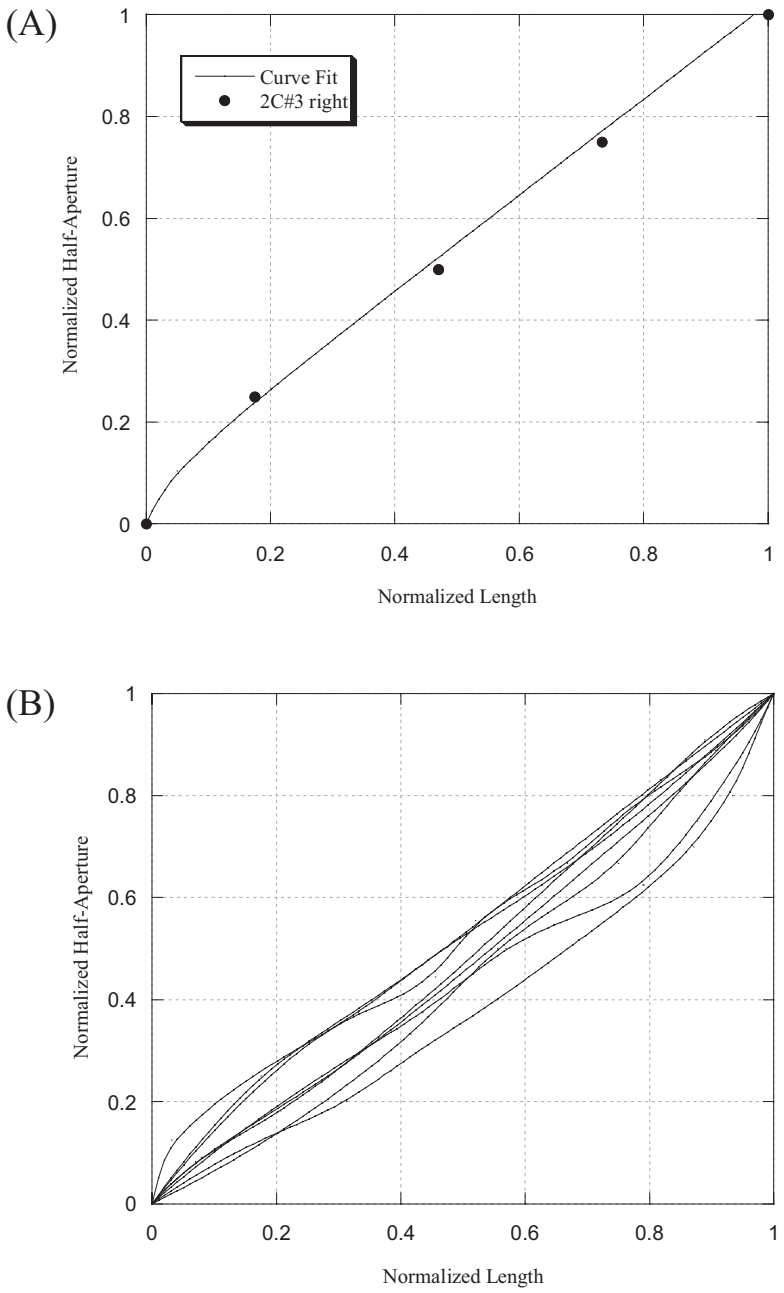

FIGURE 14. Aperture profiles of r-cleavage cracks in quartz prisms before hydrothermal annealing. A representative crack profile for sample 2C#3 right is shown (A) with aperture measurements shown as data for individual interference fringes and fit by the hyperbolic function proposed by Beeler and Hickman (2004). Half-aperture of this crack was normalized by the maximum half-aperture of 0.589 μm, following the convention of Beeler and Hickman (2004). Crack aperture profiles of other r-cleavage cracks (B) selected to show the widest range of aperture profiles measured for pre-cracked quartz prisms used in this study (quartz cracks 2C#3, 1A#2, 3D#2, 2D#3 left, 2D#3 right, 1B#5, and 2E#5 are shown). Curves represent smooth fits to interference fringe data, and in some cases do not follow a hyperbolic function.

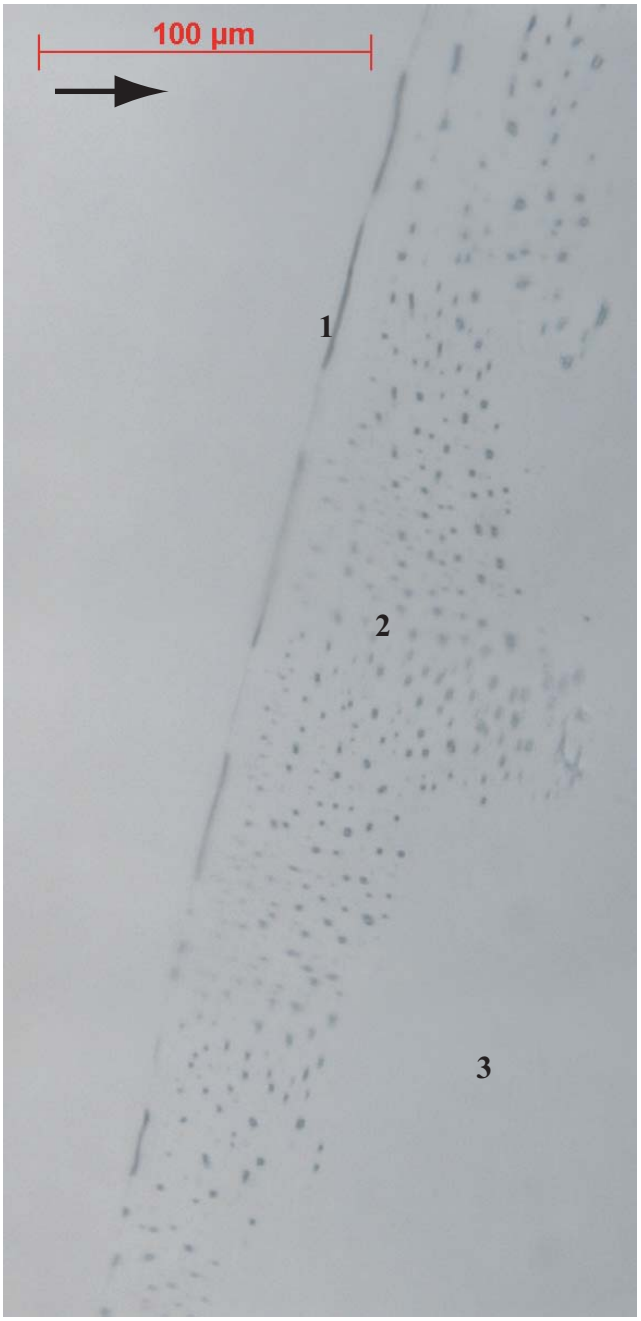

FIGURE 15. Quartz crack 2D#1 right (T = 400°C, t = 24 hrs, with distilled water) showing typical morphology of a healed crack near the tip (the r-plane is in the plane of the photograph). The black arrow shows the healing direction from the crack tip to the crack initiation point, where crack aperture is maximum. (1) Fluid filled tube. (2) Plane of fluid inclusions. (3) Healed patch without detectable fluid inclusions.

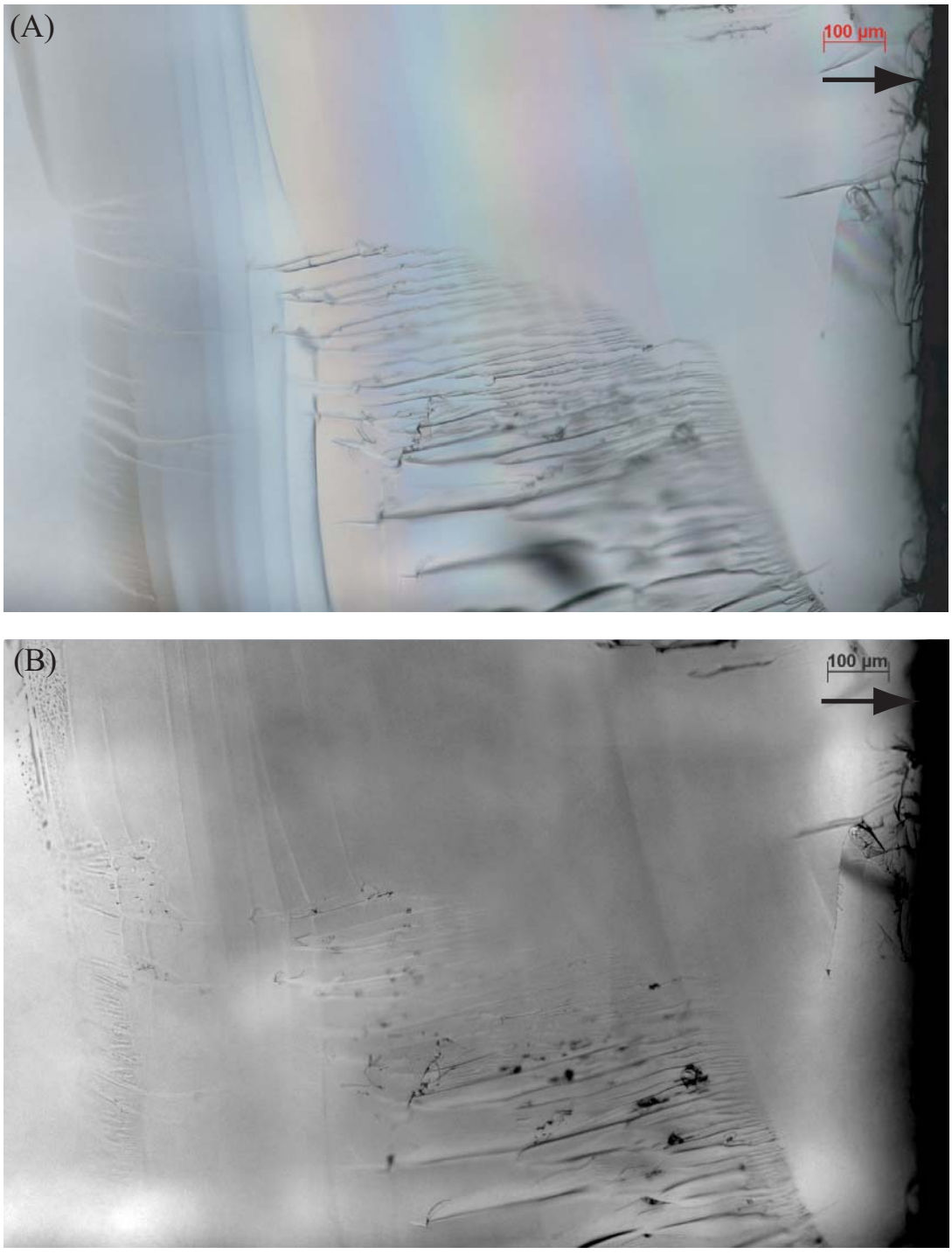

FIGURE 16. Quartz crack 3D#2 before and after healing at T= 400°C, t = 24 hrs, with distilled water, showing regions of smooth crack surface, and regions with hackle marks (r-plane in the plane of the photograph). The black arrows show the healing direction from the crack tip to the crack initiation point, where crack aperture is maximum. (A) Crack before hydrothermal annealing. (B) Crack after hydrothermal annealing.

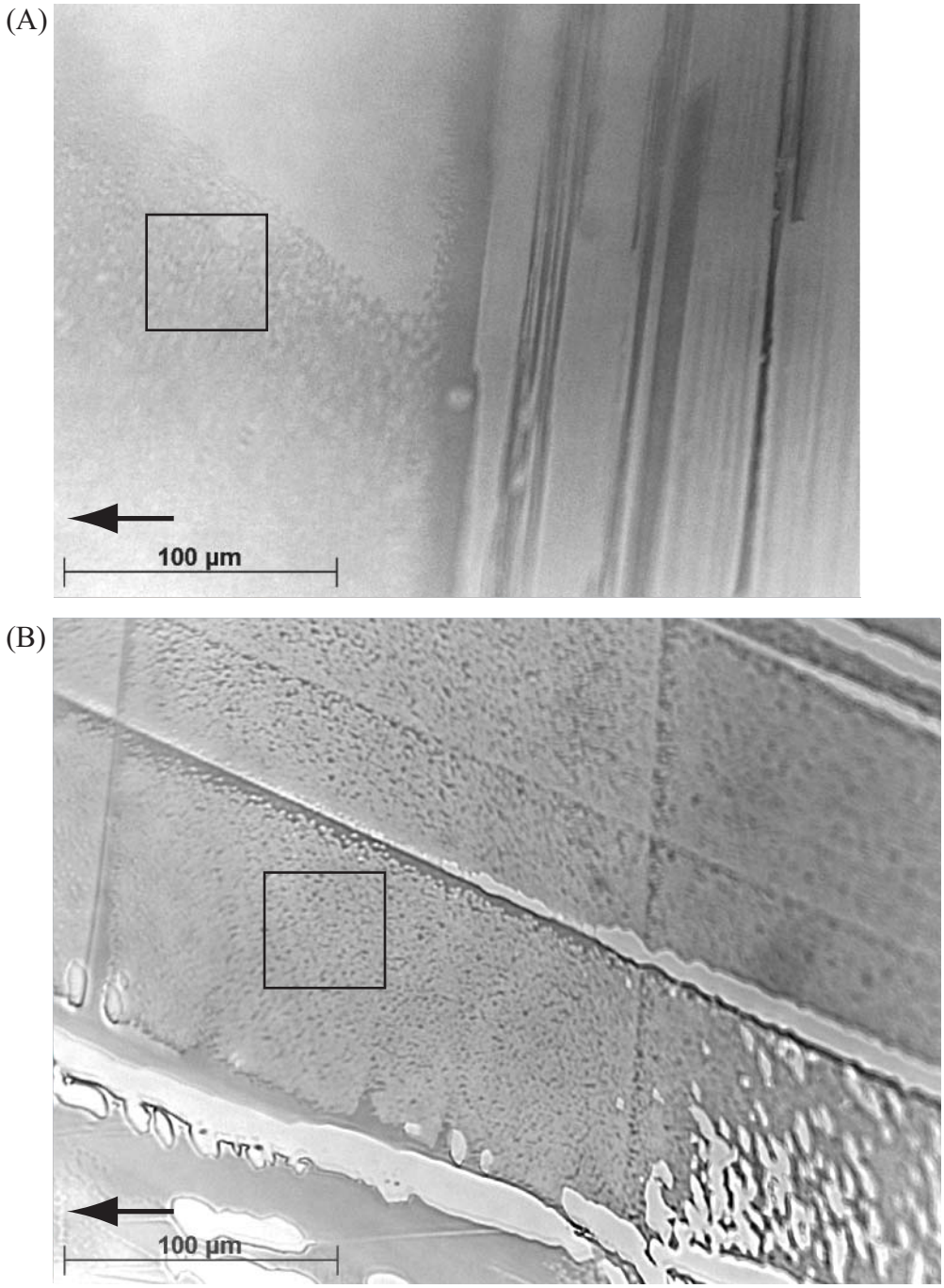

FIGURE 17. Alteration on the surfaces of open cracks after hydrothermal annealing. Surface pitting and roughening is associated with varying ammounts of dissolution and/or precipitation. (A) Quartz prism 2D#1,400°C, 24 hours, distilled water. Fluid filled tubes grade into healed and unhealed patches. Unhealed crack surface with alteration is highlighted in the black box. (B) Quartz prism 2F#2, 400°C, 24 hours, distilled water, showing altered surfaces of unhealed cracks (within box) and healed morphologies at hackles, as well as some isolated healed patches.

that cracks heal, unhealed surfaces of cracks are altered, both by dissolution and precipitation (FIGURE 17).

Healing of cracks during some hydrothermal annealing experiments was significant. The relatively smooth r-cleavage crack in 2D#1 left (T = 400°C, t = 24 hours, H_2O) shows large reductions in open crack area and crack aperture (FIGURE 18). The crack aperture profiles determined by interferometry before and after annealing show that significant crack closure (up to 90.7% of the original crack opening) occurred (FIGURE 19).

In contrast, some cracks show little or no evidence of crack healing. The branched rough cracks in sample 3F#1 (T = 400°C, t = 24 hours, H_2O) show only small reductions in crack surface area (FIGURE 20). This crack exhibits large numbers of well-developed, high-relief hackles prior to annealing, as well as subsidiary microcracks and debris, compared to the relatively smooth surface of the left crack in sample 2D#1. After annealing, fine, small aperture, subsidiary microcracks are healed, but the main large aperture crack shows little evidence of healing. Crack profiles before and after hydrothermal annealing show a reduction in aperture of only 22.8% (FIGURE 21), far less than that exhibited by the smoother crack in 2D#1.

3.3 Crack Closure and Dependence on Fracture Roughness

Many of the crack aperture profiles measured for r-cleavage cracks prior to annealing follow the hyperbolic form that Beeler and Hickman (2004) used to describe their cracks formed on the same plane of quartz. In their study of crack closure using in-situ interferometry measurements, Beeler and Hickman (2004) found that r-cleavage cracks close rapidly by up to 80% of the original crack apertures as temperature is raised. Thereafter, closure rates drop off, and crack apertures remain nearly constant. Cracks are thought to be held open by debris generated during cracking, and Beeler and

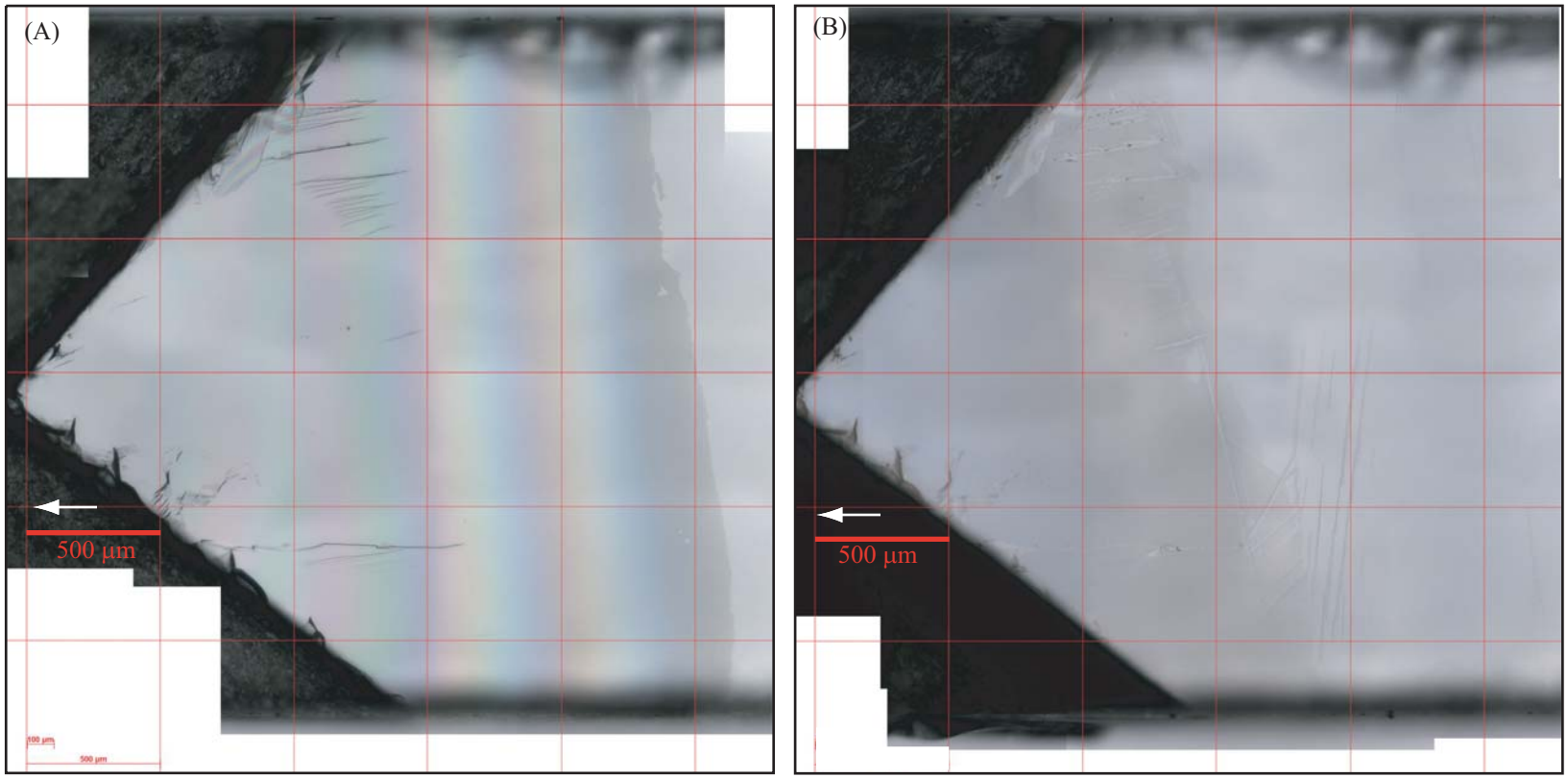

FIGURE 18. Crack 2D#1 left, with low relief hackles, shown before (A) and after (B) hydrothermally annealing the quartz prism at T = 400°C, t = 24 hours, in distilled water. Comparison of these photomontages and map

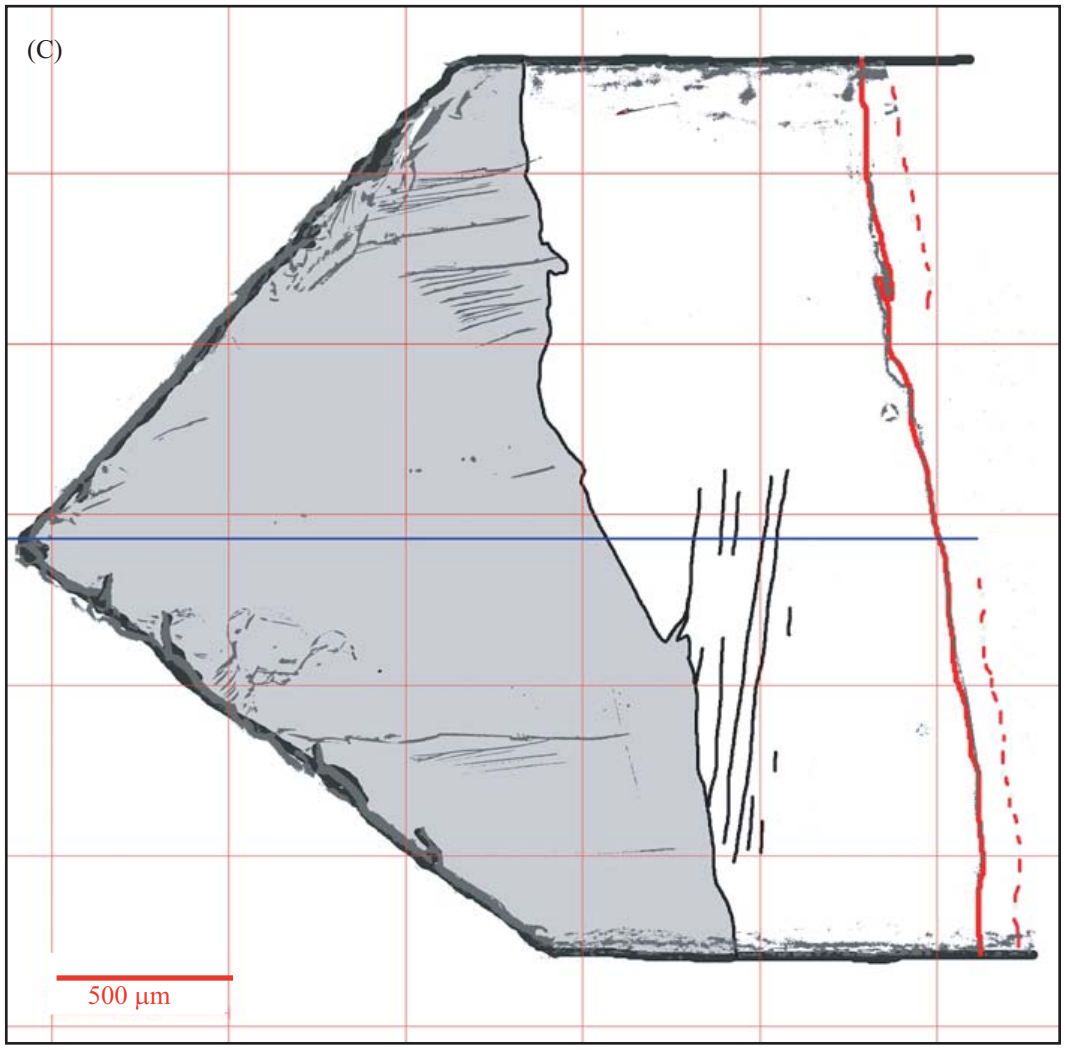

FIGURE 18, continued. (C) constructed from them shows significant regression of the crack tip and healing over a large crack area. The map also shows the location of fluid inclusion trails and hackles on the crack surface.

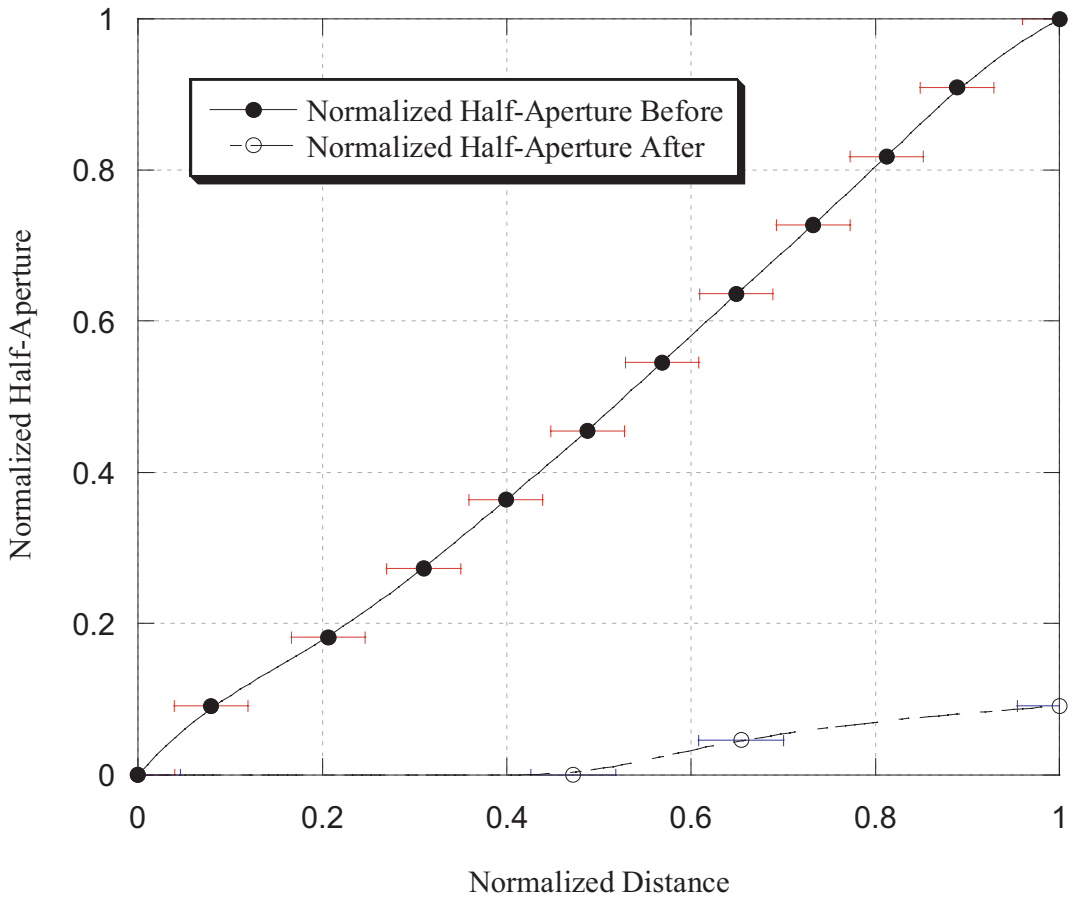

FIGURE 19. Profiles of crack aperture as a function of distance from the crack tip for Crack 2D#1 left (T = 400C, t = 24 hrs, in distilled water). The filled circles show normalized half aperture before hydrothermal annealing, while the open circles show the half aperture following hydrotherm annealing, normalized to the maximum aperture prior to annealing.

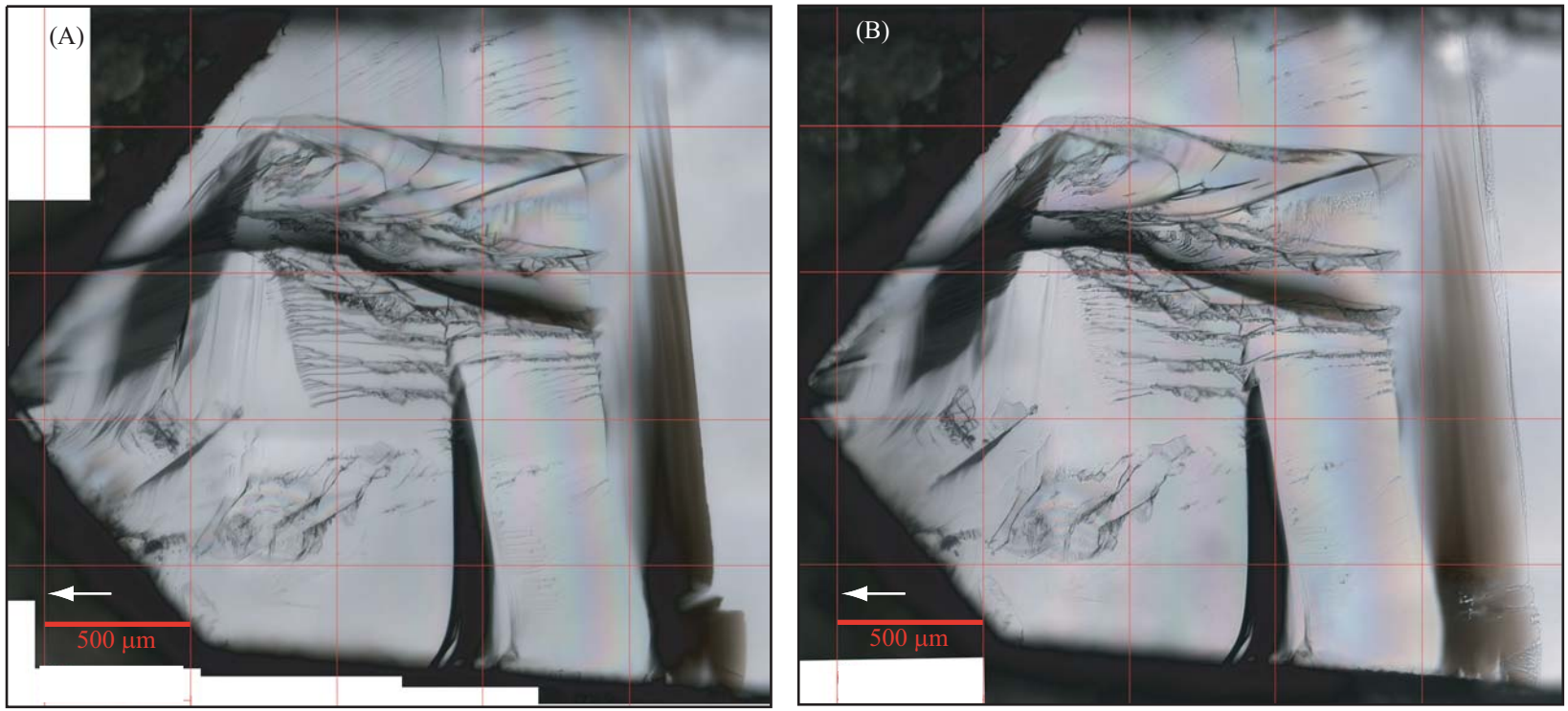

FIGURE 20. Crack 3F#1 left, with high relief hackles shown before (A) and after (B) hydrothermally annealing the quartz prism at T = 400°C, t = 24 hrs, in distilled water.

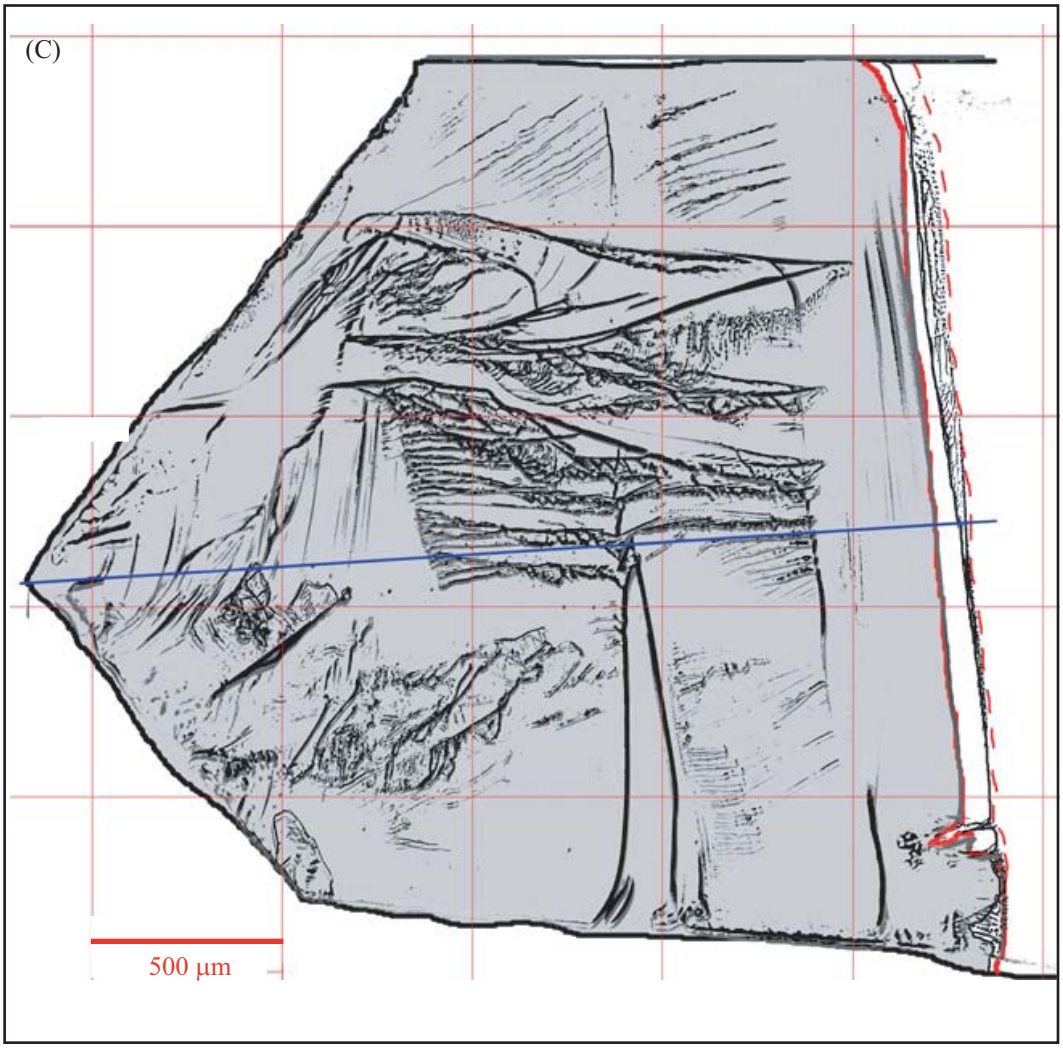

FIGURE 20, continued. Comparisons of these photo-montages and map (C) constructed from them shows only minor amounts of crack healing, primarily of fine, small aperture subsidiary cracks. Crack tip regression of the principal r-crack (which is rough and has a large aperture) is small. The map also shows hackles and branched cracks and the location of fluid inclusion trails and hackles.

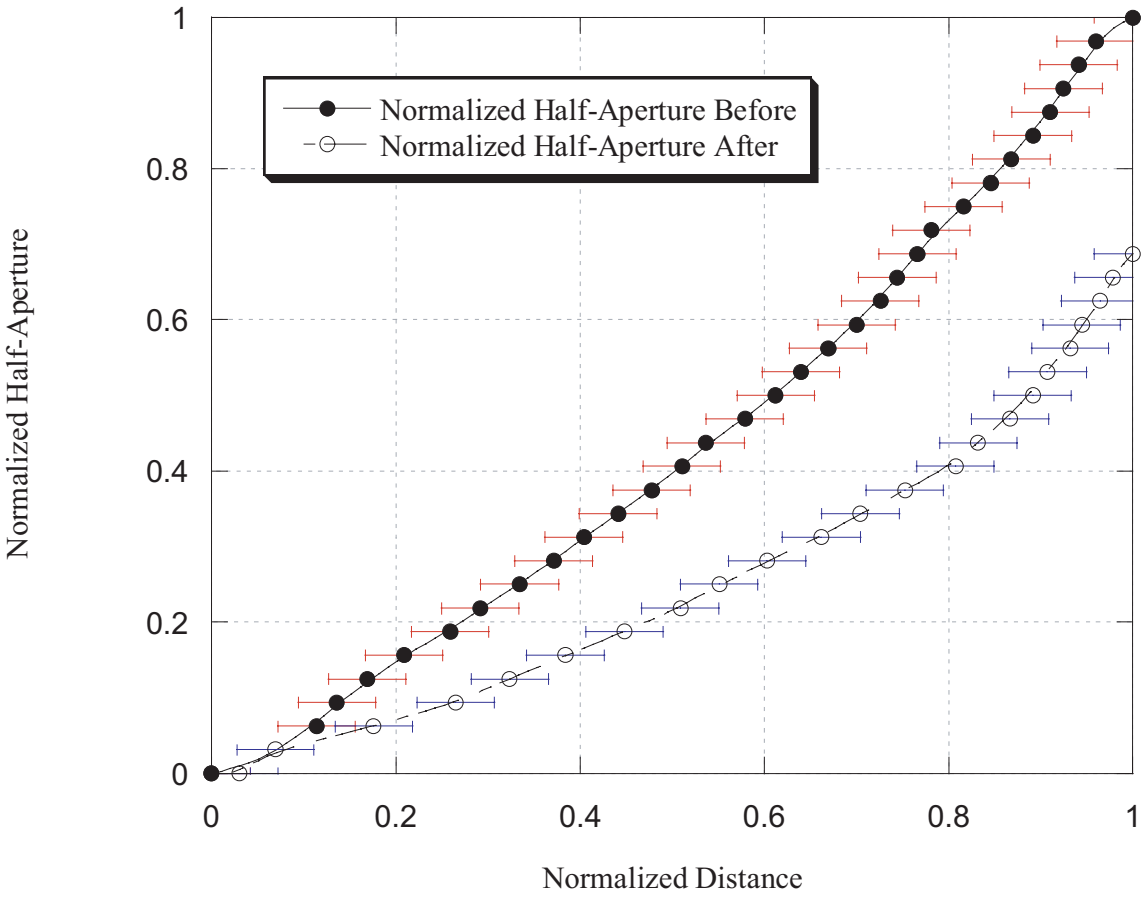

FIGURE 21. Profiles of crack aperture as a function of distance from the tip for Crack 3F#1 left (T = 400°C, t = 24 hrs, in distilled water). The filled circles show normalized half aperture before hydrothermal annealing, while the open circles show normalized half aperture following hydrothermal annealing, normalized to the maximum aperture prior to annealing.

Hickman (2004) modeled the observed crack closure by the dissolution of debris particles that prop the crack open. The reductions in crack aperture observed in these samples are similar in magnitude to those measured by Beeler and Hickman (2004) and thus, apertures determined in the annealed samples of this study reflect crack closure prior to crack healing.

The model of Beeler and Hickman (2004) suggests that the extent of crack closure scales regularly with total crack length for smooth cracks. However, measurements of crack aperture reduction of r-cracks annealed in this study suggest a dependence on crack roughness. Crack closure is greatest for smooth cracks with hackle magnitudes of 1, and smallest for rough cracks with hackle magnitudes of 3 (FIGURE 22). Large hackle magnitudes thus lead to crack apertures that are large prior to the crack healing process (FIGURE 23). Just as debris within cracks is thought to prop smooth cracks open (Beeler and Hickman, 2004), closure of rough cracks must also overcome points of contact at hackle marks and debris created during crack propagation.

3.4 Healing as a Function of Aperture

Crack healing kinetics depend on crack aperture through terms Λ and n in EQUATION 1 (Hickman and Evans, 1987) with high rates observed for small aperture cracks and low relative rates observed for large aperture cracks (Smith and Evans, 1984; Hickman and Evans, 1987; Brantley et al., 1990). Crack apertures at the onset of healing depend on the original aperture determined by interferometry before annealing and the extent of rapid crack closure once the experimental temperature is reached. Given that rough cracks show less closure than do smooth cracks (FIGURE 22), rough cracks are expected to have larger apertures and thus show less healing. The effect of crack aperture on extent of healing is illustrated by healed crack areas measured for partially healed cracks whose apertures at the experimental conditions can be estimated from

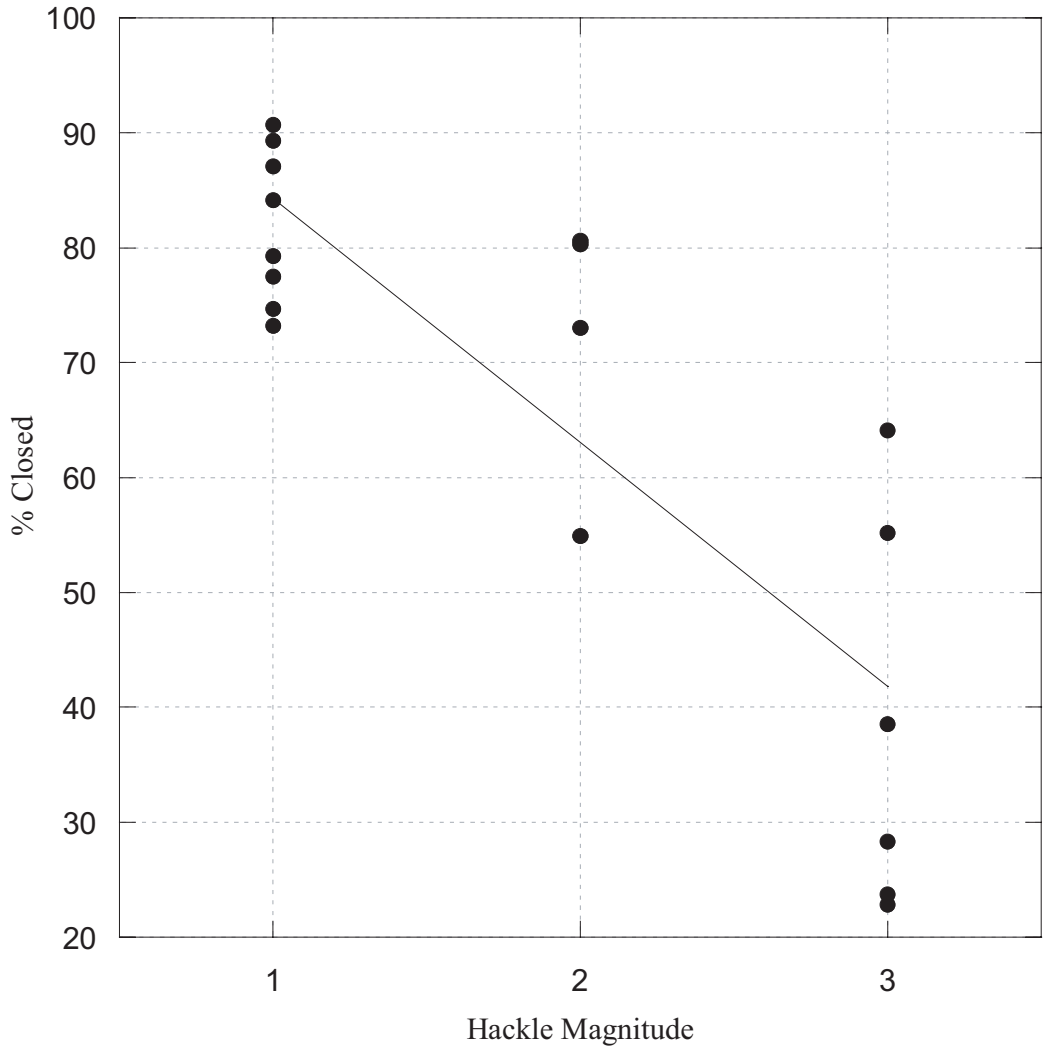

FIGURE 22. Crack closure determined by interferometry of cracks of differing roughness before and after annealing. Cracks were classified based on the largest magnitude hackle measured in the post experiment images. Crack closure data plotted here include measurements for experiments at all annealing times, temperatures, and fluids.

fringes imaged at the end of the prisms following the annealing experiments (FIGURE 23).

3.5 Healing as a Function of Crack Roughness

Close examination of open and healed cracks shows that hackle marks and crack branching do not result in uniformly large crack apertures, and that healing is highly localized. Crack healing for relatively smooth r-cleavage cracks with small relief hackle marks, such as observed in quartz prism 2F#2, show enhanced healing at hackle marks with only few visible fluid inclusions, while the smooth, slightly larger aperture crack between hackle marks healed by the formation of large numbers of fluid inclusions (FIGURE 24).

Significant crack healing is observed at hackle marks far in advance of the healing crack front between hackles (FIGURE 24, 25) where bridges of precipitated quartz prevent any further closure of the remaining open crack. Crack surfaces between healed hackle marks show some evidence of precipitation but pitted surfaces (FIGURE 24, 25) also suggest significant dissolution at these surfaces. Where hackle marks form river patterns, localized healing leads to branched quartz bridges (FIGURE 26) surrounded by open, unhealed crack. Despite the smoothness of the open crack, remaining apertures can not be reduced by closure once the quartz bridges form and they are too large for significant healing in these experimental times.

Hackle marks most commonly nucleate localized healing. However, often the relationship between hackles and the bulk crack is complex, with healed and unhealed fingers protruding from the healed crack front. In some cases, the healing crack front progresses further in the smooth regions between hackles, and leaves the hackles as unhealed tubes, or partially healed tubes that have necked down into fluid inclusions (FIGURE 27).

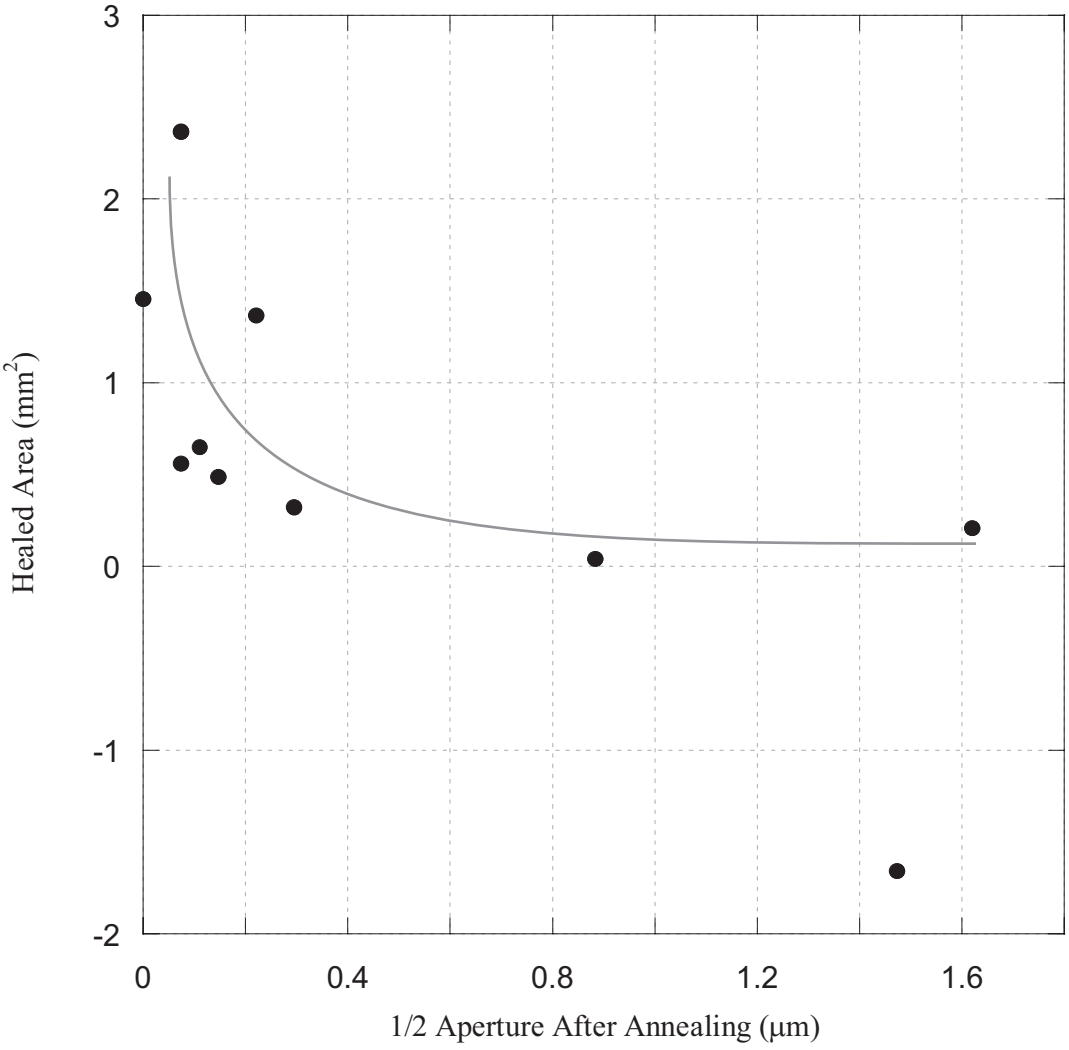

FIGURE 23. Healed area vs. maximum half-aperture at the quartz prism end. Results plotted for samples annealed at 400°C for 24 hours with distilled water as pore fluid.

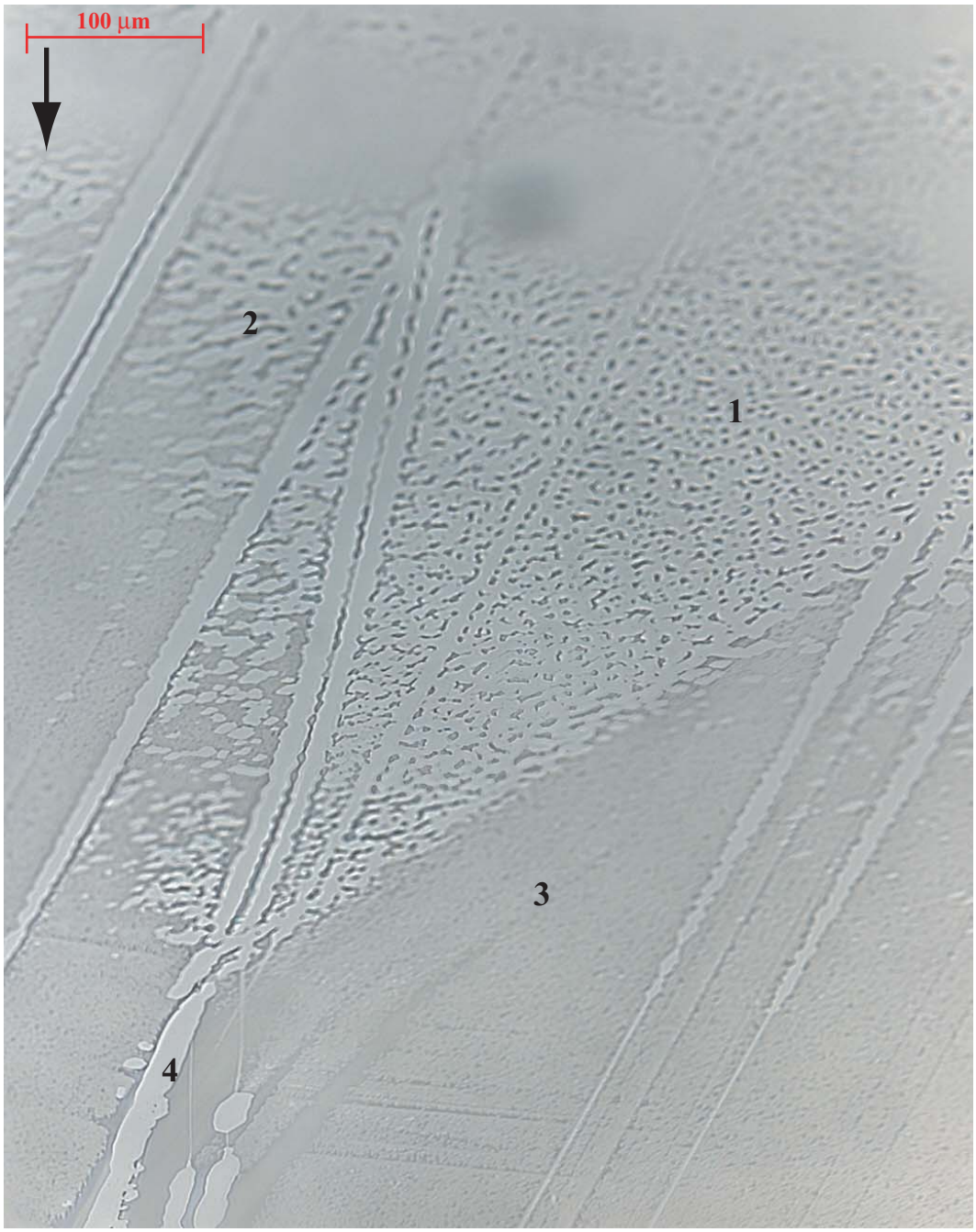

FIGURE 24. Healed crack morphologies developed at 400°C, 24 hours with distilled water (sample 2F#2) driven by surface energy for relatively smooth r-crack with small relief hackle marks. The arrow indicates the healing direction, from the crack tip to the crack initiation point. (1) Healed region with angular fluid inclusions. (2) Region where partially healed patches have coelesced to form irregularly shaped fluid inclusions. (3) Unhealed region with altered surface. (4) Quartz bridge formed by enhanced crack healing at low relief hackle mark.

FIGURE 25. Quartz bridges formed by enhanced healing of quartz at fine-scale hackle marks in quartz prism 2F#2, (annealed at 400°C for 24 hours in distilled water). The black arrow shows healing direction from the crack tip to the crack initiation point. (1) Healed hackle mark. (2) Altered crack surface with little evidence of healing.

FIGURE 26. Branched quartz bridges formed by enhanced healing of quartz at hackle marks forming a river pattern in quartz prism 2F#2 (annealed at 400°C, 24 hours, with distilled water). The healing direction, from the crack tip to the crack initiation point is shown by the black arrow. (1) A healed hackle mark. (2) Open crack with altered surface. (3) Open crack with less altered surface. (4) Fine scale river pattern that has not healed in the experimental time. (5) Microcrack that formed at a high angle to the r-plane after the start of the experiment.

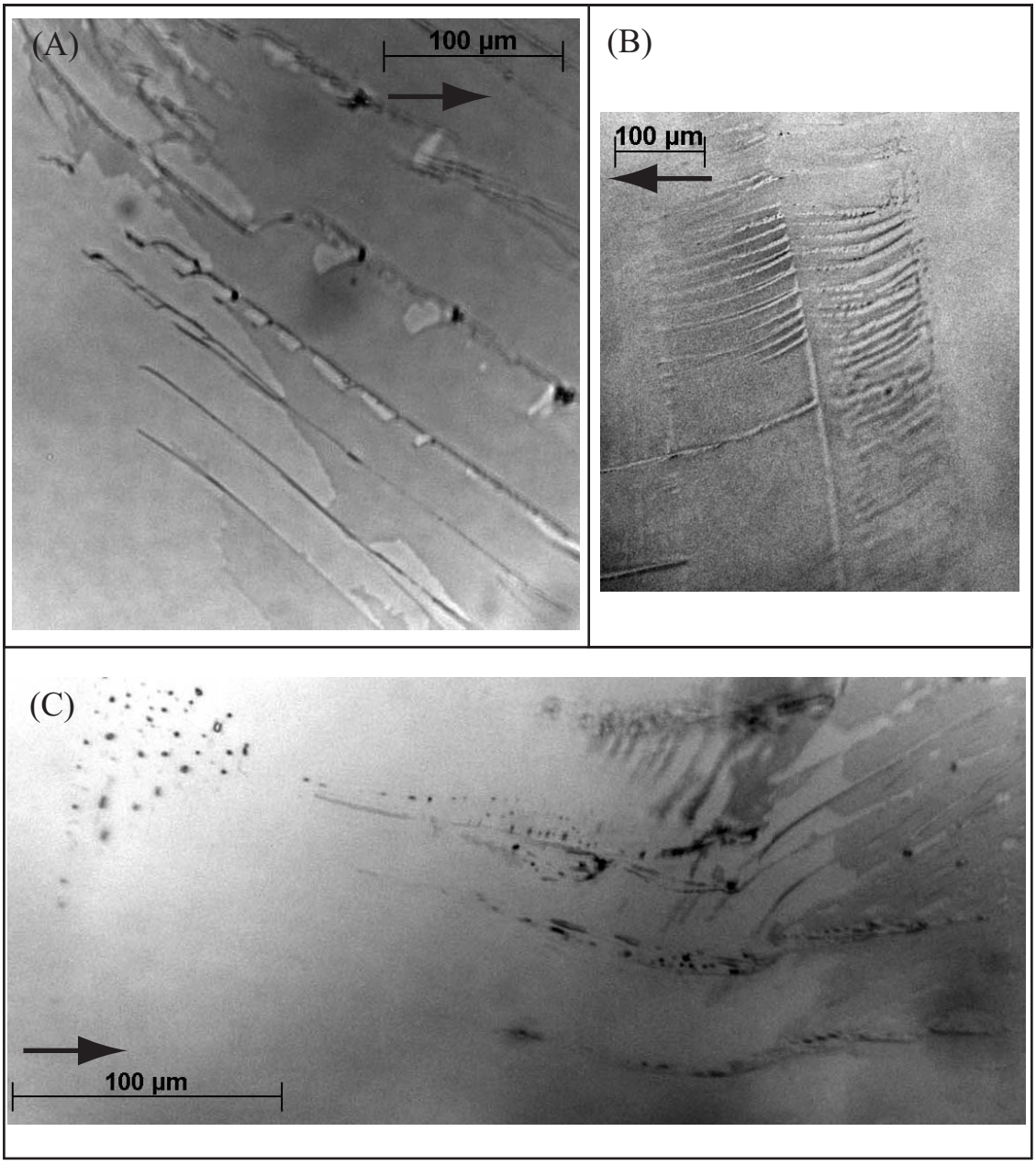

FIGURE 27. Healed morphologies showing hackles that heal less readily than the surrounding crack surfaces. The black arrows show healing directions from the crack tip to the crack initiation point. (A) Quartz prism 2B#1 (annealed at 250°C for 24 hours in distilled water). Unhealed hackles extend into healed quartz while healing is seen to simultaneously initiate at points along hackles. (B) Quartz prism 3E#2 (annealed at 400°C for 24 hours in distilled water). Hackles create healed protrusions into the open crack, interfingered with unhealed tubes extending into healed quartz. (C) Quartz prism 2D#1 (right crack) showing hackle marks which remain unhealed, extending into healed quartz as tubes, or tubes which have broken up into fluid inclusions.

Rough cracks with large hackle magnitudes typically have large crack apertures and show significant crack branching. Microstructural evidence of healing is largely absent for these large aperture cracks, yet evidence of healing is observed for the fine subsidiary cracks associated with these rough cracks. Fine subsidiary cracks exhibit precipitated quartz bridges (FIGURE 28) and fully healed subsidiary cracks are decorated by fluid inclusions (FIGURE 29). While the coarse rough cracks show little or no healing, fine subsidiary cracks that branch out from the primary crack show well-formed fluid-filled tubes and fluid inclusions (FIGURES 30 and 31).

The results of interferometry before and after annealing and observations of healed crack morphologies thus indicate that hackle marks and crack roughness limit crack healing in two ways. First, hackles and crack roughness limit crack closure prior to healing, maintaining large average crack apertures. Second, rapid healing at hackle marks, where apertures are locally small, leads to precipitated quartz bridges that prevent any further reductions in crack aperture of the remaining crack and thus limit further crack healing. As a result, healed crack areas show a strong dependence on crack roughness, as characterized by hackle magnitude (FIGURE 32).

3.6 Healing as a Function of Time

Rates of crack healing vary widely for different quartz prisms, even if results are compared for smooth cracks annealed at the same temperature in the same fluid. Maximum and minimum healing rates for smooth (hackle magnitude of 1), small aperture r-cleavage cracks vary from 2.74×10^{-5} mm/s to 3.17×10^{-6} mm/s, based on total healed areas measured, over the total annealing time. Maximum and minimum healing rates for moderately rough (hackle magnitudes of 2 and 3) cracks of intermediate aperture vary from 5.51×10^{-5} to 4.83×10^{-7} mm/s, and some rough cracks (hackle magnitude 3) show no evidence of healing in the experimental annealing times. Average crack healing rates determined for any given temperature, crack roughness, or fluid tend

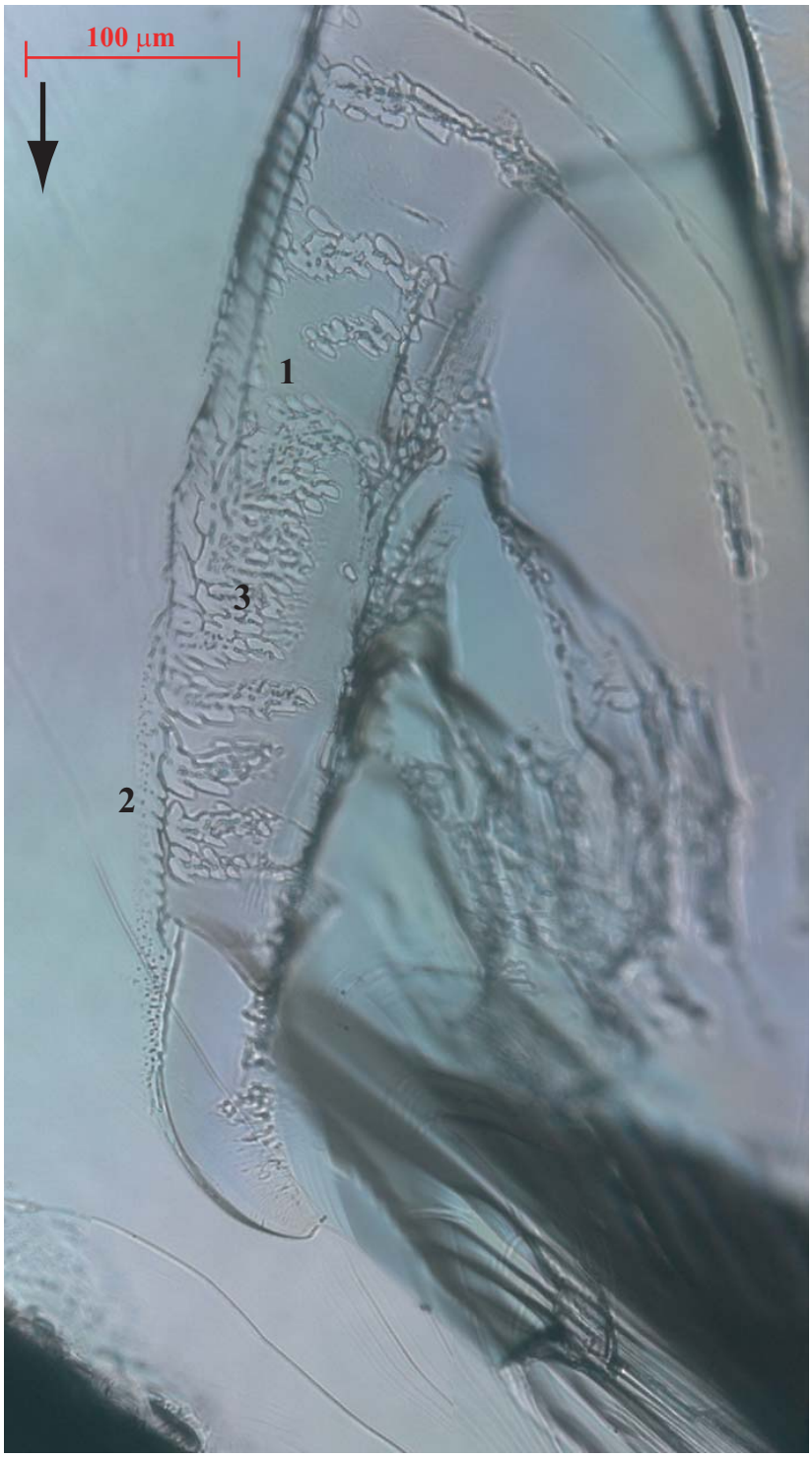

FIGURE 28. Quartz Prism 3F#1, annealed at 400°C for 24 hours with distilled water as a pore fluid. The black arrow shows the healing direction from the crack tip to the crack initiation point. (1) Large microcrack underlying the plane of the primary unhealed crack. (2) Fluid inclusion trails formed from the tip of the very thin microcrack. (3) Healing by the formation of quartz bridges across a fine microcrack is in sharp contrast to the lack of evidence for healing of the large-aperture primary crack.

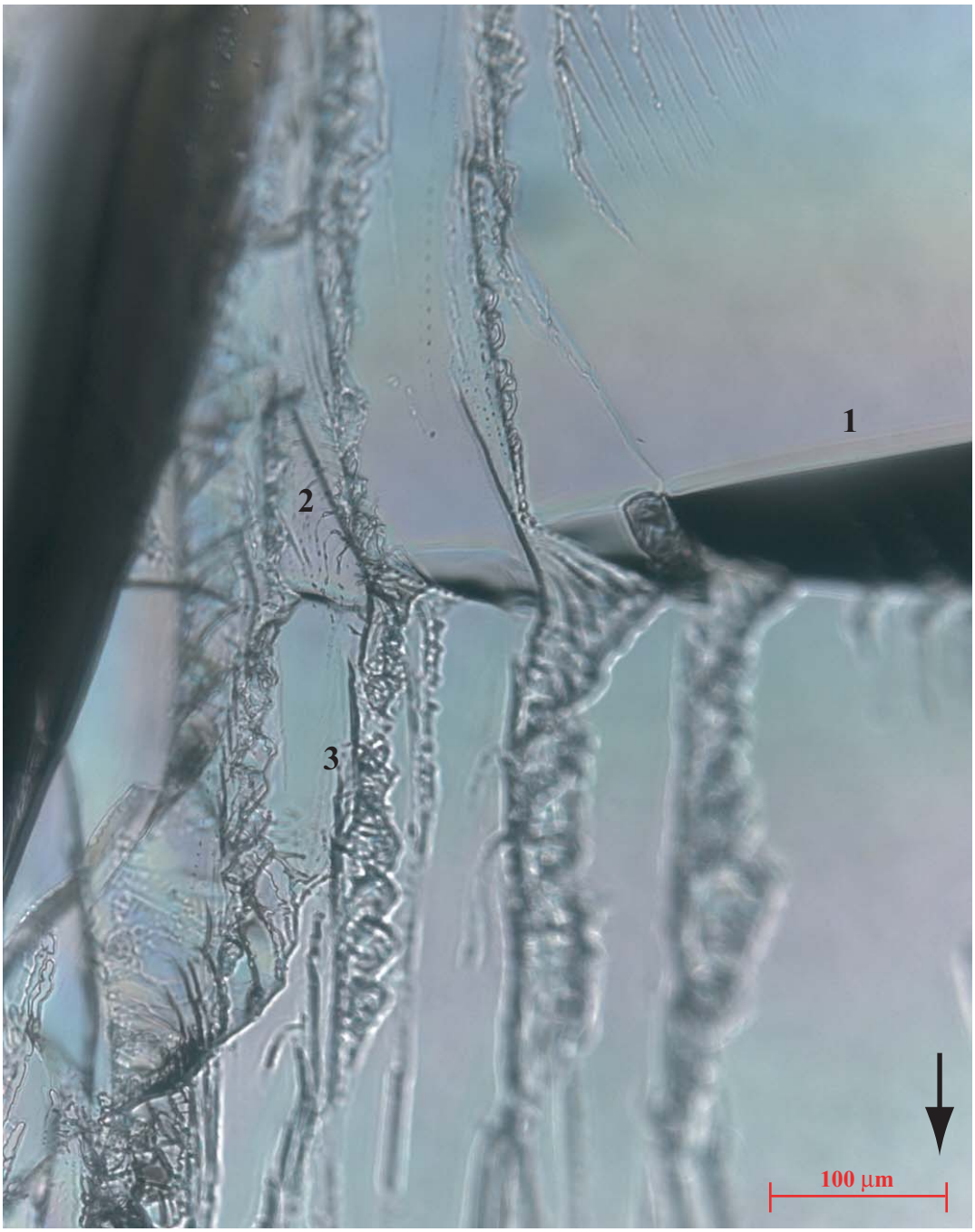

FIGURE 29. Quartz Prism 3F#1, annealed at 400°C for 24 hours, with distilled water as pore fluid. The black arrow shows the healing direction from the crack tip to the crack initiation point. (1) Large fracture step. (2) Fully healed subsidiary microcrack decorated by fluid inclusions. Almost no healing is observed for the principal large-aperture crack. (3) Complex hackles and branched cracks.

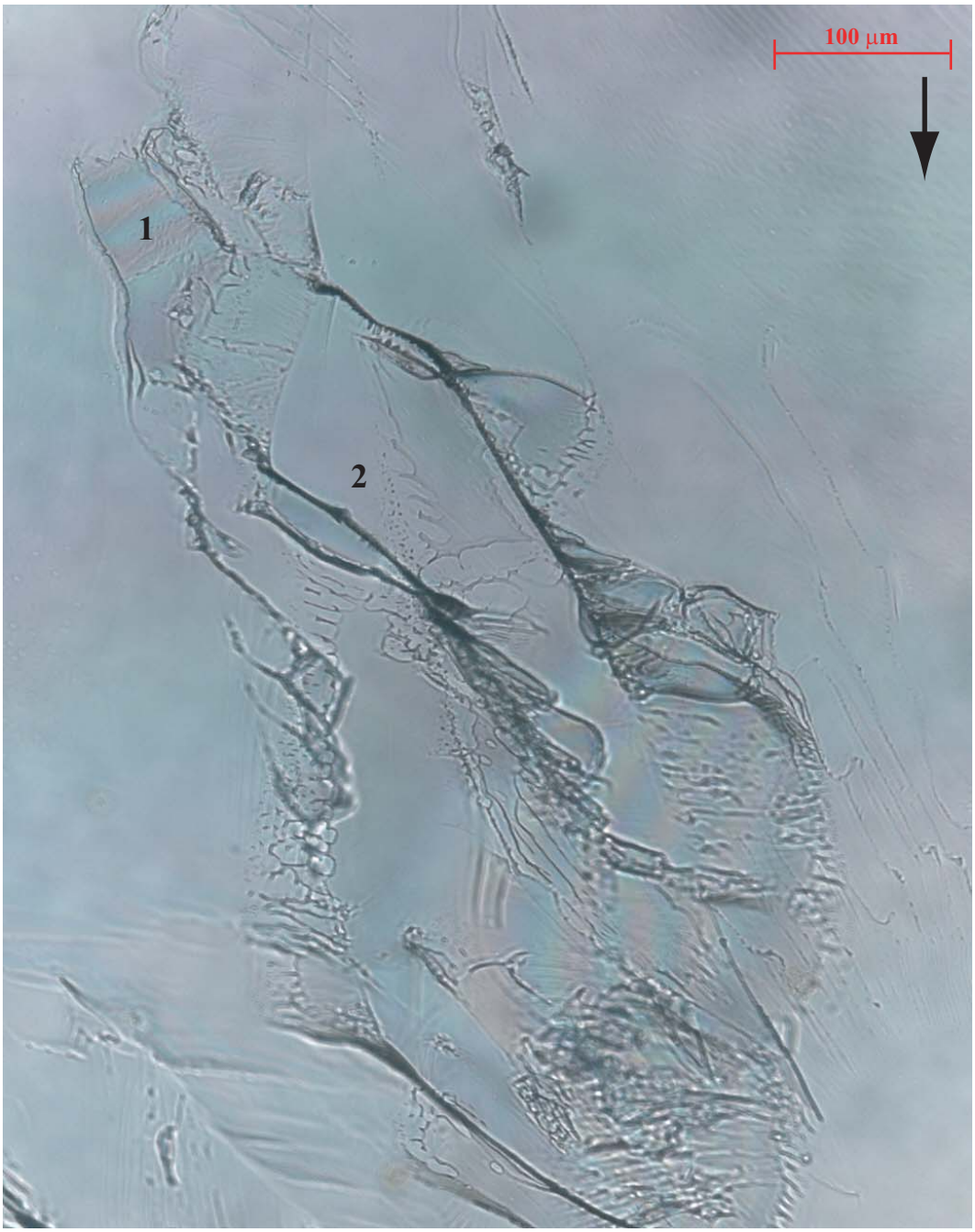

FIGURE 30. Healing of branched microcracks in quartz prism 3F#1, annealed at 400°C for 24 hours with distilled water as a pore fluid. The black arrow shows the healing direction from the crack tip to the crack initiation point. (1) Unhealed microcrack out of the plane of the main r-crack. (2) Partially healed microcracks with fluid inclusion trails, out of the plane of the main, unhealed, crack.

FIGURE 31. Healing of branched cracks in quartz prism 3F#1, annealed at 400°C for 24 hours with distilled water as a pore fluid. The black arrow shows healing direction from the crack tip to the crack initiation point. (1) Large partially healed microcrack out of plane of the main r-crack. The main r-crack is parallel to the photograph, and shows little to no healing. (2) Fluid-filled tubes and fluid inclusion trails formed at the microcrack tip. (3) Healed patches in the transition from healed quartz with fluid inclusions to open crack. (4) High angle microcrack intersecting both the main crack and the partially healed microcrack.

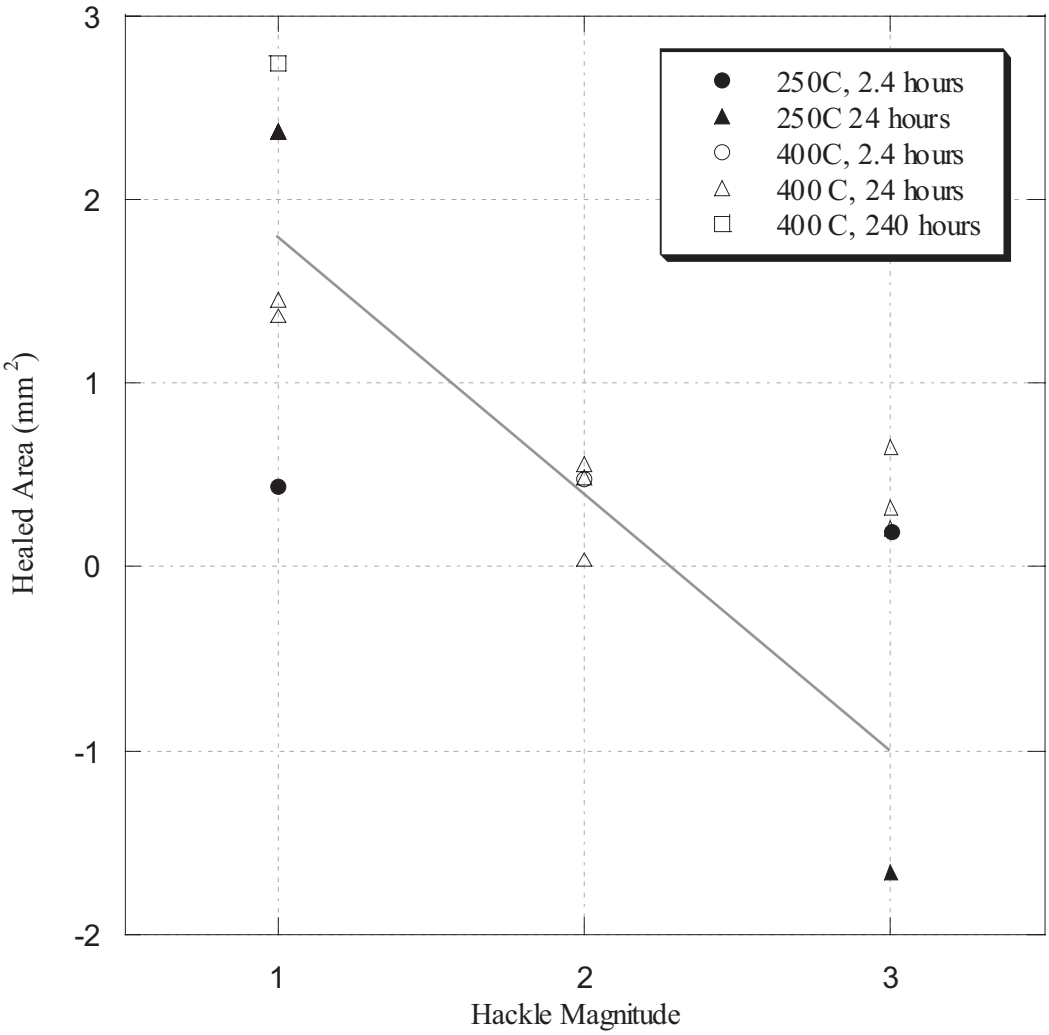

FIGURE 32. Healed area vs hackle magnitude for cracks hydrothermally annealed at T = 250°C and 400°C over periods from 2.4 to 240 hours. Cracks were classified based on the largest magnitude hackle measured. The data shown are for distilled water experiments only.

to be higher for cracks annealed for short times than those annealed over longer time intervals. This suggests that healing progresses rapidly initially, and slows down as the crack tip recedes. Reductions in healing rate of an individual crack are generally consistent with the dependence of crack healing on aperture, a hyperbolic crack aperture profile (EQUATION 2, Beeler and Hickman, 2004), and the form of EQUATION 1 if $n<1$.

Without in-situ observations of receding crack tips during an individual annealing experiment, it is difficult to evaluate variations in rate with aperture. It is also difficult to test how well EQUATION 1 fits the measured healing rates. Nevertheless, if results are selected for r-cracks that were hydrothermally annealed for periods of 2.4, 24, and 240 hours at T = 400°C in distilled water, the time dependence of healing can be described by EQUATION 1 (FIGURE 33) by plotting the log (healed area) versus log (annealing time). The slope of the healing data, recast in these terms, yields the exponent n in EQUATION 1;

$$n = \frac{\Delta \log \left| a - a_0 \right|}{\Delta \log t} \tag{4}$$

where crack areas a and a_0 are in mm^2, time is in seconds, and crack areas before and after healing are assumed to scale with crack length (ie., assuming one-dimensional healing, plotting log $a-a_0$ rather than log $|L-L_0|$ shifts the intercept in FIGURE 33 by the log of the prism width, but does not affect the slope). The value of n depends on crack geometry (Hickman and Evans, 1987), and data for cracks of differing roughness yield differing n values; n = 0.21 (+0.09 -0.15) for smooth cracks (hackle magnitude 1) and n = 0.04 (+/- 0.03) for moderately rough (hackle magnitude 2) cracks. The value of n determined for smooth cracks in this study compares favorably with the range of n values found by Brantley et al., (1990).

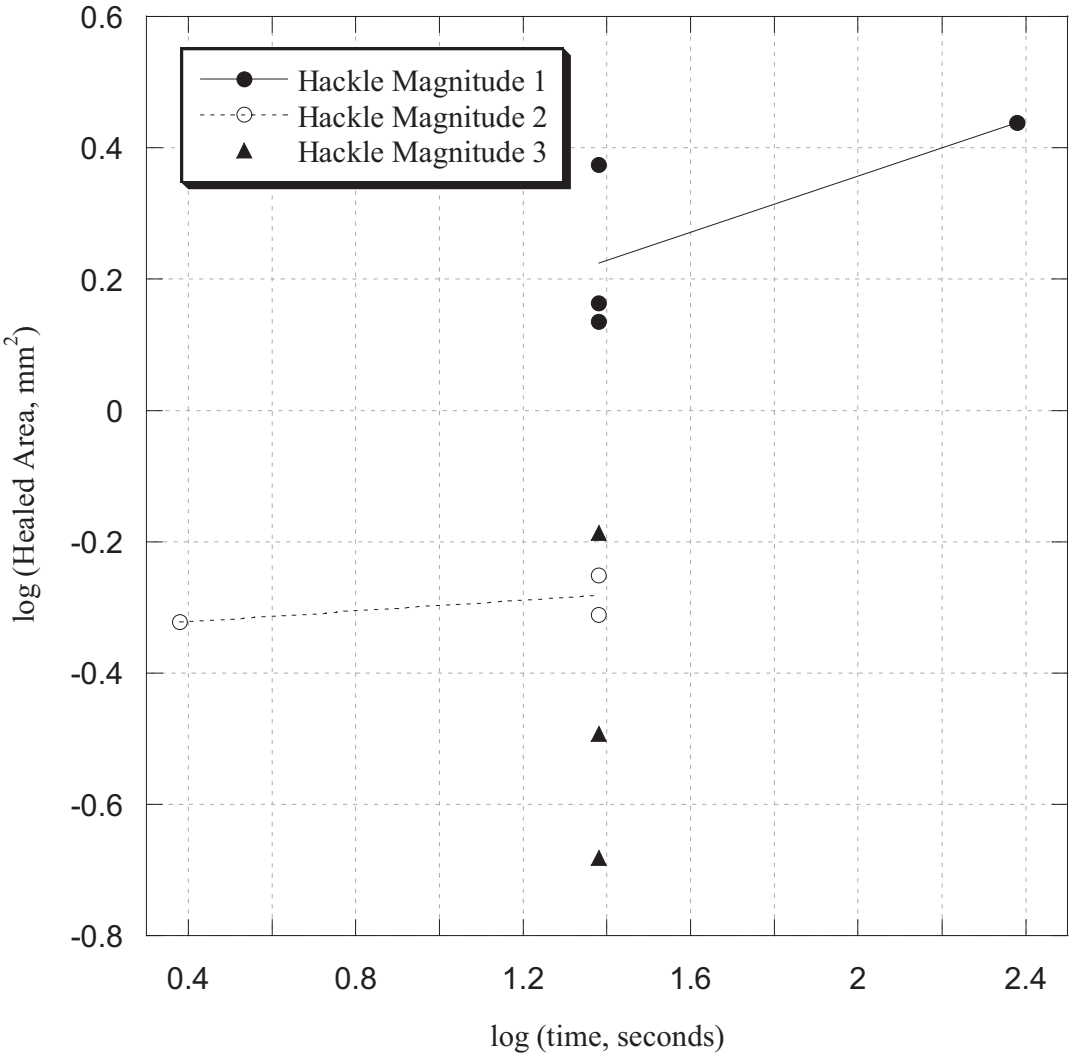

FIGURE 33. Log a-a_0 where a is the crack area after healing, and a_0 is the initial area vs. annealing log(time, in seconds) for quartz prisms annealed at T = 400°C in distilled water for different time durations. Assuming that crack growth is one dimensional with crack tips receding parallel to the long dimension of the prism, the slope of data in terms of log a-a_0 vs log t and log L-L_0 vs log t have the same slope n (eqn. 1).

3.7 Healing as a Function of Temperature

Diffusional crack healing is expected to depend on temperature through an Arrhenius term (EQUATION 1), and previous results for quartz suggest an effective activation energy for healing of 80 kJ/mol (Brantley et al. 1990). While the healed crack areas of samples annealed at T = 250°C and 400°C show too much scatter to determine an activation energy (FIGURE 34), the data can be compared with the temperature dependencies reported by Brantley et al. (1990). Recasting the data for cracks annealed in distilled water as log of healed area (log $|a-a_0|$) versus 1/T, where T is absolute temperature in Kelvin (FIGURE 34), the temperature dependence of EQUATION 1 can be expressed as:

$$\left(\frac{-nQ}{2.303R}\right)=\frac{\Delta \log\left|a-a_0\right|}{\Delta(1/T)} \qquad (5)$$

Scatter in healing data for cracks of varying aperture and roughness is large, and Q cannot be determined. However, the data can be compared with a slope (shown in FIGURE 34) defined by an activation energy Q = 80 kJ/mol determined for quartz crack healing by Brantley et al. (1990) and the value of n = 0.21 determined in this study for smooth cracks.

The character of cracks healed at T = 250°C and T = 400°C differs qualitatively. Cracks healed at 400°C (FIGURE 35) form numerous fluid inclusion trails made up of fluid filled tubes and more equant fluid inclusions, much as observed by Smith and Evans, (1984); Brantley et al., (1990); Brantley, (1992); and Beeler and Hickman, (1996). In contrast, cracks healed at 250°C appear to regress uniformly from the crack tip, without producing large numbers of fluid inclusions (FIGURE 36). This is evident even when hackles are present at crack surfaces. The blunting of crack tips and other processes that result in fluid inclusions at 400°C are characteristic of local healing and dissolution

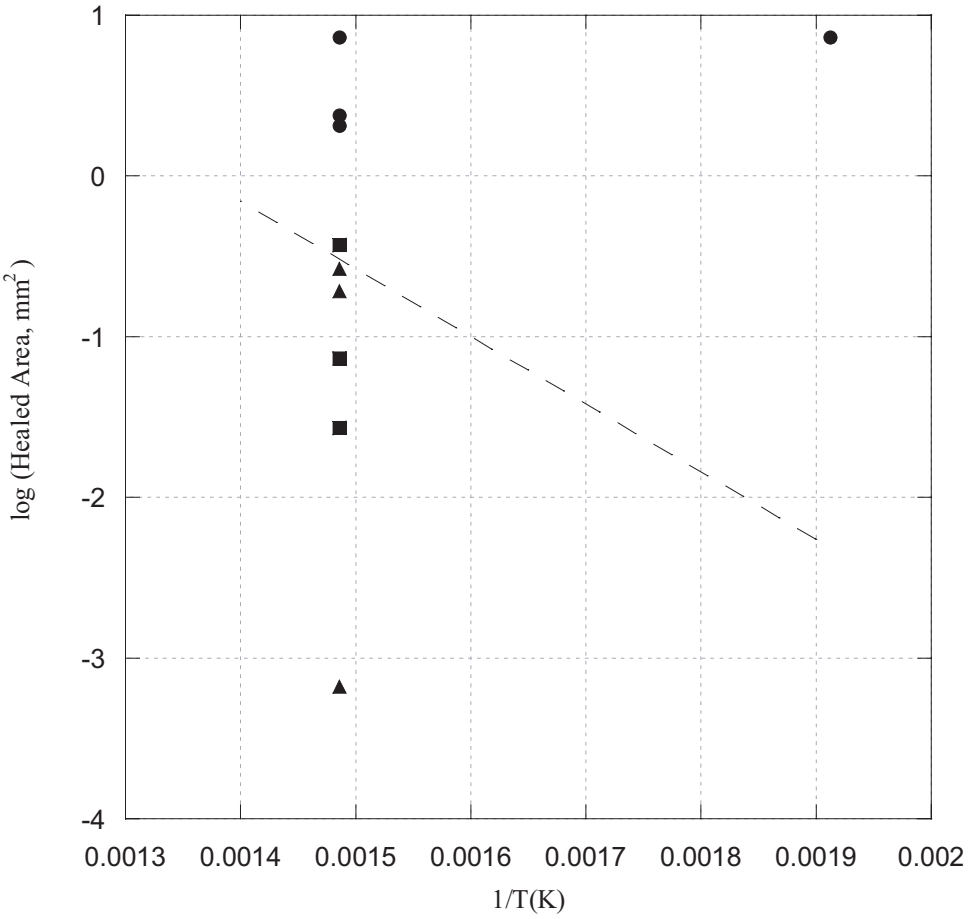

FIGURE 34. Extent of crack healing of r-cracks in quartz, as a function of temperature, shown as log $a-a_0$ versus 1/T where healed areas are in mm^2 and T is in Kelvin. Results are compared with a reference line given by the activation energy Q = 80 kJ/mol for crack healing in quartz reported by Brantley (1990) and n = 0.21 determined for smooth cracks in this study. Data are shown for 24 hour annealing experiments with distilled water.

(A)

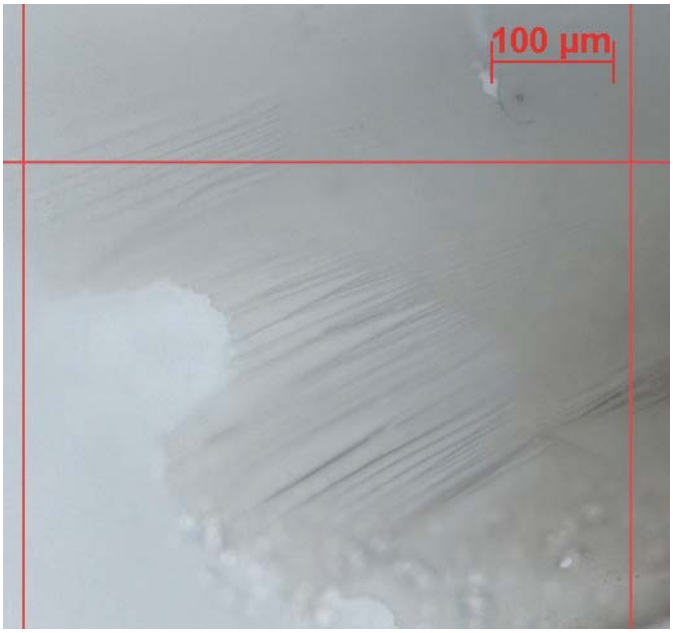

(B)

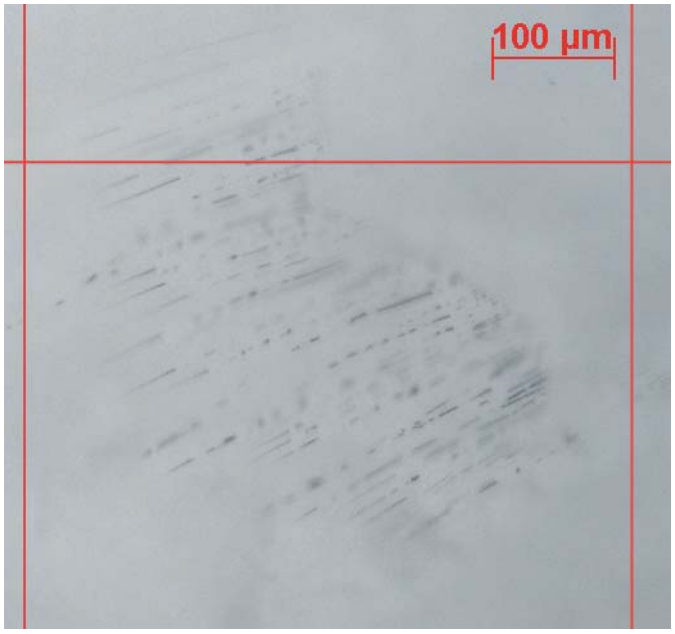

FIGURE 35. Fracture morphologies of a r-crack with fine hackle marks (A) before and (B) after annealing in distilled water at T = 400°C, t = 24 hrs (quartz prism 2A#2). Crack healing at T = 400°C typically results in numerous fluid inclusions decorating the former crack plane.

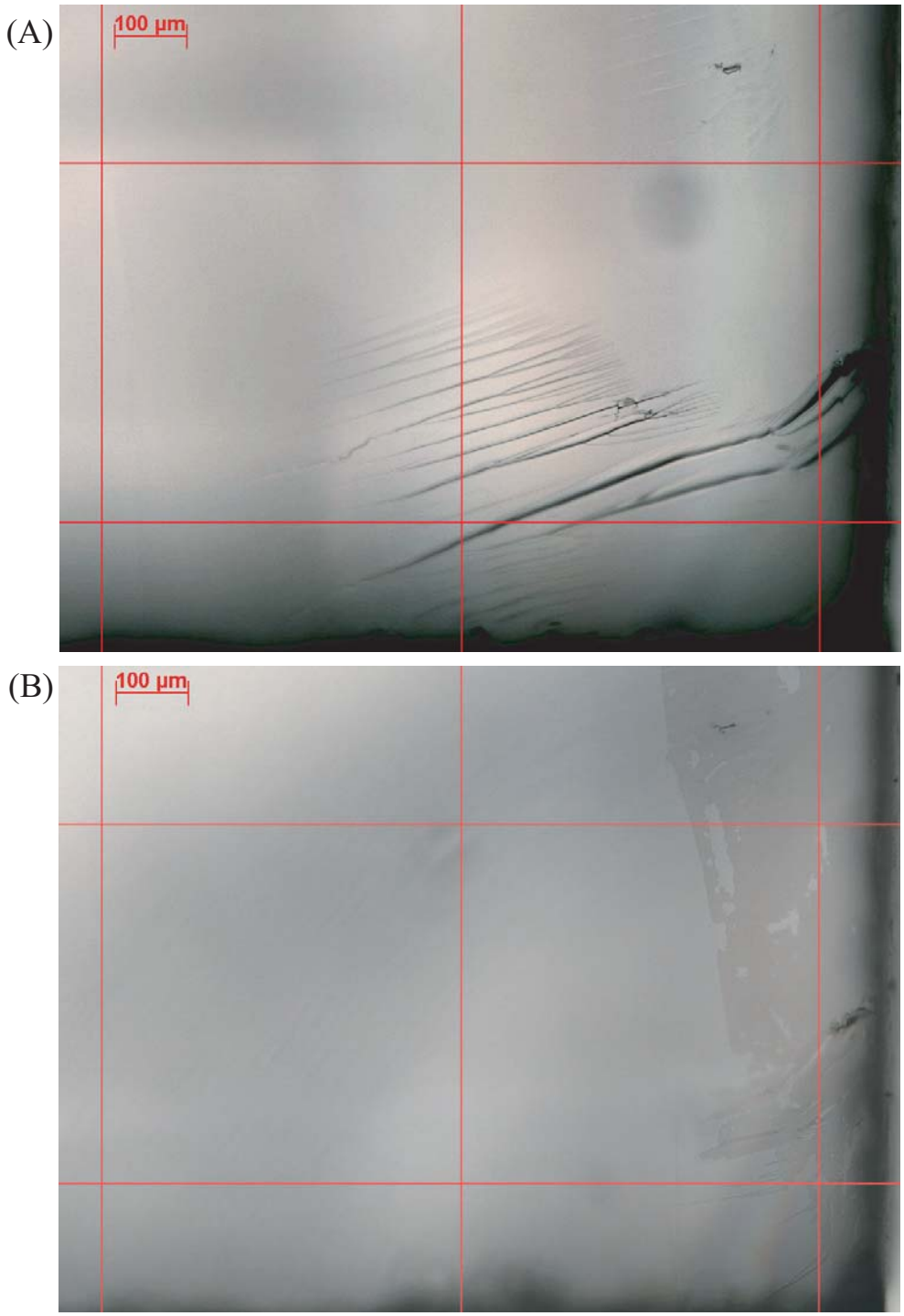

FIGURE 36. Morphologies of a r-crack with fine hackle marks (A) before and (B) after annealing in distilled water at T = 250°C (quartz prism 2B#1). Crack healing at T = 250°C typically leaves behind few fluid inclusions by comparison with those formed at T = 400°C. Note larger isolated patches of healed quartz ahead of the relatively sharp, receding crack tip.

where rates of healing are limited by rates of diffusion of solute over small characteristic distances (Nichols and Mullins, 1965; Evans and Charles, 1977, Hickman and Evans, 1987). The transition in healed crack morphology from T = 400°C to T = 250°C may thus correspond to a change in the rate-limiting mechanism, with diffusion limiting the rate of healing at T = 400°C, while dissolution or precipitation limits the healing rate at T = 250°C.

3.8 Healing as a Function of pOH^- and Quartz Solubility

Results for quartz prisms annealed at T = 250°C, P_f = 41 MPa and t = 2.4 and 24 hours reveal a significant dependence of crack healing on pOH^-, with larger areas healed for cracks annealed in NaOH solutions than for those annealed in water. Given that quartz solubility depends on NaOH concentration, healed areas may be larger at high NaOH concentration because of the silica concentration in solution. Taking solubilities reported by Simonson et al., (1989) for the NaOH solutions used in this study and for distilled water, healed areas are plotted as a function of silica concentration (FIGURE 37).

The processes of silica dissolution, diffusion and precipitation result in similar morphologies of cracks healed in distilled water and NaOH solutions with molalities up to 0.5m. Fully healed cracks may be decorated by fluid inclusions, but hackles are not visible where inclusions are absent and the precipitated quartz is optically continuous with the rest of the quartz prism (FIGURES 35, 36). Morphologies of the cracks annealed in 1.0m NaOH solution (pOH^- 1.18, experiment 2A#6) are significantly different from those that were annealed at pOH^- of 5.94 to 1.34. Fluid inclusions are sheet-like and the healed crack front is highly irregular (FIGURE 38). Where the crack has been healed, hackle marks are faint but optically detectable and the precipitated silica exhibits dendritic structures that are birefringent. Visible traces of hackles in the precipitated crack regions and the non-crystalline dendrites suggest that the material

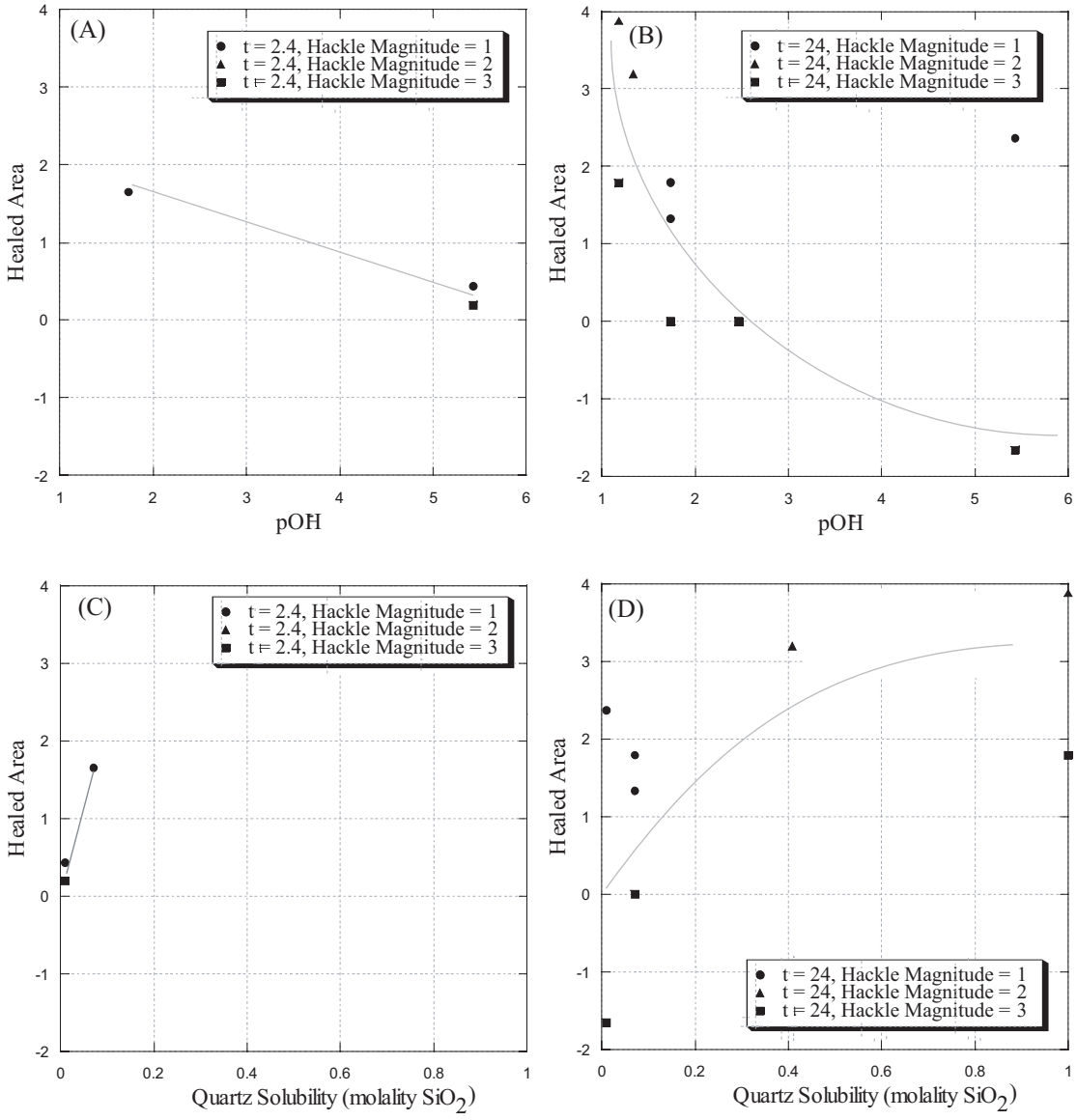

FIGURE 37. Healed areas of r-cracks in quartz prisms as a function of pOH- at T = 250°C after (A) 2.4 hours and (B) 24 hours. Healed areas of the same cracks plotted as a function of quartz solubility for (C) 2.4 hours and (D) 24 hours.

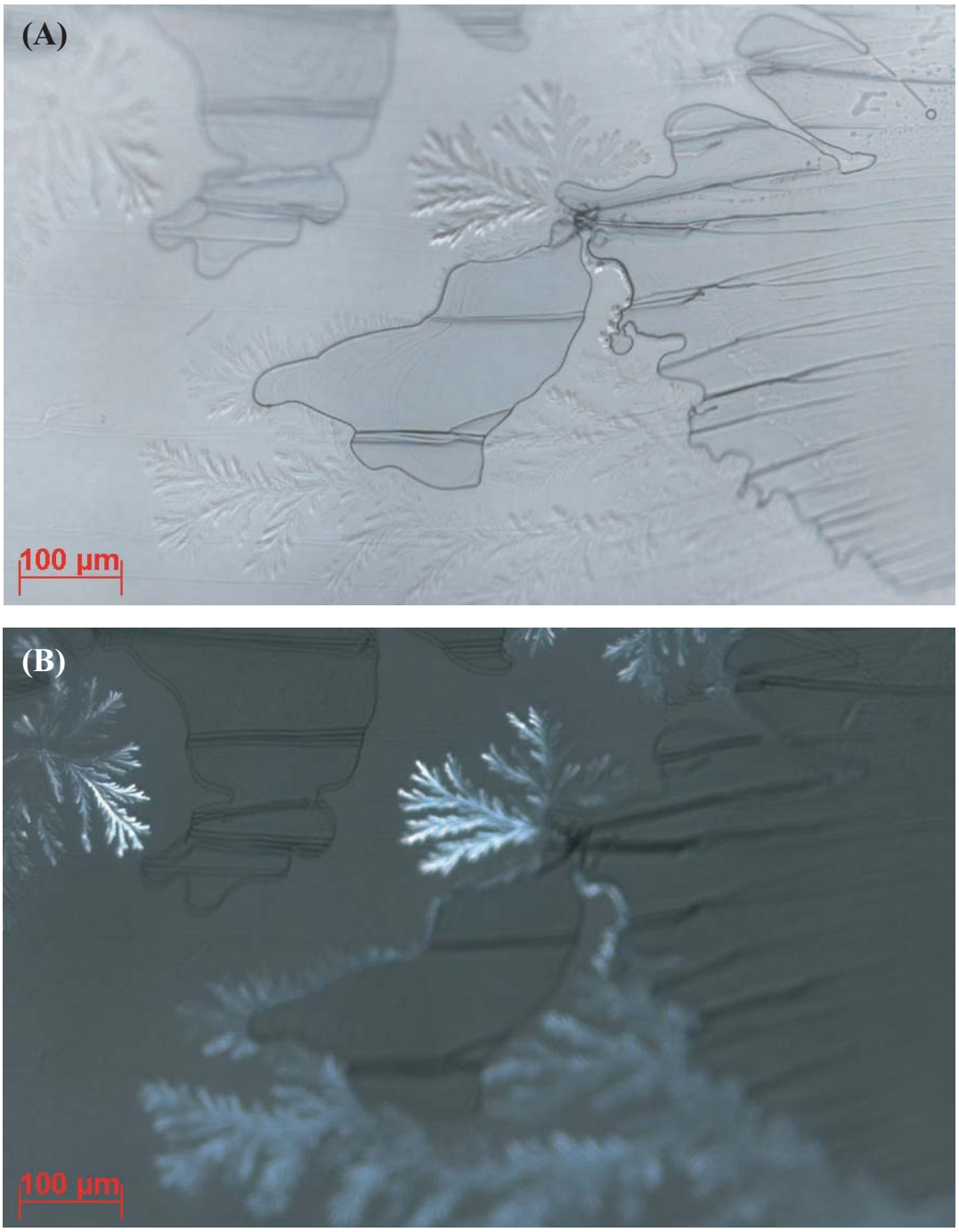

FIGURE 38. Morphologies of fluid inclusions and precipitated silica in a residual crack of quartz prism 2A#6, annealed in 1 molal NaOH at T = 250°C, t = 24 hrs. Rapid reduction in open crack area occured by precipitation of amorphous silica. (A) Healed crack shows large irregular fluid inclusions, dendritic features within the amorphous silica. Trace hackles continue to be observable because the amorphous silica has a refractive index that differs from that of quartz. (B) Between crossed nicols, dendritic features of the amorphous silica appear to be birefringent, potentially because of stresses generated between two phases of silica gel upon cooling or separation.

precipitated in these cracks has an optical refractive index that differs from that of quartz and is likely amorphous. The extensive healing of this sample is thus interpreted to result from the precipitation of amorphous silica rather than crystalline quartz. This process must be distinguished from that of crack healing in which the phase that precipitates is the same as the host phase.

3.9 Variations in Healing Rates within Individual Samples

As observed in other studies of crack healing, the scatter in healing rates determined for these experiments is large. Variations in healing rate may result from variations in initial crack morphology, leading to greatly varying crack apertures, and differences in density and magnitude of hackles and crack branching. Despite efforts to perform simple parametric experiments on smooth rhombohedral cracks (involving T, P_f, t and pOH^-), varying one key parameter while holding all others constant (TABLE 2), it was not possible to draw correlations between just two parameters from multiple experiments without introducing scatter associated with crack apertures and roughness. However, in several cases, the effect of crack surface roughness on healing can be tested for which temperature, fluid pressure, annealing time and fluid composition are constant. In some quartz prisms, two r-cracks were formed (one from either end of the quartz prism) such that variations in healing can be attributed directly to initial crack morphology. For some individual cracks, healing was detected for portions of the crack that were originally smooth and other portions that exhibit residual hackle marks.

Healed areas of cracks in the same quartz prism and subjected to identical experimental conditions are strongly dependent on crack smoothness. For each pair of cracks (FIGURE 39), healed area is larger for the smoother of the cracks (hackle magnitude 1 or 2), and lower for the rough crack (hackle magnitude 3). Healed areas of initially smooth cracks are larger than those of initially rough cracks by 30% to factors of 7.

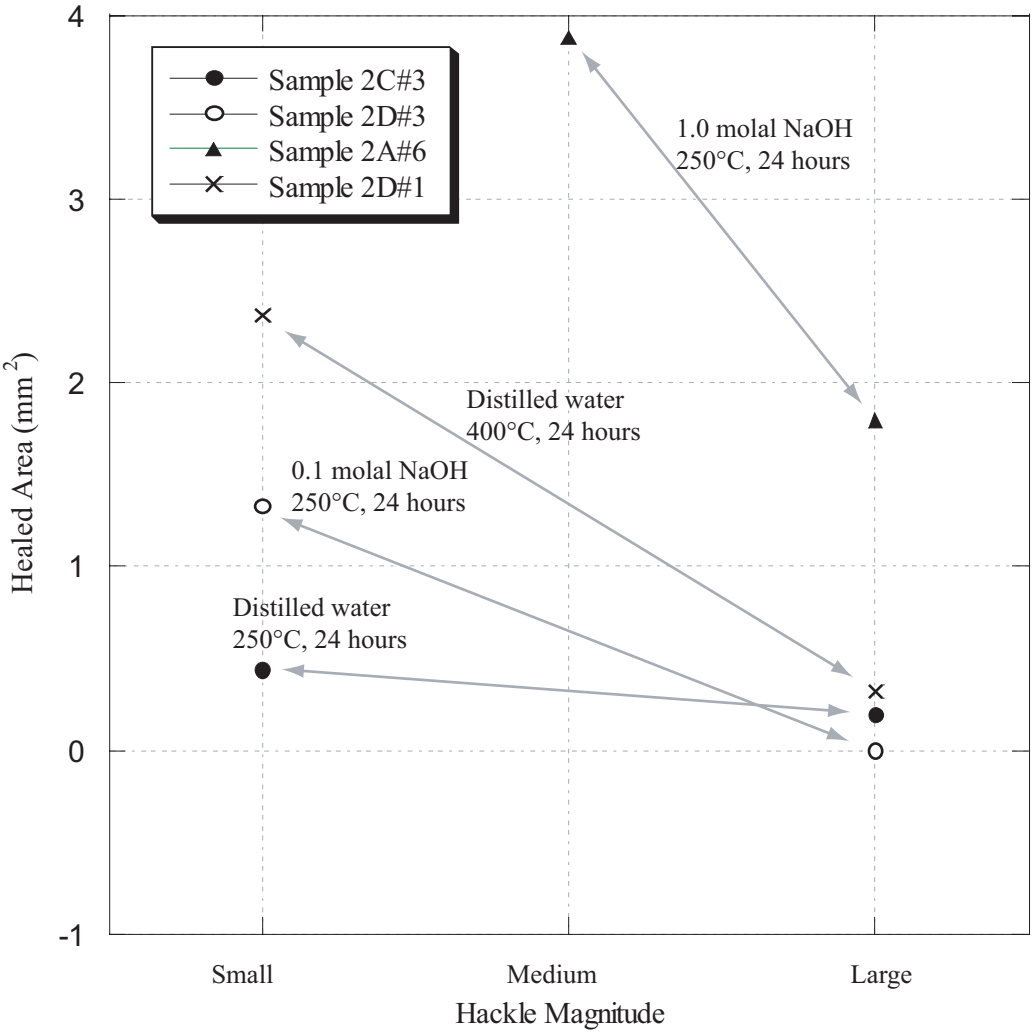

FIGURE 39. Healed area vs. hackle magnitude, for prisms which contained two cracks. Comparison of healing for pairs of cracks subject to idential experimental conditions and annealing time reveal an unambiguous dependence of healing rate on crack roughness.

While healing may be locally enhanced or reduced at hackle marks, rough cracks tend to heal less at a given set of conditions than smooth cracks. The influence of crack roughness on healing can be verified directly from observations of individual cracks with varying amounts of healing that scale with numbers of hackle marks (FIGURE 40). Initially smooth regions of a crack in quartz prism 3E#3 are well healed, while large regions of fluid filled crack remain between locally healed hackle marks.

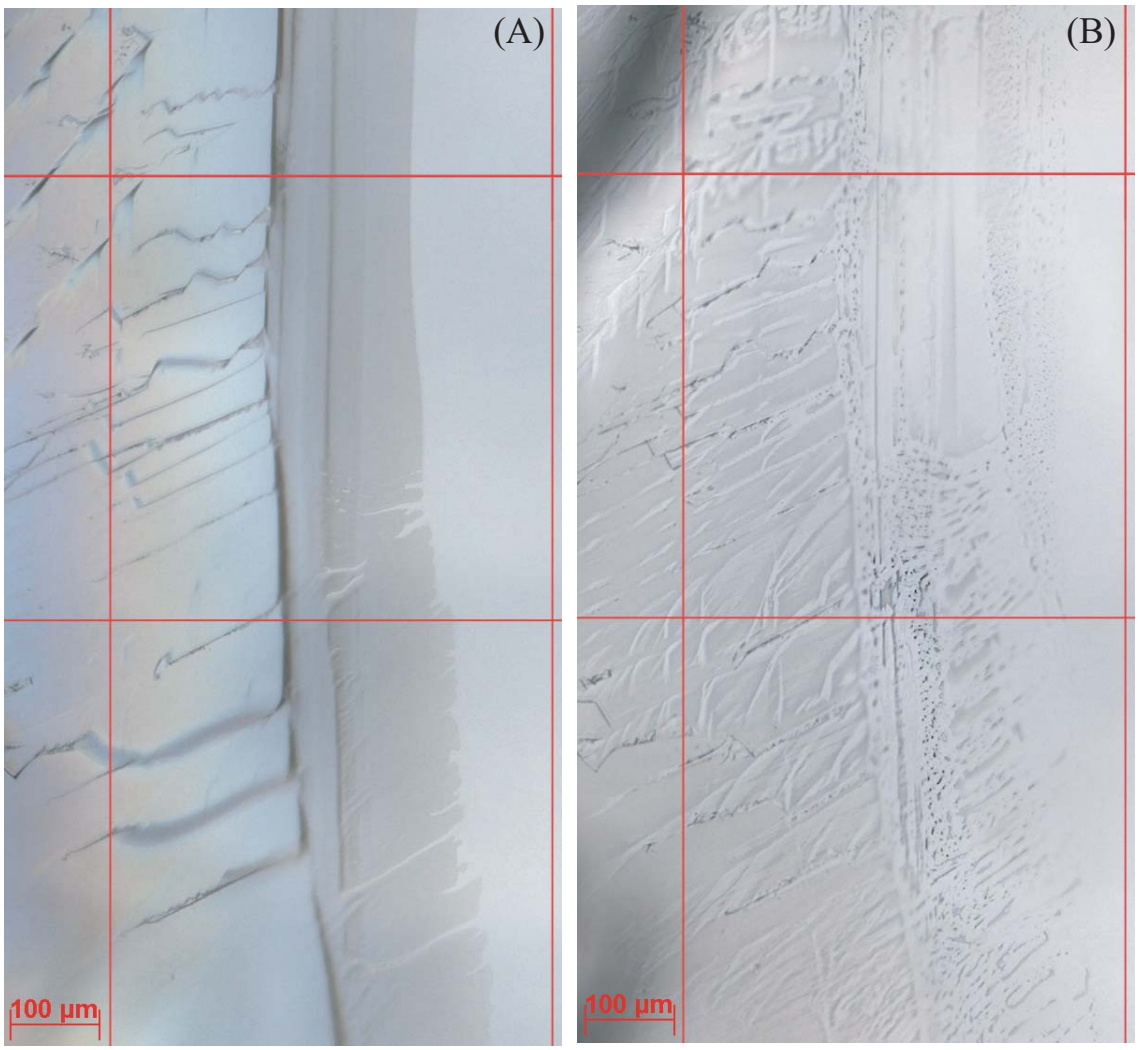

FIGURE 40. Variation in extent of crack healing resulting from differing crack roughness within the same crack (Quartz crack 3E#3 before (A) and after (B) annealing at T = 400°C and t = 24 hrs in distilled water). The smooth hackle-free crack area prior to annealing (A) is replaced by abundant fluid-filled tubes and inclusions (B) while only local healing at hackle edges is observed in rough hackled regions of the crack, leaving regions of fluid-filled crack between locally healed hackle marks.

4. DISCUSSION

4.1 Summary of Results and Comparison with Previous Studies

Healing rates determined in this study range over 4.83×10^{-7} to 1.91×10^{-4} mm/s, by processes of local silica dissolution, diffusion and precipitation, much as described by Smith and Evans, (1984) and Brantley et al., (1990). In earlier studies crack healing was observed after annealing times of 0.1 hours at T = 400°C, but not at T = 200°C (Smith and Evans, 1984). This study extends the conditions that crack healing is observed in the laboratory to T = 250°C.

Previous studies have shown that the extent of crack healing in quartz depends on T, t, aperture, and fluid salinity (Smith and Evans, 1984; Brantley et al., 1990; Brantley, 1992; Beeler and Hickman, 1996). Similarly crack healing in calcite (Hickman and Evans, 1987) appears to depend on fracture roughness, with calcite bridges formed across cracks at the former loci of hackle marks. Brantley (1992) showed that crack healing depends on fracture roughness. The results of this study confirm the dependence of healing on aperture, time, and crack surface roughness. In addition, this study shows that crack healing is enhanced at low pOH^-.

4.2 Effect of Closure

Based on the study of Beeler and Hickman (2004), rapid elastic crack closure is expected at the beginning of each annealing experiment, followed by longer term crack healing. Thus, the aperture that controls crack healing is less than the aperture determined by interferometry at room conditions for the initial crack. Given that the process of early closure was not anticipated in earlier studies, it is difficult to know what dimensions of crack apertures might have been in previous studies of quartz. Thus, direct comparisons of healing rates for a common aperture are not possible.

4.3 Effect of Roughness

Variations in crack healing for cracks of differing roughness are pronounced. Detailed microstructural observations show that hackle marks are the loci of either enhanced or reduced precipitation and healing. These variations can be explained by local variations in effective aperture and the sense of twist of opposing quartz surfaces (FIGURE 41). In addition, epitaxial quartz precipitation may be more rapid on irrational surfaces at hackle steps than rates on the low index r-plane. When opposing quartz surfaces shear relative to each other, hackle steps of the two crack surfaces locally may have small apertures or even overlap for one sense of shear, while apertures are increased for the opposite sense of shear. For reduced local apertures, healing at hackle marks may be enhanced to form curvilinear quartz bridges that prevent any further closure of the surrounding open crack. Thus, though hackles may represent sites of locally enhanced precipitation, large relative crack apertures are maintained over most of the crack, reducing the average healing rate. When hackles shear out of phase so that the hackles are pulled apart, they form a linear void with larger apertures than the opening of the surrounding crack. In these cases, the surrounding crack heals preferentially, leaving a tubular void (which may close down into a trail of fluid inclusions). These fluid filled tubes present no obstacle for healing of the surrounding crack. Quartz precipitates and quartz bridges at hackle marks appear to be more common than open fluid-filled tubes. In addition to the local variations in crack aperture, steps in the crack surfaces at hackle marks have a range of random orientations relative to crystal axes and their surface energies are likely to be higher than that of the r-face. Epitaxial growth of quartz on basal single crystal surfaces show initially high growth rates followed by much lower growth rates once equilibrium r and z faces are formed (Lander and Walderhaug, 1999; Walderhaug and Rykkje, 2000). Thus, quartz precipitation at steps in r-cleavage cracks may be rapid and contribute to locally enhanced rates of healing. Hickman and Evans (1987) note enhanced healing and precipitation at cleavage steps in cracks in calcite. Thus, for quartz, as for calcite, crack roughness has a strong effect on crack healing (Brantley, 1990).

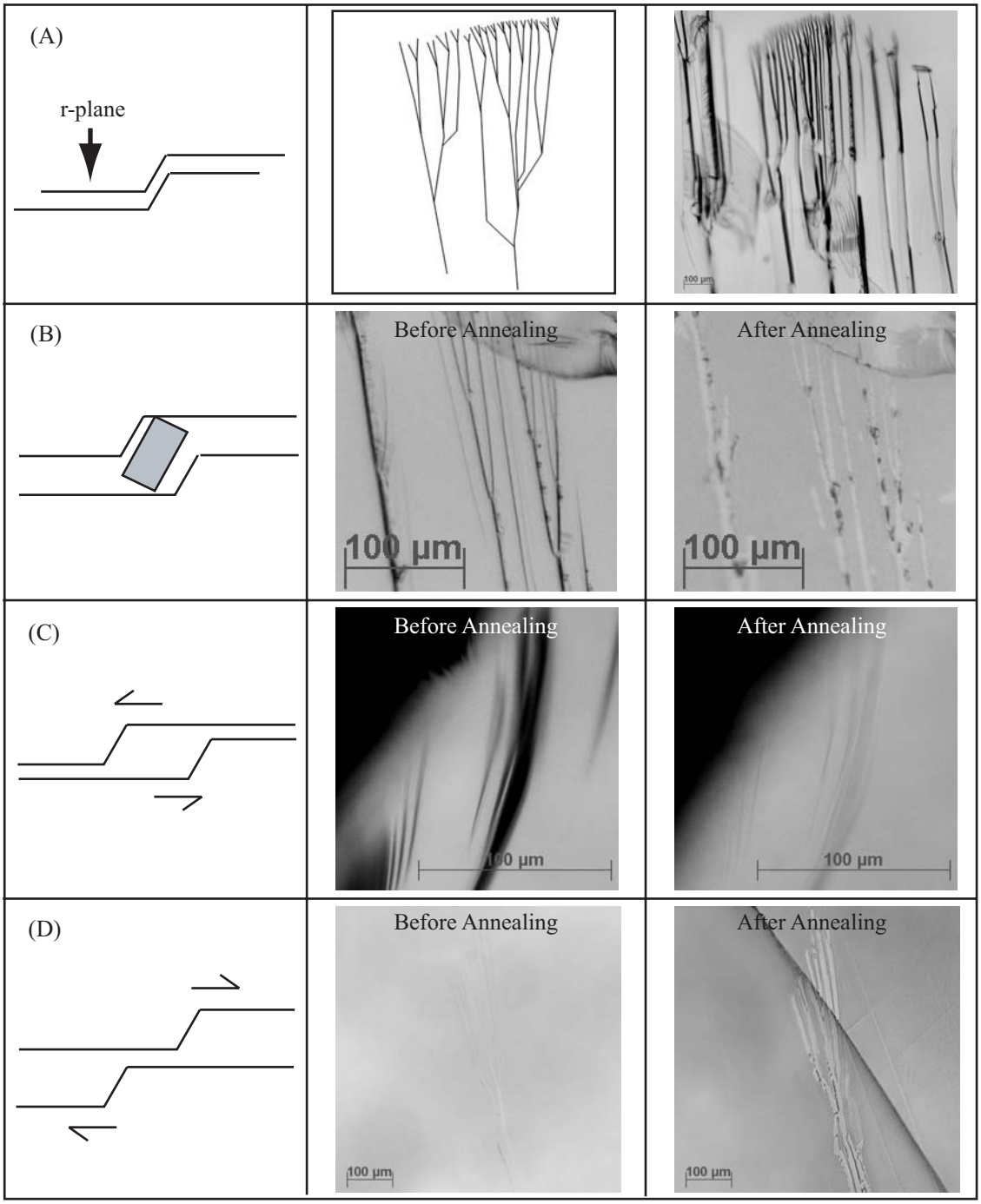

FIGURE 41. Influence of hackle marks on crack healing. (A) Hackle marks forming complex river patterns in r-crack prior to annealing, sketched in profile and plan-view, and photomicrograph of r-crack. The hackle step shown in profile may have a wide range of orientations relative to r. (B) Hackled crack held open by debris formed at hackles during crack propagation, shown schematically in cross-section, and micrographs before hydrothermal annealing, and after annealing. (C) Small angle twists of quartz on either side of crack with hackle marks may lead to fluid-filled tubes at hackles, with extensive crack healing surrounding the tube. (D) Opposite sense of twist may lead to enhanced healing at hackle mark and open, fluid filled crack surrounding healed hackles.

4.4 Effect of pOH^-

The pOH^- of the fluid has a strong effect on healing in quartz. Given that the process of healing is diffusion rate limited, low pOH^- may accelerate crack healing through its influence on SiO_2 solubility. Higher concentrations of silica in the fluid increase diffusional transport, and thus healing rates are increased through an increased diffusion coefficient that enters the pre-exponential term Λ of EQUATION 1. If so, the explanation for pOH^- effects on crack healing is the same as that offered by Brantley (1992) for increased healing rates in fluids of high salinity.

Alternatively, the rate of crack healing may be limited by rates of dissolution or precipitation. The morphologies of cracks healed at T = 400°C are similar to those described by Smith and Evans (1984), Brantley et al. (1990), Hickman and Evans (1987) and taken to support a model of diffusion-controlled reductions in surface area. However, cracks healed at T = 250°C do not show evidence of local dissolution, as noted for cracks healed at higher temperatures, and they have few fluid inclusions. Rates of healing at T = 250°C may be limited by precipitation of quartz at the crack tip or dissolution over larger, remote quartz surfaces. Increased reaction rates in this case may be explained by changes in complexes of the quartz-fluid interface that depend on pOH^-. With more OH^- molecules available, the crack surface becomes more hydroxylated and rates of dissolution and precipitation increase (Knauss and Wolery, 1987; Parks, 1990).

4.5 Crack Lifetimes Predicted by Results

Brantley et al. (1992) used experimental measurements of crack healing and an expression similar to EQUATION 1 to predict that crack lifetimes in the Earth are geologically short, even at T = 200°C. Crack lifetimes can be compared to time scales associated with burial of sediments (100m/my), and with interseismic recovery periods

of active fault zones (100-1000 years). With burial, reservoir sands subjected to lithostatic loads compact through grain crushing and associated pore collapse (Zhang et al., 1990; Zhu et al., 1997; Karner et al., 2003). Experiments performed on unconsolidated quartz sand and porous sandstones show that grain crushing occurs at a critical pressure with cracks originating at loaded grain contacts (Borg et al., 1960; Friedman, 1963; Gallagher et al., 1974; Zhang et al., 1990; Zhu et al., 1997; Karner et al., 2003). Planar arrays of fluid inclusions in association with grain contacts of reservoir sands confirm the process of grain crushing and they demonstrate that crack healing occurred following compaction.

Crack healing is expected to be particularly important in fault zones during interseismic periods between earthquakes. Cracks formed during the rapid slip of earthquakes may generate dense microcracks and gouge that affect mechanical and transport properties of the fault. During interseismic periods, ranging from 100 to 1000 years, crack healing may lead to increases in fault strength and reductions in gouge porosity and permeability.

To apply the experimental crack healing data of this study to the earth, average healing rates from this study determined at T = 400°C , EQUATION 1, the activation energy Q = 80 kJ/mol of Brantley et al. (1990), a value of n = 0.21 for smooth cracks (which agrees with values of n found by Brantley et al. 1990), and a value of n = 0.04 for rough cracks are used. Lifetimes of smooth small aperture cracks are predicted to be geologically short, on the order of 100 years at T = 100°C, and 100 days at T = 200°C. Thus, smooth cracks formed in reservoir rocks may heal rapidly during their long-term burial, and crack porosities will be negligible at all times. Interseismic healing of smooth, small-aperture cracks in fault zones may be substantial at depths where temperatures reach or exceed 200°C but cracks may remain open at shallow levels where T < 100°C. Very different predictions are obtained for rougher, large aperture cracks. Crack lifetimes predicted at T = 100°C and 200°C using n = 0.04 exceed the age of the

Earth, and would essentially never heal. However, if the equation is solved for rougher cracks using n = 0.21, more reasonable crack lifetimes of t ~ 64,000 yrs at 100°C, and t ~ 350 yrs at 200°C are obtained.

The contrasts between rough and smooth cracks, as well as the effect of (n) on calculated crack lifetimes highlight the extreme importance of geometry on healing rate. Thus, a prediction of this study, and of previous experimental studies of crack healing, is that healing rates vary greatly with aperture and crack roughness and that the extent of healing in the same rock subject to the same set of subsurface correlations will differ substantially.

4.6 Effect of Roughness Extrapolated to Real World Conditions

All of these predictions are made for rocks subject to mean stress equal to pore pressure. Crack healing rates may be increased, and crack lifetimes decreased when lithostatic loads exceed pore pressures along a hydrostat and effective stresses decrease crack apertures.

Cracks formed on the r-plane are smooth by comparison with cracks formed in quartz in all other orientations. Yet, even for r-cleavage cracks, healing rates depend critically on crack roughness. Cracks formed in other orientations of quartz are rough compared with r-cleavage cracks, with characteristic steps, and undulations that depend on the specific crack orientation (Ball and Payne, 1976; Martin and Durham, 1975). Given the dependence of crack healing on crack roughness, healing rates for rough cracks in a variety of orientations may be slower than measured in this study. Cracks in other minerals and through polycrystalline rocks can be rougher still, and healing rates are probably much slower than those measured here.

4.7 Effect of Aperture Extrapolated to Real World Conditions

For rough intra-granular cracks and large aperture fractures that transect many grains of a rock, crack healing may be insignificant, even for rocks subjected to elevated temperatures over extended geologic times. For these, the influx of large quantities of supersaturated fluids may lead to crack sealing rather than crack healing. Large aperture fractures tend to act as fluid conduits, contributing to fluid-dominated conditions and advective influx of silica (and other solutes) from remote sources. In this case, precipitation at fracture walls is driven by solute concentrations in excess of equilibrium values, with little sensitivity to crack aperture.

6. CONCLUSIONS

On the basis of hydrothermal annealing experiments and microstructural examination of rhombohedral $(10\bar{1}1)$ cracks in quartz, the following conclusions can be drawn:

1) Diffusional crack healing at T = 400°C, $P_f = P_c$ = 41 MPa is significant in short experimental times (2.4 – 240 hours) with mean healing rates of 4.83×10^{-7} to 1.91×10^{-4} mm/s.

2) Crack healing at T = 250°C $P_f = P_c$ = 41 MPa is also observed for smooth cracks with small apertures or cracks annealed at low pOH^-. Silica diffusion at T = 250°C may continue to be the rate-limiting step to crack healing, but crack blunting is not as pronounced, and fluid inclusions are not as common for cracks healed at these conditions. Thus, reaction rates cannot be ruled out as the rate-limiting process under these conditions.

3) Rates of crack healing are sensitive to crack aperture and roughness. Healing rates are highest for r-cleavage cracks with small apertures that are smooth and show little crack branching. Cracks with large numbers of hackle marks and extensive crack branching show little or no crack healing.

4) Hackle marks formed by fine scale crack branching during crack propagation are sites of locally enhanced or reduced healing depending on the sense of offset of opposing crack surfaces and local perturbations in aperture. For cracks that show enhanced quartz precipitation at hackle marks, curvilinear quartz bridges that replace the hackles serve to maintain large apertures for the surrounding fluid-filled crack.

5) Crack healing of quartz is enhanced at low pOH^-. Rates of crack healing may be increased at low pOH^- through increases in silica concentration and diffusional transport.

Alternatively, if crack healing at T = 250°C is reaction rate controlled, healing may be enhanced by increased rates of dissolution or precipitation at low pOH^-.

6) Crack lifetimes in the Earth are likely to depend critically on crack aperture and roughness. Healing rates extrapolated to geological times and conditions suggest that crack lifetimes of smooth, small aperture cracks are geologically short at temperatures T > 100°C. In contrast, rough cracks may show little crack healing over protracted geologic times and other mechanisms such as crack sealing may be necessary to reduce crack densities in rock.

REFERENCES

Atkinson, B. (1979), A fracture mechanics study of subcritical tensile cracking of quartz in wet environments, *Pageoph* 117, 1011-1024.

Atkinson, B. K., and P.G. Meredith (1981), Stress corrosion cracking of quartz: a note on the influence of chemical environment, *Tectonophysics* 77, T1-11.

Bahat, D. (1991), *Tectono-fractography*, 354 pp., Springer-Verlag, New York.

Ball, A., and W. Payne (1976), The tensile fracture of quartz crystals, *Journal of Materials Science*, 11, 731-740.

Beeler, N. M., and S. H. Hickman (1996), Crack healing in quartz: experiments and theoretical considerations, *Eos Transactions AGU*, 77(46), Fall Meeting Supplement, F696.

Beeler, N.M., and S.H. Hickman (2004), Stress-induced, time-dependent fracture closure at hydrothermal conditions, *Journal of Geophysical Research*, 109, B02211.

Bodnar, R.J., and S.M. Sterner (1985), Synthetic fluid inclusions in natural quartz. II. Application to PVT studies, *Geochimica Cosmochimica Acta*, 49, 1855-1859.

Borg, I., M. Friedman, J. Handin, and D.V. Higgs (1960), Experimental deformation of St. Peter Sand: a study of cataclastic flow, *Geological Society of America Memoir*, 79, 133-191.

Boullier, A.M. (1999), Fluid inclusions: tectonic indicators, *Journal of Structural Geology*, 21, 1229-1235.

Bourbie, T., and B. Zinszner (1985), Hydraulic and acoustic properties as a function of porosity in fontainbleau sandstone, *Journal of Geophysical Research*, 90, 1524-1532.

Brace, W.F., B.W. Pauling, and C. Scholz (1966), Dilatancy in fracture of crystalline rock, *Journal of Geophysical Research*, 71, 3939.

Brantley, S. L. (1992), The effect of fluid chemistry on quartz microcrack lifetimes, *Earth and Planetetary Science Letters*, 113, 145– 156.

Brantley, S. L., B. Evans, S. H. Hickman, and D. A. Crerar (1990), Healing of microcracks in quartz: Implications for fluid flow, *Geology*, 18, 136– 139.

Brown, S.R. (1987), Fluid flow through rock joints: the effect of surface roughness, *Journal of Geophysical Research*, 92, 1337-1347.

Brown, S.R., and R.L. Bruhn (1998), Fluid permeability of deformable fracture networks, *Journal of Geophysical Research*, 103, 2489-2500.

Brown, S.R., and C. Scholz (1985), Closure of random elastic surfaces in contact, *Journal of Geophysical Research*, 90, 5531-5545.

Brown, S.R., A. Caprihan, and R. Hardy (1998), Experimental observation of fluid flow channels in a single fracture, *Journal of Geophysical Research*, 103, 5125-5132.

Chester, F.M. (1995), A rheologic model for wet crust applied to strike-slip faults, *Journal of Geophysical Research*, 100, 13033-13044.

Cowie, P. A. (1998), A healing-reloading feedback control on the growth rate of seismogenic faults, *Journal of Structural Geology*, 20, 8, 1075-1087.

Dewers, T., and P. Orteleva (1994), Nonlinear dynamical aspects of deep basin hydrology – fluid compartment formation and episodic fluid release, *American Journal of Science*, 294, 713-755.

Domenico, S.N. (1977), Elastic properties of unconsolidated porous sand reservoirs, *Geophysics*, 42, 1339-1368.

Dove, P. M. (1995), Geochemical controls on the kinetics of quartz fracture at subcritical tensile stresses, *Journal of Geophysical Research*, 100, 22349-22359.

Dunning, J.D., D. Petrovski, J. Schuyler, and A. Owens (1984), The effects of aqueous chemical environments on crack propagation in quartz, *Journal of Geophysical Research*, 89, 4115-4123.

Evans, A. G., and E. A. Charles (1977), Strength recovery by diffusive crack healing, *Acta Metallurgica*, 25, 919-927.

Fischer D.M. and S. L. Brantley (1992), Models of quartz overgrowth and vein formation: deformation and episodic fluid flow in an ancient subduction zone, *Journal of Geophysical Research*, 97, 20043-20061.

Freiman, S. W. (1984), Effects of chemical environments on slow crack growth in glasses and ceramics, *Journal of Geophysical Research*, 89, 4072-4076.

Friedman, J. (1963), Petrofabric analysis of experimentally deformed calcite-cemented sandstones, *Journal of Geology*, 21, 12-37.

Gallagher, J.J., M. Friedman, J. Handin, and G.M. Sowers (1974), Experimental studies relating to microfractures in sandstones, *Tectonophysics*, 21, 203-347.

Gregory, A.R., (1977), Fluid saturation effects on dynamic elastic properties of sedimentary rocks, *Geophysics*, 41, 895-921.

Griffith, A.A. (1921), The phenomena of rupture and flow in solids, *Philosophical Transactions of the Royal Society*, 221, 163-199.

Hickman, S. H., and B. Evans (1987), Influence of geometry upon crack healing rate in calcite, *Physical Chemistry of Minerals*, 15, 91– 102.

Hickman, S., R. Sibson, R. Bruhn (1995), Introduction to special section: mechanical involvement of fluids in faulting, *Journal of Geophysical Research*, 100, 12,831-12,840.

Hilgers, C., K. Dilg-Gruschinski, and J.L. Urai (2004), Microstructural evolution of syntaxial veins formed by advective flow, *Geology*, 32, 261-264.

Kanagawa, K., S.F. Cox, and S.Q. Zhang (2000), Effects of dissolution-precipitation processes on the strength and mechanical behavior of quartz gouge at high-temperature hydrothermal conditions, *Journal of Geophysical Research*, 105, 11115-11126.

Karner, S.L., F.M. Chester, A.K. Kronenberg, and J.S. Chester (2003), Subcritical compaction and yielding of granular quartz sand, *Tectonophysics*, 377, 357-381.

Karner, S. L., C. Marone, B. Evans (1997), Laboratory study of fault healing and lithification in simulated fault gouge under hydrothermal conditions, *Tectonophysics*, 277, 41-45.

Knauss, K.G., and T. J. Wolery (1987), The dissolution kinetics of quartz as a function of pH and time at 70 C, *Geochimica et Cosmochimica Acta*, 52, 43-53.

Kronenberg, A.K. (1994), Hydrogen speciation and chemical weakening of quartz, *Reviews in Mineralogy*, 29, 123-176.

Lander, R.H., and O. Walderhaug (1999), Predicting porosity through simulating sandstone compaction and quartz cementation, *AAPG Bulletin*, 83, 433-449.

Laubach, S.E., R.M. Reed, J.E. Olson, R.H. Lander, and L.M. Bonnell (2004), Co-evolution of crack seal texture and fracture porosity in sedimentary rocks: cathodoluminescence observations of regional fractures, *Journal of Structural Geology*, 25, 967-982.

Lee, Y. L., and J.W. Morse (1999), Calcite precipitation in synthetic veins: implications for the time and fluid volume necessary for vein filling, *Chemical Geology*, 156, 151-170.

Lespinasse, M. (1999), Are fluid inclusion planes useful in structural geology?, *Journal of Structural Geology*, 21, 1237-1243.

Marshall, W. L., and E. U. Franck (1981), Ion product for water substance, 0-1000C, 1-10,000 bars new international formulation and its background, *Journal of Physical Chemistry Reference Data*, 10, 2, 295-303.

Martin, R.J., and W.B. Durham (1975), Mechanisms of crack growth in quartz, *Journal of Geophysical Research*, 80, 4837-4844.

Means, W. D., and T. Li (2001), A laboratory simulation of fibrous veins: some first observations, *Journal of Structural Geology*, 23, 857-863.

Michalske, T.A., Freiman, S.W., 1982. A molecular interpretation of stress corrosion in silica. *Nature* 295, pp 511-512.

Moller, K.D. (1988), *Optics*, 644 pp., University Science Books, Mill Valley California.

Nichols, F.A., and W. W. Mullins (1965), Morphological changes of a surface of revolution due to capillarity-induced surface diffusion, *Journal of Applied Physics*, 36, 1826-1835.

Parks, G. A. (1990), Surface energy and adsorption at mineral-water interfaces: an introduction, *Reviews in Mineralogy*, 23, 133-175.

Renard, F., J. Gratier, and B. Jamtveit (2000), Kinetics of crack-sealing, intergranular pressure solution, and compaction around active faults, *Journal of Structural Geology*, 22, 1395-1407.

Ritter, J.E., and R.P. LaPorte (1975), Effect of test environment of stress corrosion susceptibility of glass, *Journal of the American Ceramic Society*, 58, 265-267.

Roedder, E. (1984), Fluid inclusions, *Mineralogical Society of America Reviews in Mineralogy*, 12, 70-77.

Rumyantsev, V.N. (1993), Some specific features of quartz solubility in aqueous chloride solutions at increased temperatures and pressures, *Russian Journal of Inorganic Chemistry*, 38, 971-976.

Rumyantsev, V.N. (1995), Solubility of quartz in NaOH aqueous solutions at elevated temperatures and pressures, *Russian Journal of Inorganic Chemistry*, 40, 42-48.

Segall, P., and D.D. Pollard (1981), Joint formation in granitic rock of the Sierra Nevada, *Geological Society of America Bulletin*, 94, 563-575.

Shelton, K. L., and P. M. Orville (1980), Formation of synthetic fluid inclusions in natural quartz, *American Mineralogist*, 65, 1233–1236.

Simonson, J. M., R. E. Mesmer, and P.S.Z. Rogers (1989), The enthalpy of dilution and apparent molar heat capacity of NaOH-(aq) to 523K and 40 MPa, *Journal of Chemical Thermodynamics*, 21, 561-584.

Smith, D. L., and B. Evans (1984), Diffusional crack healing in quartz, *Journal of Geophysical Research*, 89, 4125– 4136.

Sprunt E.S., and A. Nur (1979), Microcracks and healing in granites: new evidence from cathodoluminescence, *Science*, 205, 495-497.

Sterner, S.M., and R.J. Bodnar, R.J (1984), Synthetic fluid inclusions in natural quartz I. Compositional types synthesized and applications to experimental geochemistry, *Geochimica et Cosmochimica Acta*, 48, 2659-2668.

Tenthorey, E., S.F. Cox, and H.F. Todd (2003), Evolution of strength recovery and permeability during fluid-rock reactions in experimental fault zones, *Earth and Planetary Science Letters*, 206, 161-172.

Tenthorey, E., C.H. Scholz, E. Aharonov, and A. Leger (1998), Precipitation sealing and diagenesis 1. experimental results, *Journal of Geophysical Research* 103, 23951-23967.

Valasek, J. (1949) *Introduction to Theoretical and Experimental Optics*, 454 pp., John Wiley and Sons, New York.

Walderhaug, O., and J. Rykkje (2000) Some examples of the effect of crystallographic orientation on the cathodoluminescence colors of quartz, *Journal of Sedimentary Research*, 70, 545-548.

Walther, J., and H. Helgeson (1977), Calculation of the thermodynamic properties of aqueous silica and the solubility of quartz and its polymorphs at high pressures and temperatures, *American Journal of Science* 277, 1315-1351.

Wiederhorn, S.M. (1967), Influence of water vapor on crack propagation in soda lime glass, *Journal of the American Ceramic Society*, 50, 407-414.

Wiederhorn, S.M. (1969), Fracture surface energy of glass, *Journal of the American Ceramic Society*, 52, 99-105.

Wiederhorn, S.M., and L.H. Bolz (1970), Stress corrosion and static fatigue of glass, *Journal of the American Ceramic Society*, 53, 543-548.

Wiltschko D, and Morse, J.V. 2001 Crystallization pressure versus "crack seal" as the mechanism for banded veins. *Geology* 29, 79-82.

Wiltschko D., J. Morse, Z. Sharp, W. Lamb (1998), *Analysis of veins in low temperature environments – introduction for structural geologists*, Short Course Notes for the Geological Society of America Annual Meeting, Toronto, October 24-25.

Winkler, K.W., and W.F. Murphy (1995), Acoustic velocity and attenuation in porous rocks, in *Rock Physics and Phase Relations: A Handbook of Physical Constants*, edited by T.J. Ahrens, pp. 20-34, American Geophysical Union, Washington, D.C.

Wong, T.F. (1982), Micromechanics of faulting in westerly granite, *International Journal of Rock Mechanics and Mining Sciences*, 19, 49-64.

Wong, T.F., J.T. Fredrich, and G.D. Gwanmesia (1989), Crack aperture statistics and pore space fractal geometry of westerly granite and rutland quartzite: implications for an elastic contact model of rock compressibility, *Journal of Geophysical Research*, 94, 10267-10278.

Wyllie, M.R.J., A.R. Gregory, and L.W. Gardner (1956), Elastic wave velocities in heterogeneous and porous media, *Geophysics*, 21, 41-70.

Zhang, J.X., T.F. Wong, and D.M. Davis (1990), Micromechanics of pressure-induced grain crushing in porous rocks, *Journal of Geophysical Research*, 95, 341-352.

Zhang, S.Q., M.S. Paterson, S.F. Cox (2001), Microcrack growth and healing in deformed calcite aggregates, *Tectonophysics*, 335, 17-36.

Zhu, W.L., L.G.J. Montesi, and T.F. Wong (1997), Shear-enhanced compaction and permeability reduction: triaxial extension tests on porous sandstone, *Mechanics of Materials*, 25, 199-214.

VITA

Jessica Anne Fallon

P.O. BOX 432
Boerne, TX 78006

M.S. Texas A&M University, December 2004
B.S. The University of Oklahoma, May 2001